جمهورية العراق

وزارة التعليم العالي و البحث العلمي

التحليل الديناميكي اللاخطي
بطريقة العناصر المحددة
للمنشآت الخرسانية المنحنية

رسالة

مقدمة إلى كلية الهندسة في جامعة بابل

كجزء من متطلبات نيل درجة ماجستير

علوم في الهندسة المدنية

(هندسة إنشاءات)

رنا فلاح يوسف الدهش

بكلوريوس هندسة مدنية

تموز , ٢٠٠٦

Republic of Iraq

Ministry of Higher Education

and Scientific Research

NONLINEAR DYNAMIC ANALYSIS OF REINFORCED CONCRETE ARCH STRUCTURES BY FINITE ELEMENT METHOD

A Thesis

Submitted to the College of Engineering of the University of Babylon in Partial Fulfillment of the Requirements for the Degree of Master of Science in civil Engineering

By

RANA FALAH YOUSIF AL - DAHASH

December,٢٠٠٦ B.SC.lqu□da

يتعلق البحث الحالي بموضوع التحليل الاخطي للمنشآت الخرسانية المسلحة الثلاثية الأبعاد و الناتجة عن تحميلها بقوى ديناميكية .

و لقد تم إدخال التمثيل اللاخطي للمادة في التحليل المجرى ضمن هذه الدراسة كما أخذ بنظر الاعتبار دراسة العوامل اللاخطية للمادة و تشمل تشقق الخرسانة بالسحب و انحدار الانفعال بعد التشقق و السلوك اللاخطي للخرسانة تحت الضغط مع تهشم الخرسانة و مطيلية حديد التسليح .

في هذا البحث تم تمثيل المنشأ الخرساني بموديل ثلاثي الأبعاد . و يتكون تمثيل العنصر الفضائي الواحد للكونكريت من ثمانية أو عشرين عقده و هو من نوع ال (isoparametric) يفترض أن حديد التسليح له مواصفات أحادية الاتجاه و باتجاه قضبان التسليح و لتمثيل المنشات الخرسانية المسلحة تم فرض وقوع حديد التسليح ضمني داخل عنصر الخرسانة الطابوقي الشكل و كذلك بافتراض وجود رابطة محكمة بينهما .

تتميز الخرسانة بكونها مادة مرنة خطية و لها هبوط بالانفعال (strain softening) بغد التشقق عند خضوعها لإجهاد الشد ، و بكونه مادة مرنة – لزجة – لدنة عند خضوعها لإجهاد الضغط . و قد تم اعتماد مادة مرنة – لزجة – لدنة لتمثيل الحديد .

تم حل مثالين رقميين في هذه الدراسة لغرض مقارنة النتائج التي تم الحصول عليها باستخدام طريقة العناصر المحددة مع نتائج تم الحصول عليها من طرق نظرية أخرى و من ذلك وجدنا تقارب جيد بين النتائج .

نظمت دراسات نظرية لاختيار تأثير نسبة الإخماد و درجة الانحناء و نوع المساند و عدد العناصر التي تمثل المنشأ و سمك طبقة حديد التسليح و مقدار تغير الزمن و الإزاحة البدائية على تصرف الأعتاب المنحنية المصنوعة من الكونكريت المسلح . ومن النتائج المستحصلة ، وجدنا أن الهطول و الإجهاد القصي للمنشأ بدون إخماد أكبر من الهطول و الإجهاد القصي للمنشأ عندما نأخذ الاجهاد بعين الاعتبار بمقدار (٦٠%) و(٧٩.٦%)على التوالي . و عندما مقدار التغير في الزمن يقل من (٠.٠١) ثانية إلى (٠.٠٠٥) ثانية الهطول في منتصف العتب تزداد بمقدار (٨٩%) .

النساء / الآية (١١٣)

إلى

الشمعة ألتي احترقت لتضيء طريقي

والدي

إلى

من اشعر بقربها بالحنان

والدتي

إلى

من فقدت بعده الأمان

زوجي (رحمه

الله

إلى

من أشد به أزري

أخي

The present study is concerned with nonlinear analysis of three dimensional reinforced concrete arch structures subjected to dynamic loading .

Material nonlinearity as a result of tension cracking , strain softening after cracking , the nonlinear response of concrete in compression , crushing of concrete and the yielding of the reinforcement are considered .

The three dimensional computational model is adopted in the present study. The eight and twenty noded hexahedral isoparametric elements are used for the spatial discretization of concrete , while the steel reinforcement is assumed to have uniaxial properties in the direction of the bars and it's incorporated in the concrete brick element by assuming a perfect bond .

Concrete is considered as a linear elastic strain softening material in tension and as an elasto – viscoplastic material in compression . A classical elasto – viscoplastic model is used in the present study to model the reinforcement .

Two numerical examples are worked out to compare results obtained by the finite element analysis to those available analytical results and good agreement between these results were found .

Parametric studies have been carried out to examine the influence of damping ratio , degree of curvature , boundary condition , thickness of main reinforcement layers and the initial displacement on the behavior of reinforced concrete arch structures and also the non – prismatic clamped circular arch was solved with two cases . From the results obtained , the deflection and shear stresses of arch without damping is greater than

deflection and shear stresses with damping by maximum difference about (٦٠٪) and (٧٩.٦٪) , respectively . If initial displacement happened in the supported of arch , the maximum central deflection increases , when this displacement in the direction and opposite the direction of X – axis with magnitude equals to (٠.٢,-٠.٢)cm the maximum difference of central deflection by about (٥٧.٥٪).

ACKNOWLEDGMENTS

First of all , profusely and all thanks for **ALLAH** who enabled me to achieve this work .

The researcher is indebted with gratitude to his supervisors Mr. **Abdul-Ridah S. Hadi** and **Dr. Ammar Y. Ali** for their invaluable guidance , advice and discussions throughout the research work .

I express my special thanks to **Dr. Hatham H. AL-Daami** and **Mr. Nabeel Hasan** for their help and useful discussions .

Furthermore , deepest thanks are to my friends for their help to accomplish this study , especially **Mss. Muna**, **Mss. Afrah** and for my sister **Mss. Hanan F. Yousif AL-Dahash** .

Finally , I would like to extend my sincere thanks to my family for their patience and endurance and to all those who had participated in any way or another in this research .

Rana

June , ٢٠٠٦

EXAMINING COMMITTEE CERTIFICATE

We certify we have read this thesis titled (**Nonlinear Dynamic Analysis of Reinforced concrete Arch Structures By Finite Element Method**) , and as an examining committee , examined the student **Rana Falah Yousif Al – Dahash** in it's contents and in what is connected with it and that our opinion it meet the standard of a thesis for the degree **Master of Science in Civil Engineering (Structural Engineering) .**

Signature :

Name:**Asst. Prof. Mr. Abdul–Ridah S. Hadi**

(Supervisor)

Date: / /٢٠٠

Signature :

Name:**Asst. Prof. Dr. Ammar Y. Ali**

(Supervisor)

Date: / /٢٠٠

Signature :

Name: **Asst. Prof. Dr. Mustafa B. Dawood**

(Member)

Date: / /٢٠٠

Signature :

Name:**Asst. Prof. Dr. Haider T. AL-Damarchi**

(Member)

Date: / /٢٠٠

Signature:

Name:**Asst. Prof. Dr. Nameer A. Alwash**

(Chairman)

Date: / /٢٠٠

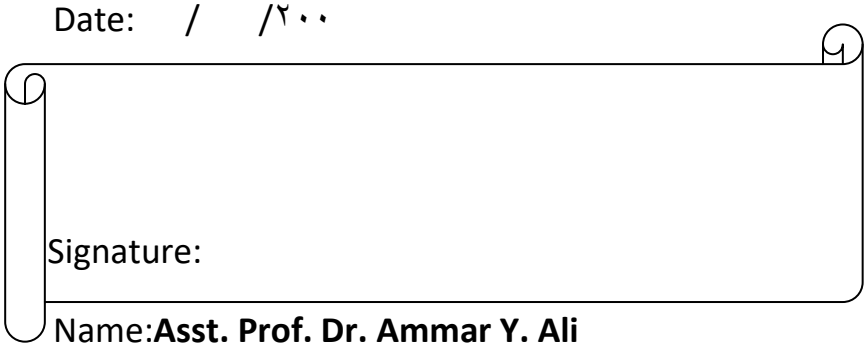

Signature:

Name:**Asst. Prof. Dr. Ammar Y. Ali**

(Head of the Civil Engineering Department)

Date: / /٢٠٠

Signature:

Name: **Prof. Abd Al-Wahid K. Rajih**

(Dean of the College of Engineering)

Date: / /٢٠٠

LIST OF CONTENTS

SUBJECT	PAGE
ACKNOWLEDGMENTS	**I**
ABSTRACT	**II**
LIST OF CONTENTS	**III**
LIST OF NOTATIONS	**VI**
CHAPTER ONE : INTRODUCTION	
١.١ General	١
١.٢ Applications of Arches Structures	٢
١.٣ Method of Analysis	٣
١.٤ Reinforced Concrete Nonlinearity	٤
١.٥ Objective and Scope	٤
١.٦ Thesis Layout	٥
CHAPTER TWO :REVIEW OF LITERATURE	
٢.١ General	٦
٢.٢ Static Analysis for Curved Beam by Finite Element	٦
٢.٣ Dynamic Analysis for Curved Beams	١٠
CHAPTER THREE : MODELING OF MATERIAL PROPERTIES	
٣.١ General	١٦
٣.٢ Concrete Modeling	١٦
٣.٢.١ Stresses – Strain Relationship	١٧
٣.٣ Traditional Elasto / Viscoplastic Model	١٨
٣.٤ Strian Rate Sensitive Elasto/Viscoplastic Model for Concrete	١٩
٣.٤.١ Yield and Strength Limit Surfaces	٢٠
٣.٤.٢ Viscoplastic Strain Rate	٢٣
٣.٤.٣ Determination of Model Parameters	٢٣
٣.٥ Modeling of Cracked concrete	٢٤
٣.٥.١ Cracking Criterion	٢٥
٣.٥. ٢ Strain – Softening Rule (Tension Stiffening)	٢٨
SUBJECT	**PAGE**
٣.٥.٣ Shear Transfer Across the Crack	٣٣
٣.٦ Modeling of Reinforcing Steel	٣٣
٣.٦.١ Stresses – Strain Relationship	٣٣
٣.٦.٢ Reinforcement Representation	٣٥
٣.٦.٣ Reinforcing Steel	٣٥
CHAPTER FOUR : NONLINEAR DYNAMIC ANALYSIS	

BY FINITE ELEMENT METHOD	
٤.١ General	٣٦
٤.٢ Finite Element Equilibrium Equations	٣٦
٤.٣ Formulation of ٣ – D Brick Element	٣٧
٤.٣.١ Concrete Element Modeling	٣٧
٤.٣.١.١ Shape Functions	٣٨
٤.٣.١.٢ Stresses and Strain Fields	٤٠
٤.٣.١.٣ Formulation of Load Matrix	٤٤
٤.٣.٢ Steel Layer	٤٤
٤.٤ Dynamic Equilibrium Equations is Semi – Discrete Form	٤٥
٤.٤.١ Mass Matrix Formulation	٤٥
٤.٤.٢ Modeling of Damping	٤٧
٤.٥ Nonlinear Solution Technique	٤٧
٤.٥.١ General	٤٧
٤.٥.٢ Direct Integration Methods	٤٨
٤.٥.٢.١ The Newmark Method	٤٨
٤.٥.٢.٢ Computational Algorithm Form of Newmark's Method	٤٩
٤.٥.٣ Selection of the Time Step Size for Viscoplastic Model	٥١
٤.٥.٤ Convergence Criteria	٥٢
٤.٦ Computer Program for Dynamic Analysis	٥٢
CHAPTER FIVE :NUMERICAL APPLICATION AND PARAMETRIC STUDY	
٥.١ General	٥٥
٥.٢ Numerical Applications	٥٦
٥.٢.١ Semi–Circular Arch Subjected to Step Loading	٥٦
٥.٢.٢ A clamped Reinforced Concrete Circular Arch Subjected to Uniformly Distributed Normal Load	٥٩
٥.٣ Parametric Study	٧٠
٥.٣.١ Effect Subtended Angle on Curved Cantilever Arch	٧٠
٥.٣.٢ Non- Prismatic Reinforced Concrete Clamped Circular Arch Structure with Subtended Angle (١٧٠°)	٨٠
٥.٣.٣ Simply Supported Reinforced Concrete Arch Structure Under A concentrated Load	٩٣
SUBJECT	**PAGE**
٥.٣.٤ Effect of Boundary Conditions on Reinforced Concrete Arch Structures	١٠٤
٥.٣.٥ Simply Supported Reinforced Concrete Arch Under Concentrated Load with Harmonic Excitation Load – Time Function	١٢٠

٥.٣.٦ Reinforced Concrete Clamped Circular Arch Structure of Continuously Varying Cross – Section	١٢٧
CHAPTER SIX : CONCLUSIONS AND RECOMMENDATIONS FOR FUTURE WORKS	
٦.١ Conclusions	١٣٦
٦.٢ Recommendations for Future Works	١٣٧
REFERENCES	١٣٩

LIST OF NOTATIONS

– Latin Symbols	
Symbol	**Description**
$\{a\}^e$	Nodal displacements .
a_1 , a_o	Fluidity parameters .
$[B_s]$	Strain – displacement matrix of steel .
[B]	Strain – displacement matrix .
c	Damping parameter .
[C]	damping matrices .
[D]	Elasticity matrix
$[D_s]$	Stresses – strain matrix of steel .
E_O	Elastic **Young's** modulus .
E_s	**Young's** modulus of steel .
E_c	**Young's** modulus of concrete .
F_c	Ultimate compressive strength for concrete .
F_t	Tensile strength for concrete .
F.	Yield surface .
F_f	Strength limit surface .
F_y	Yield stresses for steel .
F_{xi} ,F_{yi} ,F_{zi}	External nodal forces in x , y and z – direction respectively .
f_1 ,f_2 , f_3	X , y and z components of gravity direction vector .
{F}	Vector of external applied forces .
G_f	Fracture energy .
G_o	Shear modulus of uncracked concrete .
G_c	Reduced shear modulus of cracked concrete .
G_t	Fictitious tensile strain normal to crack plane .
g	Gravity constant .
I_c	Characteristic length .
I_1	First stresses in variant .

J_2	Second deviatoric stresses invariant .

Symbol	Description
[J]	**Jacobian** matrix .
[K]	Total stiffness matrix .
$[K_c]$, $[K_s]$	Concrete and steel stiffness matrices respectively .
k	Hardening parameter .
[M]	Mass matrices .
N_i	Shape function .
n	Number of nodes per element .
{R}	Vector of internal resisting forces .
t_{sx}	Steel equivalent layer thickness .
t	Total element thickness .
t_f	Time energy density at the strength limitb.
{U}	Vectors of nodal displacement .
$\{\dot{U}\}\{\ddot{U}\}$	Vectors of nodal velocities and acceleration respectively .
U ,V ,W	Displacement components in x , y and z – direction respectively .
u_i , v_i , w_i	Nodal displacement .
v	Element volume .
w	Crack width .
X , Y , Z	Global or cartisian coordinates .
x_i , y_i , z_i	Global coordinates of ith node .

ii - Greek Symbols

Symbol	Description
α_c	Yield surface function .
α	Softening parameter .
β	Reducing factor .
β_o , β_1	Failure surface function .
β , δ	Parameters of **Newmark** method .
ε_e^{eff}	Uniaxial elastic strain .
$\dot{\varepsilon}_e^{eff}$	Uniaxial elastic strain .
ε_{cr}	Cracking strain .
ε_c	Fictitious crack strain .
ε_{ref}	Maximum tensile strain reached across the crack .
$\dot{\varepsilon}_c$	Fictitious crack strain rate .
ε	Strain .
$\dot{\varepsilon}$	Strain rate .

ε_s	Strain in steel .

Symbol	Description
ε_e , ε_{vp}	Elasto and alasto – viscoplastic strain .
$\dot{\varepsilon}_e$, $\dot{\varepsilon}_{vp}$	Elasto and alasto – viscoplastic strain rate .
$\varepsilon_.$	Strain at cracking .
$\dot{\varepsilon}_s$	Strain rate in steel .
$\{\varepsilon\}$	Strain vector .
ε_{cu}	Ultimate concrete strain .
γ	Fluidity parameter .
$\gamma_\cdot$, $\gamma_.$	Damping ratio .
φ	Angle of friction .
$\dot{\Pi}_s$	Rate of energy dissipation in the crack .
$\dot{\Pi}_v$	Rate of energy dissipation in the valume .
ρ_s , ρ_c	Mass density for steel and concrete respectively .
ρ_x	Reinforcement ratio in the direction of local element x – axis .
σ	Stresses .
$\{\sigma\}$	Stresses vector .
$\{\dot{\sigma}\}$	Stresses rate vector .
σ_{ref}	Corresponding stresses .
σ_s	Current stresses level in steel .
σ_o	Yield stresses .
σ_f	Failure stresses .
υ	Poisson's ratio .
ω_p	Viscoplastic energy density .
$\omega_p{}^f$,	Viscoplastic energy density at the strength limit .
ξ , η , τ	Natural coordinate system .
$\{\psi\}$	Vector of residual forces .
$\{\psi^i_t\}$	Vector of residual forces for ith iteration of time step .

We certify that this theses titled (**Nonlinear Dynamic Analysis of Reinforced concrete Arch Structures By Finite Element Method**) was prepared by **Rana Falah Yousif Al – Dahash** under our supervision at University of Babylon in partial fulfillment of the requirement for the degree of **Master of Science in Civil Engineering (Structural Engineering) .**

Signature :	Signature :
Name:**Asst. Prof. Mr. Abdul – Ridah S. Hadi**	Name:**Asst. Prof. Dr. Ammar Y. Ali**
(Supervisor)	(Supervisor)
Date: / /٢٠٠	Date: / /٢٠٠

CHAPTER TWO
REVIEW OF LITERATURE

٢.١ General

With the advent of modern computers and sophisticated analytical techniques of concrete structures , an intense research effort has been used recently to model the concrete under short – time loading for one , two or three – dimensional stresses states . The objective of this chapter is to give a brief review of the previous studies on the application of dynamic analysis of reinforced concrete arch structures . In this chapter , a review to the available methods for analysis of reinforced concrete arches .

٢.٢ Static Analysis for Curved Beam by Finite Element

Curved members finite element developed by many studies based on exact strain energy or natural shape functions , others are based on assumed displacement fields . In some study the strain element is based on independent strain components rather than displacement .

Martine (١٩٦٦) [٦٢] derived exact two dimensional stiffness matrix for curved beam in which axial stiffness and shear stiffness are neglected . The strain energy expression used is :

$$U= R/\text{٢}EI_Z \int_{\text{٠}}^{\beta} M^{\text{٢}}_Z \; d\Phi \qquad (\text{٢.١})$$

where ; M_Z : the moment about z – axis

R : radius of curvature of centroidal

$\mathcal{B}$: is the subtended angle by the element

Φ : is the polar angle

Morris (١٩٦٨) [٦٣] included the effect of the axial deformation in the strain energy expression and derived a three dimensional exact stiffness matrix for curved beam :

$$U=R/2EI_Z \int_{\mathcal{B}} M'^2_Z \, d\Phi + R/2EA \int_{\mathcal{B}} F'^2_Z \, d\Phi + R/2EI_n \int_{\mathcal{B}} M'^2_n \, d\Phi + R/2GJ \int M'^2_S \, d\Phi \quad (٢.٢)$$

where ; F_Z = the force in z – axis

A = cross section area

M_S = the moment about alongitudal axis

Dabrowski (١٩٦٨) [٣٢] examined the behavior of thin – walled beam for non deformable cross – section for different loading and boundary conditions . The effects of secondary shear deformation on closed box sections was considered and so was the effect of curvature on the overall static behavior . The effects of curvature on the transverse distribution of stresses was not considered .

Ashwell (١٩٧١) [٨] gave models based both on independently - interpolated displacement components of up to cubic order and strain distributed were considered . The degree of the interpolation polynomial is increased to represent rigid body modes implicitly with an acceptable accuracy there are used in the analysis of two dimensional element .

Dawe (١٩٧٤) [٣١] used a curved beam finite element for analyzing shallow and deep arches in which he considered high order models mainly . He used many types of strain displacement equation and high order independent polynomial function is the strain element , which is based on a constant axial strain and a linear axial bending strain

Evans and **AL-Rifaie** (١٩٧٥) [٣٦] success fully employed both sand and araldite and steel box girder models to establish the accuracy of the finite element method in analyzing box girders curved in plane . Eighteen models of different curvature were studied . Each under different loading condition to study the elastic behavior of box girders curved in plane .

Yamada and **Ezawa** (١٩٧٧) [٩١] derived natural shape function (i.e. a function which defines the exact deformed shape of the element) by integrating the strain – displacement equations for circular arches and the natural shape function . The two displacement functions are interrelated by terms arising from deformations cannot be represented exactly by polynomial functions .

Chaudhuri (١٩٧٧) [٢٨] and **Yoo** (١٩٨١) [٩٠] took the influence of the warping on the thin – walled section due to torsion when which were obtained the stiffness matrix of the curve element by natural shape function were obtain for thin – walled curved element of open cross section . The torsion that cause the warping influence on the normal stresses distribution .

Meck (١٩٨٠) [٦٤] used circular ring element to discuss an inextensional and extensional deformation and assumed shape function to derive the stiffness matrix for this element . He also derived the stiffness matrix for extensional deformation by using this Equation :

$$D_n = R\varepsilon_\circ - a_2 - 2a_3\Phi - 3a_4\Phi^2 - 4a_5\Phi^3 - 5a_6\Phi^4 \qquad (٢.٣)$$

Where : $R\varepsilon_\circ = dD_S / d\Phi + D_n$

Meck also discussed the curved beam in his studies and he found that when neglecting the coupling between normal and tangential displacements the results obtained from their element were only with in ٠.١٪ error , but for the thick element the error became larger because the strain distribution a cross the thickness is not linear .

Just (١٩٨٢) [٥٢] derived the stiffness matrix for two – dimensional element by integrating the equilibrium equations to get a natural shape function and **Just** considered the axial and flexural action in the derived stiffness matrix for circularly curved beams .

Prathap (١٩٨٢)[٧٢] proposed the concept of (membrane locking) phenomenon to explain the very poor behavior of exactly integrated low order independently interpolated polynomial fields . But **Prathap**[٧٣] explained that (membrane locking) originated from the inability of these simple interpolation polynomial to produce a

membrane strain field that can vanish in a (consistent) way so that only and in-

extensional constraints are enforced in the physical limits of extreme thinness .

Palaninathan (١٩٨٥) [٧٥] derived stiffness for curved beam element matrix of order (١٢*١٢) which was formulated by using castigliano's theorem . It is also included in the program developed in this work .

Antoon (١٩٨٥) [١٠] developed a circular coplanar static of three – dimensional curved element which takes into account the nonlinear distribution of longitudinal strains and stresses over the cross section due to the initial curvature of the element. Exact strain energy expression was established and solved to get the flexibility matrix which is upon inverting , yields the stiffness matrix .

Waldron (١٩٨٥) [٨٧] considered curvature effects in the calculation of the various section parameters and studied the effects of warping restraint in thin – walled fixed – fixed girders .

Prathap (١٩٨٦) [٧٤] derived the stiffness matrix for the thick curved element by using the same procedure of **Prathap** (١٩٨٥) [٧٣] by neglected the shear and membrane locking and used the curvilinear deep shell theory .

Tessler (١٩٨٦) [٨٣] derived stiffness matrix for the curved beam including shear deformation and rotary inertia effects which was derived from Hamilton's variation principle . Different degree polynomials were used to interpolate the kinematics variables .

Akhtar (١٩٨٧) [١١] used strain energy in derivation stiffness matrix for curved beam element which have uniform cross section and assumed that the radius of curvature is so greater than the beam depth so that the effect of shear deformations was neglected . He also obtained a fixed end action due to concentrated load at any point of the member , making any angle with the radial direction at this point .

Abdul-Hameed (١٩٩٢) [١٢] presented a theoretical analysis of the plastic behavior of non-prismatic hinged-hinged arches for the purpose of determining their plastic hinge locations as well as evaluating the collapse loads . Two analytical methods were adopted , namely , the limit analysis and the finite element method .

Shanmugam (١٩٩٥) [٨١] determined the ultimate load – carrying capacity of steel I-beam with intermediate lateral restrained and examined the effects of curvature on the behavior of these beams under bending loads . A finite – element analysis was used to analyze the behavior of curved I – beam with intermediate lateral restrain . The triangular element is a three – noded flat facet shell , which does not includ shear deformation .

AL-Naimi,H.A. (١٩٩٦) [٣] studied stresses analyses of the three dimensional reinforced concrete structures subjected to static or dynamic loadings . Nonlinear material and time dependent effects are included in the analysis . This research is concerned with creep and shrinkage as a time dependent behavior of concrete . The material nonlinearities as a results of tension cracking , strain softening after cracking , the nonlinear response of concrete in compression , crushing of concrete and the yielding of the reinforcement are considered .

Litewka and **Rakoski** (١٩٩٨) [٥٧] analyzed the plane curved beam element with six degree of freedom in which the effect of flexural , axial and shear deformation were taken into account . They assumed the constant curvature for curved beam element and used the strain energy formula , the stiffness matrix for shear – flexible and compressible arch element was formulated .

AL- Daami,H.H.M. (٢٠٠٠) [١٣] developed a space curved beam element and used the exact strain energy expression . In the normal strain , the influence of the axial force , bending moment , bimoment , direct shear forces and torsion moment are included . This research includes warping deformations for that the stiffness matrix can be used for thin – walled section . Besides its application to solid of revolution , the semi – analytical method can be applied to prismatic solids .

٢.٣ Dynamic Analysis for Curved Beams

Many structure are subjected to time – varying loads such as impulse blast , impact or earthquake loading .

Duham (١٩٦٧) [٣٣] and **Ghosh** (١٩٦٩) [٣٨] derived the stiffness matrix , mass matrix and load vector from strain energy , kinetic energy and work expression by using **Hamilton's** variation principle . They solved the stiffness and mass matrices by used numerical integration .

Veletsos (١٩٧٢) [٨٤] used **Rayleih** technique with curved beam theory and shallow shell theory when he found that the natural frequencies for thin arch applications and neglected the effect of shear and rotary inertia . But **Austin** (١٩٧٣) [١٦] developed the work of **Veletsos** by including the shear deformation and rotary inertia ; correction factors were introduced to the previous approximate formulas for this purpose .

Tene (١٩٧٥) [٨٢] used a general analytical and numerical procedure based on the linear theory for the elastic stresses and deflection analysis of arbitrary plane curved beam subjected to arbitrary static and dynamic loads . The equation admits shear deformation and rotary inertia . The numerical solution is obtained by Houbolt's method and by finite differences .

Noor (١٩٧٩) [٦٨] used the explicit central difference method in addition to Newmark's average acceleration and Park's stiffly stable method to study the nonlinear dynamic analysis of curved beam .

Owne (١٩٨٠) [٦٩] presented a program for nonlinear dynamic stresses analysis with implicit , explicit solution or combined implicit/explicit solution . Two dimensional plane stresses plane strain and axisymmetric formulations using ٤,٨, and ٩ noded isoparametric quadrilaterals were presented .

Henrych (١٩٨٠) [٤٨] derived lengthy deformation equation by using elementary theory of elasticity when he studied the in plane dynamic behavior of elastic arches .The effects of shear deformation , rotary inertia and damping were

also considered . Account was taken for the effects due to changes in the radius of curvature , cross sectional area , relative weight moment of inertia , relative mass moment of inertia . Numerical solution was presented for simplified cases in which some of the previous variables were ignored .

AL-Maroof (١٩٨٧) [٦] studied the dynamic behavior of curved members based on the linear theory by the finite element method . He solved many free and forced vibration examples . . He concentrated with reconstructing an existing element to include warping restraint effects .. Effects of shear deformation and rotary inertia on the natural frequencies are studied and compared with the results of recent theoretical studies . A wide range of dynamic analyses are performed .

This includes earthquake effects , moving loads , blast pressure , impact loads and response spectrum analysis .

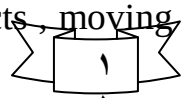

Darzy (١٩٨٨) [٣٥] developed a software based on a relatively simple and accurate method , that is the finite prism method and to develop this software for the analysis of three dimensional bridge structures , with a view to overcome the complexities or limitation of the conventional methods used for the static and dynamic analysis of medium/short span simply supported reinforced concrete bridges . In this method the three dimensional problem is reduced to a series of two dimensional one due to the decoupling properties of the chosen Fourier series terms .

Hinton (١٩٨٨) [٤٤] developed a three dimensional , nonlinear , transient dynamic analysis with special emphasis on various structures . Two types of structural materials were considered ; steel and reinforcement concrete . For steel structures , a classical elasto – viscoplastic constitutive model was adopted . A related model was used for concrete structures but allowance was made for the rate dependency and damage accumulation in the concrete .

Gutierrez (١٩٨٩) [٣٩] studied the determination of the dynamic response , elastic stability configurations and critical buckling load in arch – type structures is of fundamental importance in practically all fields of engineering . They studied the dynamic behavior of arch – type structures of variable cross section and it solved by using polynomial coordinate functions and the Ritz method to generate the frequency equation .

AL-Da'ami (١٩٩٢) [٧] studied the transient and the dynamic response of non prismatic straight members and prismatic and non prismatic arches are being investigated by modeling an axial and flexural wave transmission a long such structures using the method of characteristics . The effect of coupling between axial and flexural waves due to the unsymmetrical variation of the cross sectional area about the longitudinal axis are considered .

Krauthammer (١٩٩٢) [٥٥] modified an approximate analytical approach and applied it for the study of shallow buried reinforced concrete arches under severe dynamic loads . The approach contains a closed form solution for wave propagation of soil , transfer functions for simulation of soil – structure interaction , and a layered beam finite element for representing the structure . Several modifications were incorporated in the original approach , for improving the applied loads and for insuring cross sectional equilibrium in the analysis

Sabir (١٩٩٤) [٧٩] studied the free – vibration natural frequencies of circular arches subtending a considerable range of central angles and having a wide range of ratio of radius of curvature to radius of gyration (R/r) are obtained . Arches that are fixed at both ends , hinged at both ends and one end fixed whilst the others pinned are analyzed . A strain – based curved beam element , using Timoshenko's deep – beam formulation in a system of curvilinear coordinates is obtained and employed in the analysis .

Hsiao (١٩٩٥) [٤٩] presented a co-rotational finite element formulation for the dynamic analysis of a polar curved Euler beam . An Incremental – iterative method based on the **Newmark** direct integration method and the **Newton** – **Raphson** method is employed here for the solution of the nonlinear dynamic equilibrium equations . Numerical examples are presented to determined the effectiveness of the proposed element and to investigate the effect of the initial curvature on the dynamic response of the curved beam structures .

Lee (١٩٩٦) [٦٠] presented the behavior of elasto – plastic planar arches subjected to dynamic load . The governing equations are formulated through the dynamic equations and compatibility conditions . The latter is established by applying the generalized conjugate segment analogy . Bending moments at the nodes and axial forces in the members are considered as primary variables in the elastic regime . They are supplemented by the rotations at the nodes and dislocations in the elements when plastic hinges occure . **Newmark - β** method is adopted in the time marching process .

Ali (١٩٩٩) [٤] presented a theoretical analysis for estimating the in plane large displacement elastic stability behavior of structures with prismatic or tapered

members subjected to static and dynamic loading . In the static analysis , the load – deflection path is traced by using the modified arc – length method . This method allows for the analysis to be continued beyond the limit point and handles snap – back . The formulation of the tangent stiffness local and global coordinates of tapered beam column , which takes into account the geometrical nonlinearity has

Park (١٩٩٩) [٧٦] investigated a bout the dynamic characteristic of a rotating curved beam . The equations of motion include all dynamic effects such as **Coriolis** force , centrifugal force and acceleration . The natural frequencies for curved beams of various radii of curvature are then calculated as the rotating speed increases . The effects of tip mass on the dynamic response of the beam are also studied .

The dynamic behavior of a shallow arch subjected to periodic excitation with internal resonance is explored in detail by **Dai** (٢٠٠٠) [٣٤] . The parametric plane is then divided into different types of regions by the transition boundaries according to the types of the steady state solutions . A time – integration scheme is used to find the numerical solutions in these regions , which agree with the analytical results .

Liu (٢٠٠١) [٥٨] investigated in – plane free vibrations of circular arches using the generalized differential quadrature rule proposed recently . The **Kirchhoff** assumptions for thin beams are considered , the natural axis is taken as inextensible . Several examples of arches with uniform , continuously varying , and stepped cross sections are presented to illustrate the validity and accuracy of the rule .

Xu (٢٠٠٢) [٨٩] studied a shallow arch with elastic supports subjected to impulsive load and he used as a theoretical model to investigate the dynamic stability problem of inner windings of power transformer under short – circuit condition . First the series solution representing the corresponding nonlinear integration – differential equation . Secondly , the equivalent relation n\between short – circuit load and impulsive one , and the electrical forces transferred pattern between the coils of inner windings are assumed .

Huang (٢٠٠٣) [٥٠] derived the first known equations governing vibrations of preloaded , shear – deformable circular arches are derived according to a variation principle for dynamic problems concerning an elastic body under equilibrium initial stresses. Convergence to accurate results is obtained by increasing the number of elements or by increasing both the number of terms in the series solution and the number of terms in the **Taylor** expansion of the variable coefficients . They

clarify the effects of the opening angle and thickness - to – radius ratio on vibration frequencies and buckling loads .

Wu (٢٠٠٤) [٨٨] investigated the radial (in plane) bending – vibration responses of a uniform circular arch under the action of a moving load by means of the arch (curved beam) elements . Then the dynamic responses of a typical segmental circular arch , with constant curvature , due to a concentrated load moving along the circumferential direction were discussed .

Chen (٢٠٠٥) [٢٩] discussed the (١/٢) sub harmonic bifurcation and universal unfolding problems for an arch structure with parametric and forced excitation in their research . The amplitude frequency curved and some dynamical behavior have been shown for this class of problems by Liu et al. . He studied singularity theory

in the case of strict (١:٢) internal resonance , the bifurcation behavior of the amplitude with respect to a parameter (which is related to the amplitude of the live load imposed on the arch structures) .

Zong (٢٠٠٥) [٩٢] presented the analytical and experimental dynamic analysis of a concrete – filled steel tubular half – through arch bridge . A three – dimensional finite element model is developed and an analytical modal analysis is carried out to obtain natural frequencies and mode shapes . The initial finite element model is then corrected with the help of measured natural frequencies and mode shapes by varying some influential parameters of the bridge making use of engineering intuition

Lee (٢٠٠٦) [٥٩] studied of the antisymmetric response to the symmetric sinusoidal excitation of a clamped – clamped curved beam. The autoparametric responses of the antisymmetric modes are obtained from a two – mode equation with nonlinear coupling which is solved using the Rung – Kutta numerical integration method . The measurement of the antisymmetric modes was separated from the measurement of the symmetric mode by the special configuration of the strain gauge sensor systems .

The present study concerned with stresses analyses of three dimensional reinforced concrete arch structures subjected to dynamic loadings . Nonlinear material are included in the analysis . Material nonlinearities as a result of tension cracking , strain softening after cracking . The nonlinear response of concrete in compression , crushing of concrete and yield of the reinforcement are considered. The eight and twenty nodded hexahedral isoparameteric element are used for the

spatial discretization . In the idealization of the reinforced concrete structures , the steel reinforcement is incorporated in the concrete brick element by assuming perfect bond . Concrete is considered as a linear elastic strain softening material in tension and as an elasto – viscoplastic material in compression . The steel reinforcement is assumed to have uniaxial properties in the direction of bars . A classical elasto – viscoplastic model is used in the present study to model the reinforcement .

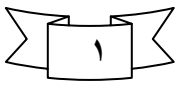

CHAPTER ONE

INTRODUCTION

١.١ General

In the past , the arch represents one of the few structure systems which make it possible to cover large spans . The earliest inhabitants developed the arch as an important element of their architectural objects as expressed by old bridges , aqueducts and large public buildings .

Today , the same importance is presented especially in construction of bridges and arched structures which are constructed in different shapes and from various materials such as brick , steel , reinforced concrete , Ferro cement and timber. The main aim of the arch is to enhance the load carrying capacity more than straight beam . This may be attributed to the stiffening behavior of the membrane action which leads to reduce the bending moment , shear forces and axial force. Arching , not only reduces the bending moments in the arch in comparison with a straight member of same properties and loading patterns , but even more the shear forces [٨٥] . On the other hand , an axial force is introduced due to the arch action . This state of action is compatible with the concrete material , which is relatively weak in carrying tension and shear stresses but adequate in carrying compressive stresses . The reinforced concrete is a composite material made up of concrete and steel and it is efficient in the construction of some arched structures such as gable frames and arched bridges .

Although prismatic shaped members are usually the most widely used members in engineering construction , but the economy in material and architectural necessities make the use of non prismatic members designed to resist a given applied load can be considerably lighter than a prismatic members designed

to resist the same load ; so because the material in the former is well distributed and the load can be resisted in a more efficient manner [٧٨] , these reasons have led to the continuity of using non prismatic arches as one of such structures .

١.٢ Applications of Arch Structure

a - Arch roofs : the search for structures which cover long spans and large areas without intermediate support , and which do so using a minimum of material , has long occupied the structural engineering profession . If a flat plane surface is not necessary to meet the functional requirements of a structure , then singly or doubly curved members such as arches and thin shells offer important advantages, see Figure (١-١) .

b - Arch dam : is a solid concrete dam , curved upstream in plane , which transmits a major part of the imposed load to the canyon walls by thrust . The shape of most arch dams in plane is circular, but some have been designed and constructed with elliptic , parabolic, multi centered and other complex shapes . In cross section arch dams may have vertical , inclined or curved upstream and/or downstream faces, as shown in Figure (١-٢) , (١-٣) and (١-٤) .

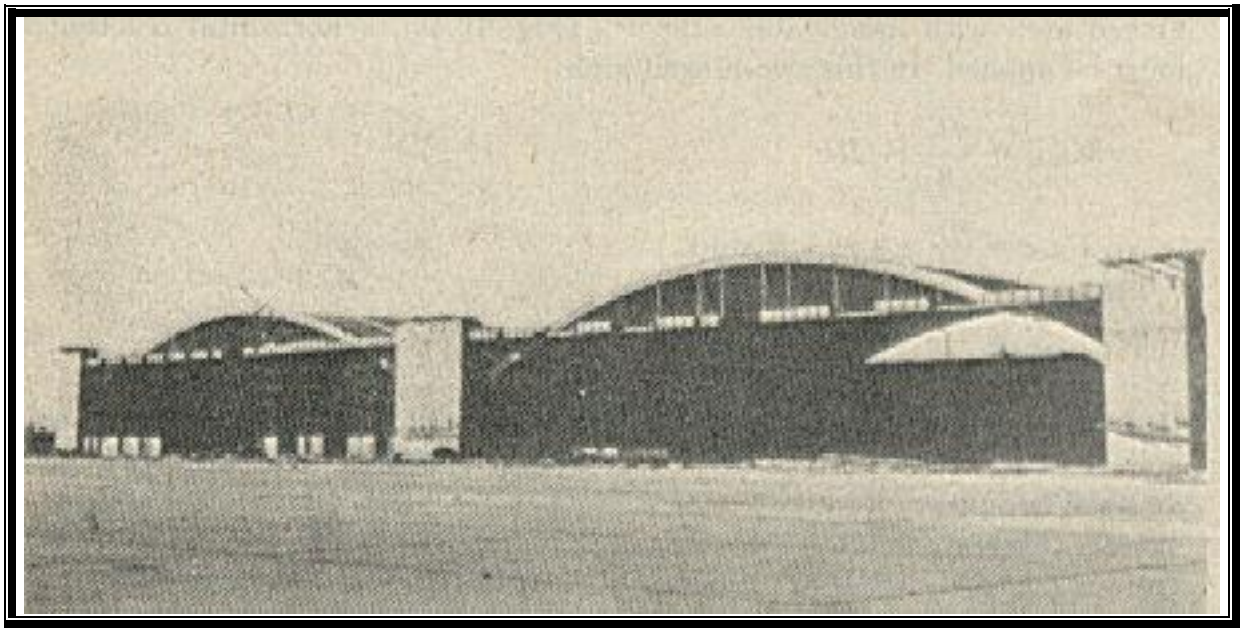

Figure (١-١) Fixed Arches Roofs [٨٥]

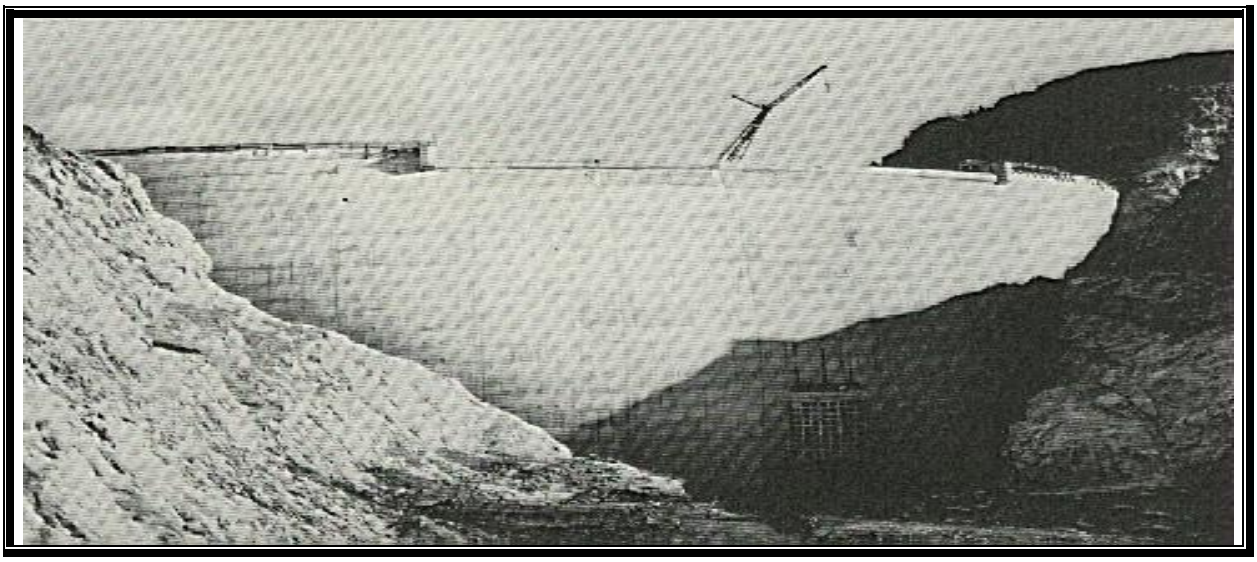

Figure (١-٢) Arch Dam [٨٦]

١.٣ Method of Analysis

Nonlinear dynamic analysis of arch structure is too complex to be analyzed by classical methods (finite difference , straight beam element , curved beam element , ….) and hence numerical methods should be adopted among these methods . Recently the finite element method receives much attention nowadays because of it's effectiveness and versatility . In this method , the structure is divided into small but finite elements . The primary advantage of the finite element method it is generality and can be utilized to solve linear or nonlinear problems , homogenous and continuum , and two or three dimensional structures and for different loading point or surface load static or dynamic . All reinforced concrete structures such as reactor buildings , domes , multistory buildings and bridges are three dimensional bodies but usually modeled as several two dimensional smaller problems to descriptive their spatial configuration and hence simplify their analyses . Generally , the analysis of such structures as a fully three dimensional has been made possible largely by the development of the modern digital computer .

١.٤ Reinforced Concrete Nonlinearity

Reinforced concrete structures exhibit two different forms of nonlinearity ; geometrical nonlinearity and material nonlinearity . Geometrical nonlinearity results from the nonlinear strain – displacement relation and form the finite changes in geometry of the members . Hence , geometrical nonlinearity becomes a significant factor when the level of loading is sufficient to cause large displacements . This is true in the case of slender structures such as ; long columns , towers , flexible arches and some thin shells . Material nonlinearity results from many factors among them are ; nonlinear stress – strain relation of the material , tensile cracking and time dependent deformation . The stress – strain relation is the important factor among them . Several idealized curves with different degrees of accuracy have been developed to represent this relation . However , concrete has a complex behavior and an exact constitutive relation not yet found [٢١]. Material nonlinearity occurs in all reinforced concrete structure and it may play the major role in controlling the behavior during loading . If a realistic nonlinear analysis of a concrete structure can be carried out , the safety is increased and the cost can frequently be reduced [٢٠,٢١] .

١.٥ Objective and Scope

This study is concerned with three dimensional , nonlinear transient dynamic analysis of arch structures . The reinforced concrete is used as a structural material . Eight – and twenty – noded , hexahedral , isoparametric finite elements are used for the spatial discrimination. In the idealization of the reinforced concrete structures , the steel reinforcement is incorporated in the concrete brick element by assuming perfect bond .

Due to the complexity of these structures and the nature of the materials involved , there is a need to employ highly sophisticated numerical analysis procedure , such as the finite element method to ensure safety and economy of such structures . Dynamic and stability predictions for arch – type structures are of great practical importance in practically all fields of engineering . In spite of the fact that many excellent studies the plane vibrations of arches there is a very limited number of studies available in the open literature on the dynamic behavior of arch – type structure of variable cross – section .

For the dynamic analysis , the direct integration method with unconditionally stable implicit scheme , namely **Newmark's** method , is adopted to solve the equations of motion . In this work , the program from **Hinton** [٤٤] Is considered to solved the examples .

An investigation to the effects of the damping ratio , degree of curvature , boundary condition , thickness of main reinforcement layers and effects the initial displacement on the behavior of reinforced concrete arch structures and also the non – prismatic clamped circular arch was solved with two cases .

١.٦ Thesis Layout

This thesis consists of six chapters :**Chapter One** introduces and explains briefly the problem in hand , the aim of the study and the subjects included in other chapters .**Chapter Two** is devoted to the review of literature . Outlines of some previous research works on arch structures are presented . **Chapter Three** material modeling concerning an elasto – viscoplastic model used for concrete in compression is described . A smeared crack model that is used to model the concrete in tension , strain – softening rule is also described . An elastic – linear model used to simulate the reinforcement is also given . **Chapter Four** contains a finite element method and the formulation of the governing equilibrium equations . The adopted quadratic brick element , the steel representation and integration rules used in evaluating the element stiffness matrix are also described . Load , mass and damping matrices and dynamic equilibrium equations are formulated in this chapter . The incremental – iterative **Newmark's** method and the nonlinear solution techniques used for solving the set of nonlinear equations are also presented . The outline of the computer program is also presented in this chapter . **Chapter Five** several numerical examples are presented and verified in the previous analytical studies . **Chapter Six** gives the conclusions and recommendations .

CHAPTER THREE

MODELING OF MATERIAL PROPERTIES

٣.١ General

Reinforce concrete is a composite material made up of concrete and steel . For steel structures , a classical elasto / viscoplastic constitutive model is adopted . Concrete , however , is aheterogeous and has completely different properties in tension and in compression . A related model is used for concrete structures but allowance is made for rate dependency and damage accumulation in the concrete . Furthermore , tensile cracking is considered using the smeared crack approach and the constant fracture energy release concept , where the strain softening effect is related to the element size to make the response prediction mesh – size dependent . The amount of shear stresses can be transferred across the rough surfaces of cracked concrete . Material nonlinearities of reinforced concrete in compression are described as inelastic response by elastic – plastic relationships .In the idealization of the reinforced concrete structures, the steel reinforcement is incorporated in the concrete brick element by assuming perfect bond [٤٤] .

٣.٢ Concrete Modeling

In present study , the concrete is considered as a linear elastic brittle fracture material in tension and as an elasto – viscoplastic material in compression .

٣.٢.١ Stresses – Strain Relationship

Atypical stresses – strain relationship for concrete subjected to uniaxial compression is shown in Figure (٣.١) .

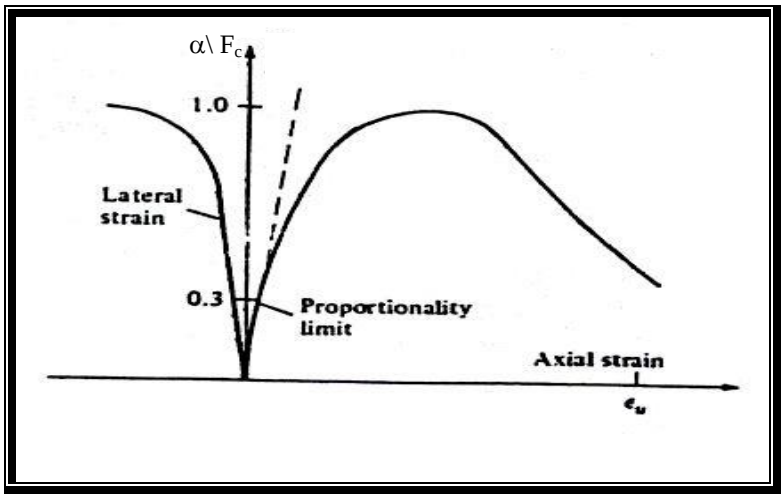

Figure (٣.١) Typical Plot of Compressive and Lateral Strain of Concrete [٢٣] .

The stresses – strain curve has a nearly linear elastic behavior up to about (٣٠) percent of it´s maximum compressive strength F_c for stresses above this point , the curve shows a gradual increase in curvature up to about (٠.٧٥ F_c) to (٠.٩ F_c) , whereupon it bends more sharply and approaches the peak point at F_c . Beyond this peak , the failure occurs at some ultimate strain ε_{cu} [٢٣] .

The curve is nearly linear up to about (٦٠) percent of the uniaxial tensile strength F_t . A reasonable value for the onset of unstable crack propagation will therefore be about (٧٥) percent of F_t [٢٣] . Some uniaxial and biaxial dynamic test results are available . **Hatano** [٤٠] conducted some valuable direct tensile tests on notched cylinders under impulsive loading . **Nelissen** [٦٦] has performed biaxial test under a different rate of straining . Where result for direct tensile testes , **Hatano** [٤١] , direct compressive tests , **Hatano** [٤٢,٤٦] , and low cycle fatigue testes , **Hatano** [٤٠,٤٧] are plotted . For these experimental results , the principal features of the behavior of plain concrete under dynamic loading conditions **Bic′anic′** [١٧,١٨] are now listed :

a - The strength of plain concrete depends on the straining rate .

b - The initial elastic modulus depends on the straining rate .

c - The failure strain remains almost constant for any rate of straining for a particular concrete .

d - Cyclic compressive loading produces a pronounced hysteresis effect in the stresses – strain curve , and

e – For the stresses – strain curves under compressive load histories there is a bounding curve which may be considered identical to the stresses – strain curve under the constant strain – rate test [٤٤] .

A typical uniaxial stresses – strain curve is shown in Figure (٣.٢) .

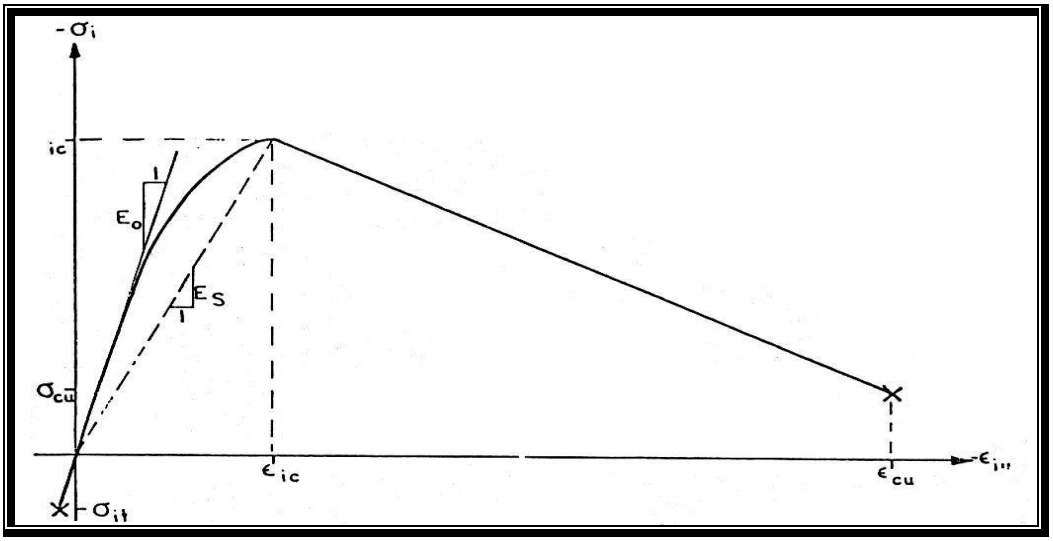

Figure (٣.٢) Equivalent Uniaxial Stresses – Strain Curve of Concrete [٣].

٣.٣ Traditional Elasto / Viscoplastic Model

In the theory of elasto / viscoplasticity , the total strain ε and strain rate $\dot{\varepsilon}$ are decomposed into elastic and viscoplastic parts as :

$$\varepsilon = \varepsilon_e + \varepsilon_{vp} \quad \text{.....} \quad (٣.١a)$$

$$\dot{\varepsilon} = \dot{\varepsilon}_e + \dot{\varepsilon}_{vp} \quad \text{.....} \quad (٣.١b)$$

The stresses rate $\{\dot{\sigma}\}$ is related to the elastic strain rate $\{\dot{\varepsilon}_e\}$ by the elasticity matrix [D]

according to :

$$\{\dot{\sigma}\} = [D] \{\dot{\varepsilon}_e\} \quad \text{.....} \quad (٣.٢)$$

where ($\dot{}$) represents differentiation with respect to time . Viscoplastic flow occurs for positive values of a scaler yield function F. :

$$F.(\sigma) = F(\sigma) - \sigma.(k) \quad \text{.....} \quad (٣.٣)$$

Where $\sigma.$ is a value defining the position of the yield surface , and k is a hardening or softening parameter . For associated elasto / viscoplasticity , the viscoplastic flow rule by **Perzyna** [٧١] has been widely used . The viscoplastic strain rate is given as :

$$\dot{\varepsilon}_{vp} = \gamma \langle \phi (F.) \rangle \partial f / \partial \sigma \quad \text{.....} \quad (٣.٤)$$

in which γ is the fluidity parameter . The expression $\langle \phi (F.) \rangle$ is equal to $\phi (F.)$ for positive value of F. and zero otherwise .
In this work , the flow function is defined to be :

$$\phi (F.) = F./\sigma. = (f(\sigma) - \sigma.) / \sigma. \quad \text{.....} \quad (٣.٥)$$

The term $\partial f / \partial \sigma$ is a vector normal to the potential surface and it defines the direction of the viscoplastic flow [٣] .

٣.٤ Strian Rate Sensitive Elasto/Viscoplastic Model for Concrete

In the present study , there are two main differences when compared with the traditional elasto – viscoplastic model :
a – The fluidity parameter is not constant , and it is assumed to be dependent on the elastic strain rate (or stress rate) .
b – A variable strength limit surface is introduced to monitor the damage caused by viscoplastic flow . If the stresses point reaches the strength limit surface , then the degradation of the yield surface is initiated [٤٤] .

٣.٤.١ Yield and Strength Limit Surfaces

The yield surface F. , defining the onset of viscoplastic behavior , and the strength limit surface F_f , defining the initiation of material degradation will be described in terms of the first and second invariants only . They can be expressed as:

$$F.(\sigma , \sigma_o) = CI_1 + (C^2 I_1^2 + 3\beta J_2)^{1/2} - \sigma_o = 0 \quad \text{(٣.٦a)}$$

$$F_f(\sigma , \sigma_f) = CI_1 + (C^2 I_1^2 + 3\beta J_2)^{1/2} - \sigma_f = 0 \quad \text{(٣.٦b)}$$

Where ; I_1 and J_2 are the first and second stresses invariants . The correlate well with **Kupfer's** test results [٥٣] . During inelastic straining both surfaces F. and

F_f change depending on the viscoplastic energy density ω_p :

$$F.(\sigma , \sigma_o(\omega_p , k)) = 0 \quad \text{(٣.٧a)}$$

$$F_f(\sigma , \sigma_f(\omega_p)) = 0 \quad \text{(٣.٧b)}$$

Where ;

$\sigma_o(\omega_p , k)$ defines the change of the yield stresses level in uniaxial compression σ_o,

$\sigma_f(\omega_p)$ define the change of the failure stresses level in uniaxial compression σ_f ,

ω_p Is the viscoplastic energy density defined as :

$$\omega_p = \int_0^t \sigma^T \dot{\varepsilon}_{vp} \, dt \quad \text{(٣.٨)}$$

k is the viscoplastic work density in the softening rang . It is defined as :

$$k = \omega_p - \omega_p^f = \int_{t_f}^t \sigma^T \dot{\varepsilon}_{vp} \, dt \quad \text{(٣.٩)}$$

and t_f and ω_p^f are the time and viscoplastic energy density when the strength limit

is reached .

While the stresses path remains inside the yield surface , the behavior of concrete is linearly elastic , no viscoplastic straining is developed , the yield and failure surfaces remain stationary . When the stresses path is outside the yield surface , inelastic straining occurs , and the values of σ_f vary . If hardening is considered , σ_o increases with the viscoplastic work and the yield surface expands .

However , σ_f decreases with the increase of damage , and the strength limit surface shrinks . The strength limit surface is only a monitoring device t_o define where and when the failure occurs , when the stresses path reaches the strength limit surface , degradation of the material is initiated . After that , the strength limit surface is no longer considered , and the yield surface begins to shrink according to the post – failure dissipated energy density k . Figure (٣.٣) summarizes the process [٤٤] .

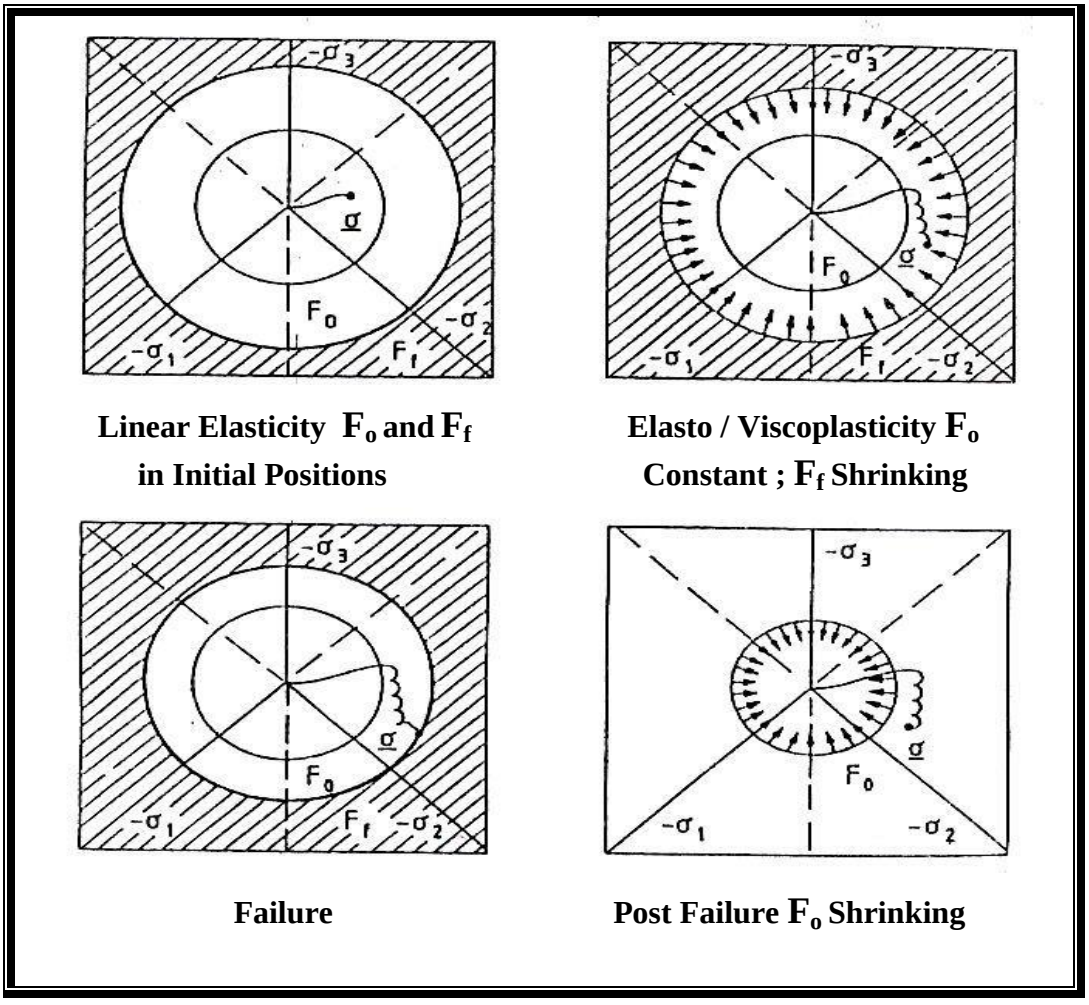

Figure (٣.٣) Evaluation of the Yield and Failure Surfaces [٤٤] .

In this works , no hardening will be considered for concrete and an exponential function will be used to describe the post – failure behavior . Therefore , the function $\sigma_o(\omega_p , k)$ is defined by the expression :

$$\sigma_o(\omega_p , k) = \alpha_1 F_c \qquad \omega_p \le \omega_p^{\,f} \qquad \text{(٣.١٠a)}$$

$$\sigma_o(\omega_p , k) = \alpha_1 F_c \;) \qquad \omega_p > \omega_p^{\,f} \qquad \text{(٣.١٠b)}$$

$$\exp(-\alpha_c$$

In which α_1, defines the limit for elastic behavior (typically = ٠.٣ - ٠.٤) and α_c models the degradation after failure . The parameter F_c is the static compressive strength of concrete . The failure stresses will be assumed to be a linear function of the viscoplastic energy density , and the function can be define by the expression :

$$\sigma_f(\omega_p) = \beta_o F_c (1 - \beta_1 \omega_p) \qquad 0 < \omega_p \le \omega_p^{\,f} \qquad (3.11)$$

The parameters β_o and β_1 are determined from experiments and $\beta_o F_c$ is the compressive strength obtained with infinite load rates and no inelastic strains . Figure (٣.٤) shows the yield and failure stresses vary with the dissipated energy .

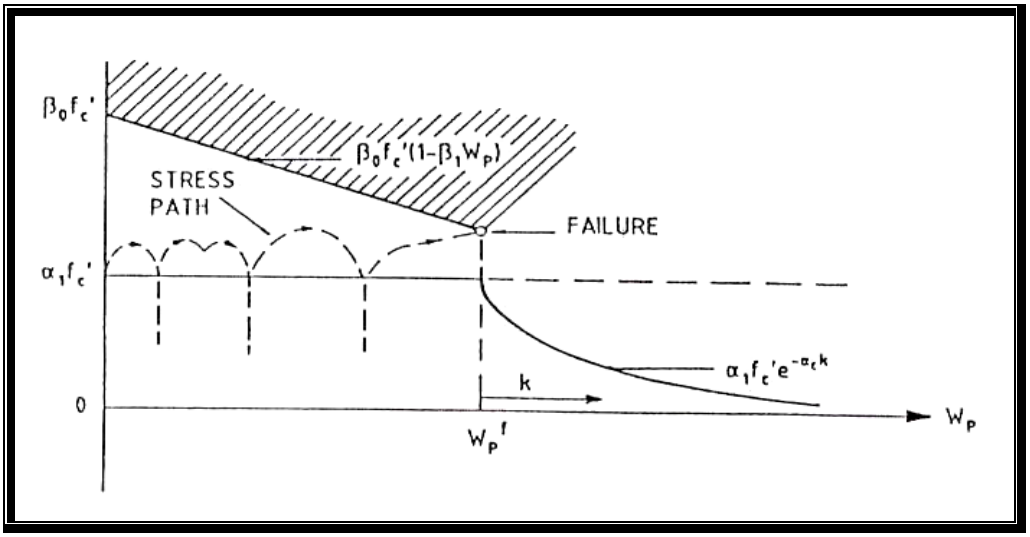

Figure (٣.٤) Variation of the Yield and Failure with the Dissipated Energy Density [٤٤].

٣.٤.٢ Viscoplastic Strain Rate

The rate of viscoplastic straining in equation (٣.٤) is modified to depend on the rate of elastic strain (or loading) and on the position of the yield surface . It is written as :

$$\dot{\varepsilon}_{vp} = \gamma(\dot{\varepsilon}_e) \langle \phi(F.) \rangle n \qquad (٣.١٢)$$

Where ; $n = \partial f / \partial \sigma$

$\phi(F.) = F. / \alpha_١ F_c$

The fluidity parameters is related to the elastic strain rate through an exponential function of an effective elastic strain rate :

$$\gamma(\dot{\varepsilon}_e) = a_o(\dot{\varepsilon}_e^{eff})^{a_١} \qquad (٣.١٣)$$

Where a_o and $a_١$ are parameters which must be determined experimentally . The effective elastic strain is defined as :

$$\varepsilon_e^{eff} = (٣ J'_{٢e} / (١-\upsilon)^٢)^{١/٢} \qquad (٣.١٤)$$

because deviatoric strains cause most damage to concrete and ε_e^{eff} is equal to the uniaxial elastic strain for a uniaxial stress state .

٣.٤.٣ Determination of Model Parameters

In the present study , the model of concrete requires only uniaxial tests to identify the material parameters needed . Parameters F_c , $\alpha_١$ and α_c can be determined from uniaxial static tests . Whereas , parameters β_o , $\beta_١$, a_o and $a_١$ defining σ_f as a function of the viscoplastic energy density and the elastic strain rate respectively , and can be determined from dynamic monotonic direct compression test .

Bic′anic′ [١٧,١٨] describes how these dynamic parameters can be determined from

experimental data . **Hatano** considered three different equalities of concrete mixes (١:٢:٤) , (١:٣:٥) and (١:٤:٧) under several loading conditions . The model parameters identified from **Hatano's** tests are shown in Table (٣.١) .

Table (٣.١) Model Parameters Identified from Hatano's Tests [٤٤] .

Fc (kg/cm^{٢})	a_o	$a_١$	β_o	$\beta_١$
٦٠٥.٠	٠.٤٠٥	٠.٨٣١	١.٩٦٧	٠.٧٩٢
٤٤٤.٠	٠.٣٠٦	٠.٧٦٠	١.٨٣٦	١.٠٨٨
٢٧٥.٠	٠.٤١٣	٠.٧٤٧	٢.٢٩١	٢.٣٦٥

Assuming linear relationship between the failure stresses and the dissipated energy density in Equation (٣.١١) ; it will be considered as a crude approximation for all ranges of straining [٤٤] . When only moderate and fast strain rates are considered , the assumed linear dependency appears to be satisfactory .

٣.٥ Modeling of Cracked concrete

Probably the main feature of plain concrete material behavior is low tensile strength , which results in tensile cracking at a very low stresses compared to the failure stresses in compression . A number of early studies numerically predicted the behavior of reinforced concrete structures in the condition of cracking . In the finite element method , two main mathematical models used for crack representation discrete crack model and smeared crack model .

a – Discrete Crack Model

This model represents the individual cracks as actual discontinuities in the finite element mesh . This model was first used by **Ngo** and **Scordelies** [٦٥] to analyze simply supported reinforced concrete beam . Cracking initiated when failure criterion at a certain node is achieved and crack discontinuity is represented by physically splitter that node . An obvious restriction of such a model is that the cracks must be formed along the element boundaries . This makes crack patterns

dependent on the local mesh refinement . Furthermore , when a crack forms the topology of the mesh varies , and the updating procedures are time – consuming . These difficulties have resulted in a very limited acceptance of this model in general structural applications .

b – Smeared Crack Model

This model does account for real discontinuities in the mesh . It was introduced by Reshid (١٩٦٨) and is adopted in this study . Cracked concrete is assumed to remain a continuum and material properties are modified to account for the damage due to cracking . Concrete is initially isotropic , but cracking induces anisotropy . After cracking , concrete is assumed to become orthotropic , with the principal material axes oriented along the directions of cracking . Material properties are varied depending on the state of strain and stresses . The Young's modulus is reduced in the direction perpendicular to the crack plane , and Poisson's effect is usually neglected due to the lack of continuity of the material . The shear modulus parallel to the crack plane is also reduced . **Lin** and **Scordelies** [٥٦] introduced the retained shear modulus term , where the shear modulus of uncracked concrete and a reducing factor in the range of zero to one .

The smeared approach is used for most structural engineering applications , sine it offers :

١ – Unchanging of topology of the mesh throughout the analysis , and only the stresses – strain relationship need to be updated when cracking occurs .

٢ – Complete generality in possible crack direction .

٣ – Computational efficiency .

A smeared crack model will be adopted in this work to be described such a model requires the following items :

١ – A cracking criterion .

٢ – A strain – softening (or tension – stiffening) rule .

٣.٥.١ Cracking Criterion

The tensile strength of uncracked plain concrete can be obtained from laboratory tests .In the presence of reinforcement , cracking is further complicated . Due to the bond stresses developed between the steel and the surrounding concrete

, the concrete is capable of carrying tension between adjacent primary cracks . Simple criteria are favored by most analysts to predict tensile strain criterion is used for this purpose .

In the present study , concrete in tension is modeled as a linear elastic – strain softening material and the maximum tensile stresses criterion will be employed to distinguish elastic behavior from tensile fracture . For a previously uncracked sampling point , when the principal stresses and their corresponding strain exceed a limiting value , a crack is formed in a plane orthogonal to this stresses . Thereafter , the behavior of the concrete is no longer isotropic , it becomes orthotropic , and the local material axes coincide with the principal stresses directions . It should be noted that the direction of the crack remains fixed (fixed crack approach) . A maximum of two sets of cracks are allowed to form at each sampling point . For simplicity , the crack directions are assumed to be orthogonal . Under further Loading , secondary cracking may occur at a sampling point that was originally cracked in one direction . Three variants are available to determine the direction of the second set of cracks :

a - The principal material axes can be rotated to coincide with the current principal stresses or strain directions , which is known as the rotating crack model . Although this approach is reported to produce results which are in good agreement with experimental results , the model could be physically objectionable since it implies rotation of defects within the material .

b – The material axes are fixed in the directions corresponding to the principal stresses directions when the primary cracks occurred , irrespectively of the possible rotation of the stresses .

c – Keeping the direction of the first set of cracks fixed , a search is performed to determine the maximum stresses in the plane parallel to the existing crack . For this computation only the normal and shear stresses action on that plane are considered. As shown in Figure (٣.٥) , if the maximum stresses exceeds the limiting value , the new set of cracks is formed perpendicular to it , and the local material axes are fixed .

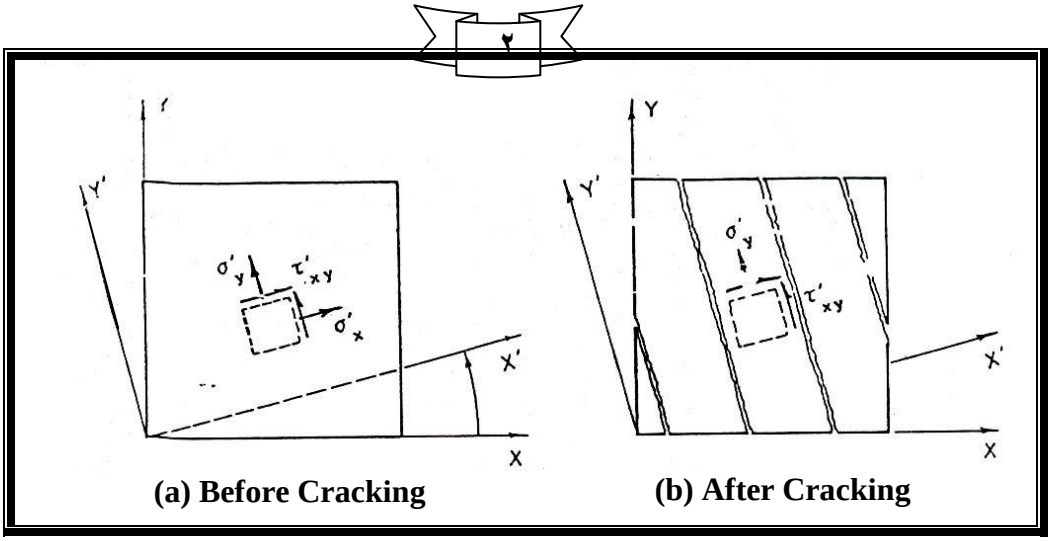

Figure (٣.٥) Smeared Crack Stresses Distribution [٣] .

This is the option that will be used in this study . When the first cracking occurs , it is assumed that only the normal stresses perpendicular to the cracked plane σ'_x is released . After the formulation of the first (primary) crack , the element is regarded capable to sustain further loading . A uniaxial failure criterion is assumed to control further cracking or crushing of concrete by considering only the stresses and strain parallel to the primary crack [٢٣]. When the tensile strain exceeds the cracking strain ε_{cr} at a previously cracked sampling point , an additional set of (secondary) cracks is allowed to form perpendicular to the first set . The current state of stresses at the point just before fracture is assumed to be released completely .

Upon unloading , the crack is assumed to be closed only when the strain across the crack becomes negative . Some probable sequences for concrete to experience through the entire loading history are illustrated in Figure (٣.٦) .

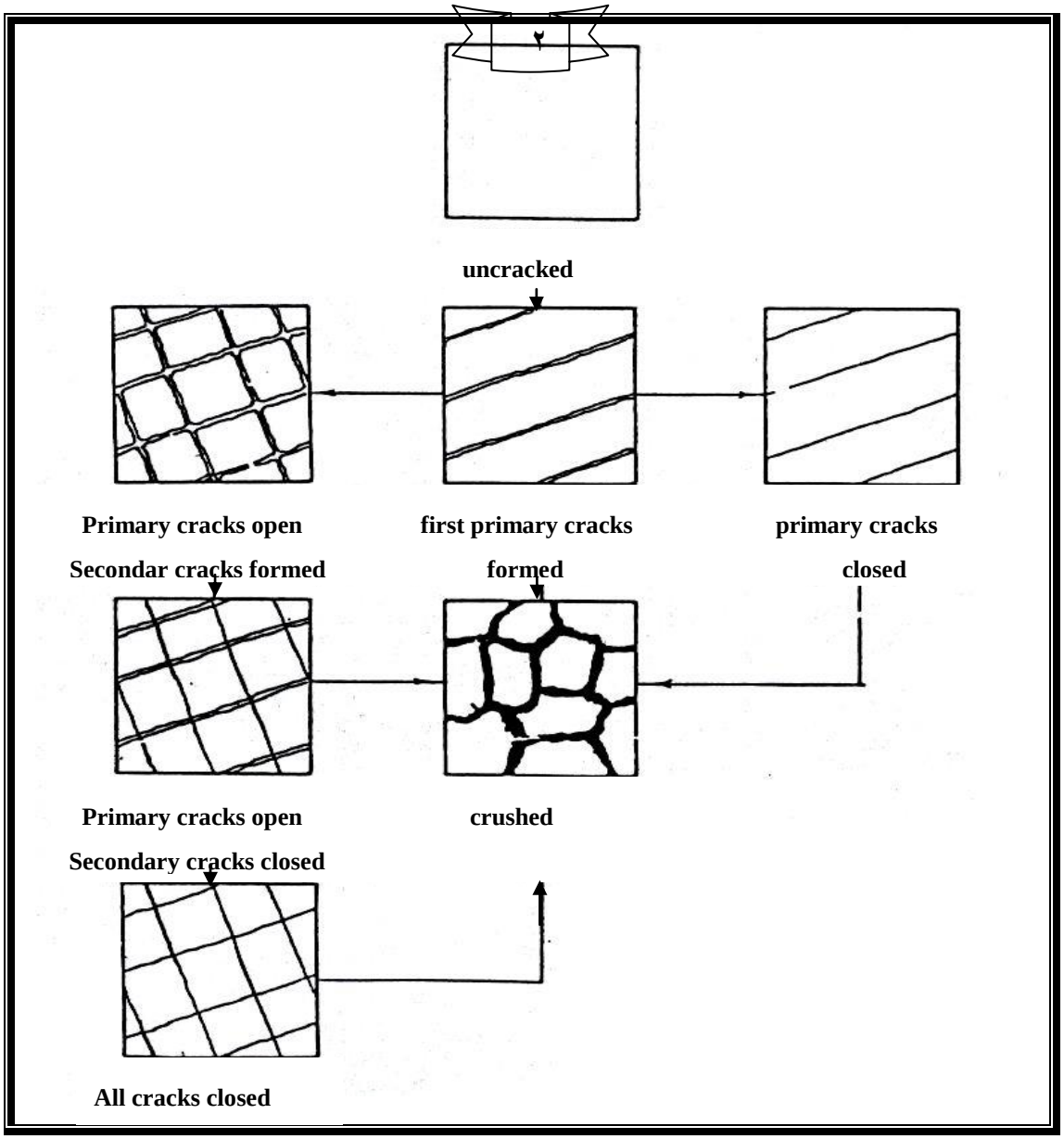

Figure (٣.٦) Possible Crack Formations in Post – Cracking Level [٢٣] .

Crushing of a previously singly cracked element can occur when the transverse compressive strains exceed the ultimate compressive strain of concrete ε_{cu} .

٣.٥.٢ Strain – Softening Rule (Tension Stiffening)

The first studies done on numerical analysis of reinforced concrete structures assumed concrete to be an elastic – brittle material in tension . When cracking

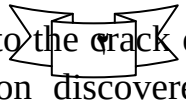

occurred , the stresses normal to the crack direction was immediately released and dropped to zero . It was soon discovered that this procedure leads to great convergence difficulties , and more importantly , to results that strongly depend on the size of the finite elements used in the analysis .

Due to bond forces , cracked concrete carries between the cracks and a certain amount of tensile stresses normal to the cracked plane . The concrete adheres to the overall stiffness of the structure. This effect is known as (tension – stiffening) . It can be incorporate into the computational model in two indirect ways :

a –Assuming that the loss of tensile strength in concrete occurs gradually after cracking [٨٠] .

b – Modifying the steel stresses – strain curve [٣٧] .

The first option assumes unloading in cracked concrete takes place gradually according to a special softening phenomenon . **Scanlon** [٨٠] used a stepped unloading diagram shown in Figure (٣.٧c) , **Lin** and **Scordelis** [٥٦] propose a smooth softening model shown in Figure (٣.٧b) . The concrete is considered as an elastic – strain softening material in tension , and has been extensively used in computational analysis of reinforced concrete structures .

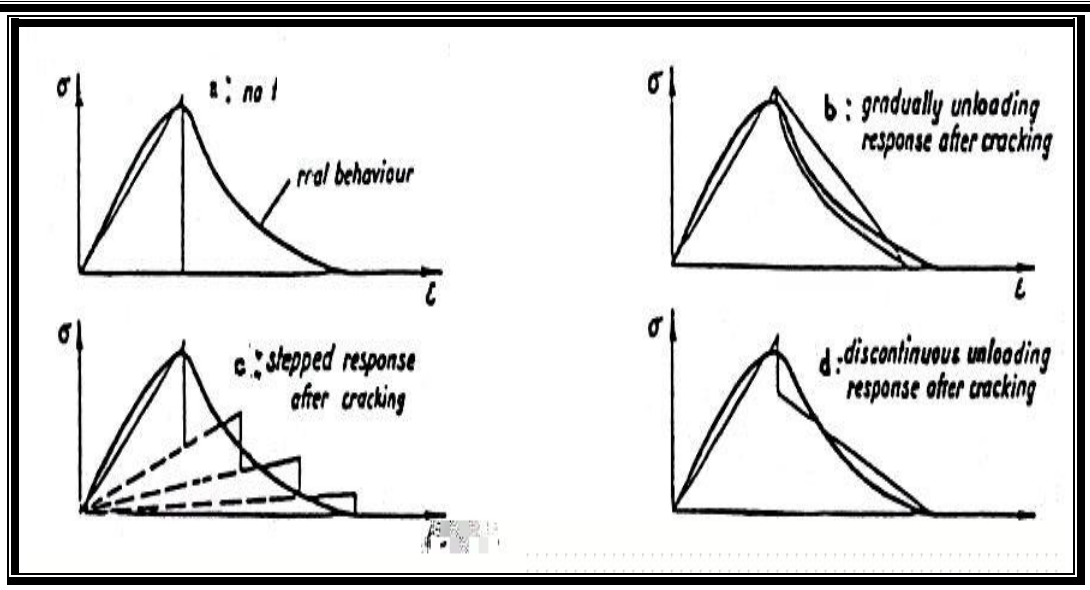

Figure (٣.٧) Some Possible Assumptions for Strain – Softening of Concrete After Cracking [٦١] .

However , two main problems remained unsolved . The first one is that there is no objective way of measuring how much tension – stiffening should be included in the model . It is easy to choose a tension – stiffening curve that will adequately fit experimental results , but is very difficult to make any prior predictions . Secondly , the effect , if explained in terms of bond interactions with the reinforcing steel , cannot be applied to plain concrete structures , or , to concrete located at a certain distance from the reinforcement .

Bazant [١٩] the using of some fracture energy concepts in the material modeling of concrete . The main concept borrowed from fracture mechanics to develop the composite damage models is the assumptions that the fracture energy release rate , (G_f), is a material property , rather than the local stresses – strain curve . In the case of assuming (G_f) is constant , the concept loads to that the local strain softening low depends on a characteristic length (I_c) depending on the finite element mesh .

In defining a curve to model the strain – softening effects , two aspects have to be considered ; the shape of the adopted curve and the value of the parameters needed to define it . In most of the cases , either a simple straight line shape , or a bilinear shape have been used . The assumption used to select the parameters defining such a curve are more important than the shape of the strain – softening curve selected – assuming that the stresses , σ , across on opening crack is a function of the crack

width , w , the fracture is defined as :

$$G_f = \int_{.}^{\infty} \sigma_{(w)}\, dw \qquad \text{(3.15)}$$

G_f represents the energy needed to separate the two crack surfaces . Typical values of the fracture energy for normal concretes are in the range of (٥٠ to ٢٠٠ N/m) . The smeared approach does not represent individual cracks , so the crack width , w , must be smeared into an equivalent by a characteristic length , I_c , Figure (٣.٨) . By assuming that when the crack is formed , all inelastic deformations inside the control volume takes place in the crack , the rate of energy dissipation in the crack is :

$$\Pi^{\cdot}_s = \int \sigma\, w^{\cdot}\, ds \qquad \text{(٣.١٦)}$$

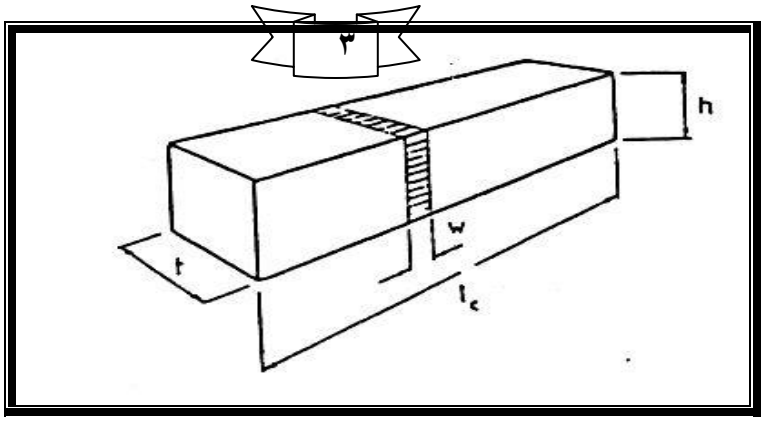

Figure (٣.٨) Illustration of Characteristic Length for A prismatic Control Volume [٤٤] .

By assuming that the control volume is subjected to the same state of stresses as the crack , but strained by the equivalent strain , the rate of energy dissipation in the volume is :

$$\Pi^{\cdot}_v = \int_v \sigma\, \varepsilon^{\cdot}_c\, dv \qquad \text{(٣.١٧)}$$

From Equation (٣.١٦) and (٣.١٧) , the relationship between the crack width and fictitious crack strain is :

$w = (v/s)\ \varepsilon_c = I_c\ \varepsilon_c$ ..... (٣.١٨)

In the present study , an exponential function is used to simulate the strain – softening effect , as shown in Figure (٣.١٠) .

$\sigma = E_O \varepsilon_. [\ \exp(-(\varepsilon - \varepsilon_.) / \alpha)]$ ..... (3.19)

Where E_O : is the elastic Young's modulus ,

$\varepsilon_.$: is the strain at cracking ,

ε : is the normal tensile strain in the crack zone ,

α : is the softening parameter .

The softening parameter , α , is determined by the evaluation of the integral in Equation (٣.١٥) , and by introducing Equation (٣.١٨) , the relation can be :

$(G_f - ١/٢ E.\varepsilon_.^{٢}\ I_c) / E.\varepsilon_.\ I_c > ٠$ ..... (٣.٢٠)

$\alpha =$

In the present work , the characteristic length is computed for each sampling point as :

$I_c = (dv)^{١/٣}$ ..... (٣.٢١)

Where dv is the volume of concrete represented by the sampling point . It should state that this approach for computing the strain – softening is only directly applicable to plain concrete . The classical tension – stiffening effect due to the presence of reinforcement has not been account for. The effect of the reinforcement can be included by assuming a higher fracture energy for reinforced concrete than for plain concrete .

Further loading or redistribution of stresses due to cracking in other sampling points , any force some of the previously – opened cracks to close partially or fully . This behavior is allowed in the present model . If the current strain is smaller than the strain ε_{ref} , the stresses normal to the crack , σ , is :

$\sigma = (\sigma_{ref} / \varepsilon_{ref}) * \varepsilon$ ..... (٣.٢٢)

In which ε_{ref} is the maximum tensile strain reached across the crack , σ_{ref} is

the corresponding stresses , as shown in Figure (٣.٩) . The re – opening of the crack follows the same path until ε_{ref} is exceeded .

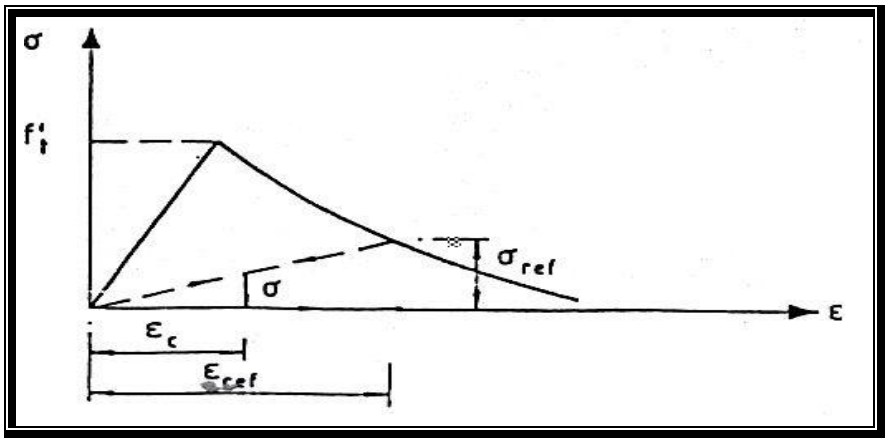

Figure (٣.٩) Strain – Softening Curve with Secant Unloading and Re – Loading [٤٤] .

٣.٥.٣ Shear Transfer Across the Crack

In plain concrete , the main shear transfer mechanism is aggregate interlock and the main variables involved are the aggregate size and grading . In reinforced concrete dowel action will play a significant role , the main variables being the reinforcement ratio , the size of the bars and the angle between crack and bars , the shear transfer capacity being reduced as the crack width increases . The process used to define the reduced shear modulus is :

$$G_c = \beta G_o \qquad (٣.٢٣)$$

G_o is the shear modulus of uncracked concrete and β is a reducing factor in the range of zero to one . In this work , the following value is used[٤٤] :

$$\beta = ١ - (\varepsilon_t / ٠.٠٠٥)^{k_١} \qquad (٣.٢٤)$$

Where ε_t is the fictitious tensile strain normal to the crack plane , and $k_١$ is a parameter in the range of (٠.٣ to ١.٠) .

٣.٦ Modeling of Reinforcing Steel

٣.٦.١ Stresses – Strain Relationship

In contrast to concrete , the mechanical properties of steel reinforcement are well known . The uniaxial stresses – strain relation for steel is idealized as a bilinear curve . This relation is assumed to be identical in tension and compression . During unloading , a linear elastic constitutive relation is assumed . Figure (٣.١٠) represent the static stresses – strain relation of steel .

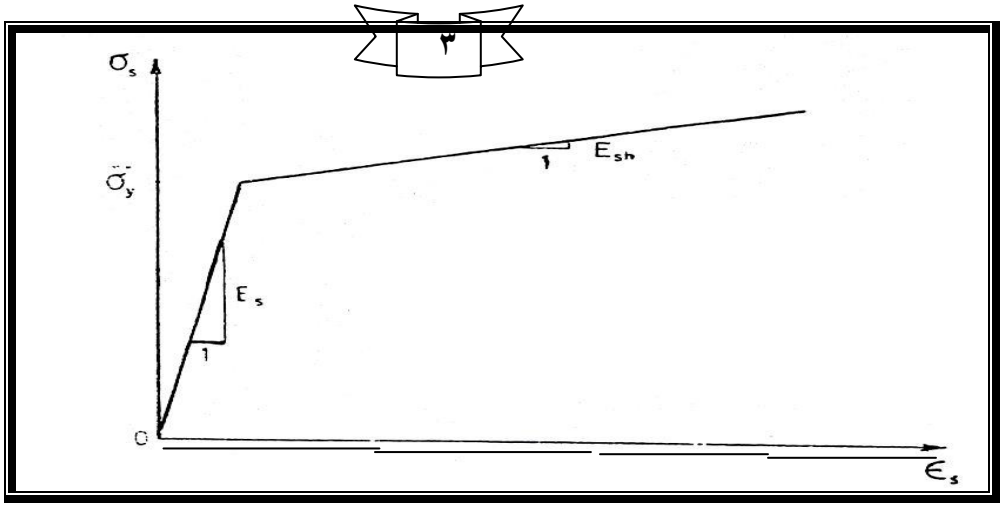

Figure (٣.١٠) Typical Stresses – Strain Curve for Steel [٣] .

From dynamic uniaxial tests , most conclusions can be drawn :

a – The yield stresses and the ultimate stresses of steel increase with the straining rate ,

b – The initial elastic modulus is relatively unaffected by the straining rate ,

c – Ductility is observed to decrease with increasing straining rate , and

d – The rate effects are approximately equal in tension and compression .

Figure (٣.١١) shows some of these features .

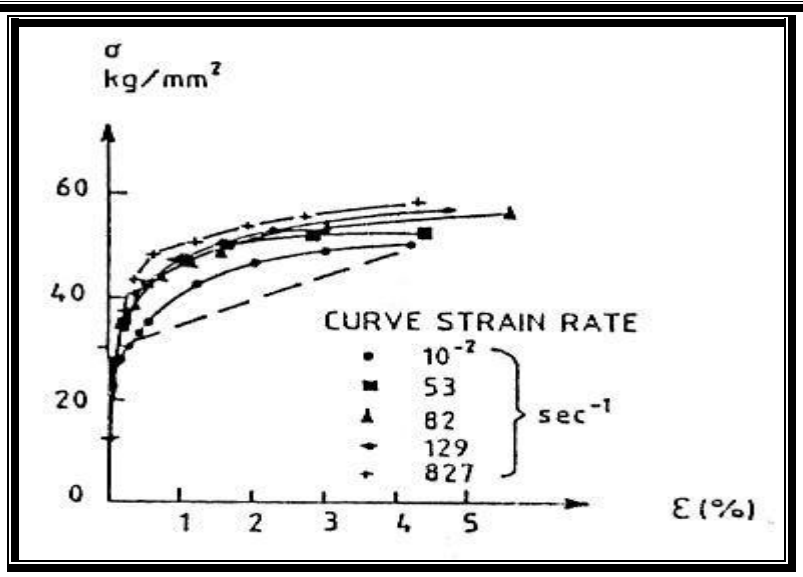

Figure (٣.١١) Dynamic Stresses – Strain Diagram for Steel [٤٤] .

٣.٦.٢ Reinforcement Representation

Concrete and reinforcement are represented with a single element and perfect bond is assumed between the reinforcement and the surrounding concrete .

The stiffness and internal forces associated with the reinforcement are integrated and added to those of the concrete to get the total stiffness and internal forces of the element .Each set of reinforcing bars is smeared as a two – dimensional membrane (layer) of equivalent thickness (and hence equal area) . The layer is placed inside the solid element to coincide with the surface corresponding to (ξ , η , constant) , (ξ , constant , τ) and (constant , η , τ) as appropriate .

The proposed restriction has the advantage of an easy definition of the sampling points used to perform the necessary surface integration over the steel reinforcement membrane . Reinforcing bars are assumed to only resist axial stresses in the bar direction .

A local Cartesian coordinate system must be set up at each integration point in the bar direction . Stresses and the local stiffness matrix for the reinforcement , are first evaluated this local system , and then transformed into the global system [٤٤] .

٣.٦.٣ Reinforcing Steel

Reinforcing steel is assumed to have uniaxial properties in the direction of the bars . A classical elasto – viscoplastic model is used in the program with :

$$\dot{\varepsilon}_{vp} = + \gamma (\dot{\varepsilon}_s) (|\sigma_s| - F_y) / F_y \quad \text{(٣.٢٥)}$$

where ; σ_s is the current stresses level in the steel and F_y is the yield stresses of the material which is assumed to be constant , although strain rate sensitivity may be readily included [٤٤] .

CHAPTER FOUR

NONLINEAR DYNAMIC ANALYSIS BY FINITE ELEMENT METHOD

٤.١ General

This chapter is concerned with three dimensional , nonlinear , transient dynamic analysis with special emphasis on curve beam structures . Eight and twenty – nodded , hexahedral , isoparametric finite elements are used for the spatial diseretisation . The steel reinforcement is incorporated in the concrete brick element by assuming perfect bond .

٤.٢ Finite Element Equilibrium Equations

Numerical method of stresses can be subdivided into two groups , direct numerical solution of the developed differential equations , and matrix methods based on discrete – element idealization . The finite element method belongs to the second **Gategory** . The continuous domain is subdivided into sub – regions known as elements . Stiffness , mass and load matrices are formulated for each element and the results are assembled to form the total system matrices . A variational principle of mechanics , such as the principle of minimum potential energy , is usually employed to obtain the set of equilibrium equations for static analysis . The variational principle for problems in dynamics is **Hamilton's** principle . The functional for this approach is the **Lagrangion** [٩٣] . Weighted residual methods and mainly the **Galerkin** method is used especially for problems

where the functional is difficult or impossible to form . The resulting equations are solved in the time domain using a numerical step – by – step direct integration procedure .

٤.٣ Formulation of ٣ – D Brick Element

The general finite element procedure to fully three – dimensional problems of stresses analysis is rarely used . In many problems the various two dimensional approximations give an adequate and more economical analyses the use of isoparametric elements satisfy the constant strain state , including all the rigid body modes and maintaining (c°) continuity .

٤.٣.١ Concrete Element Modeling

The three dimensional computational model is adopted in the present study . The eight and twenty node hexahedral isoparametric element are used , see Figure (٤.١) .

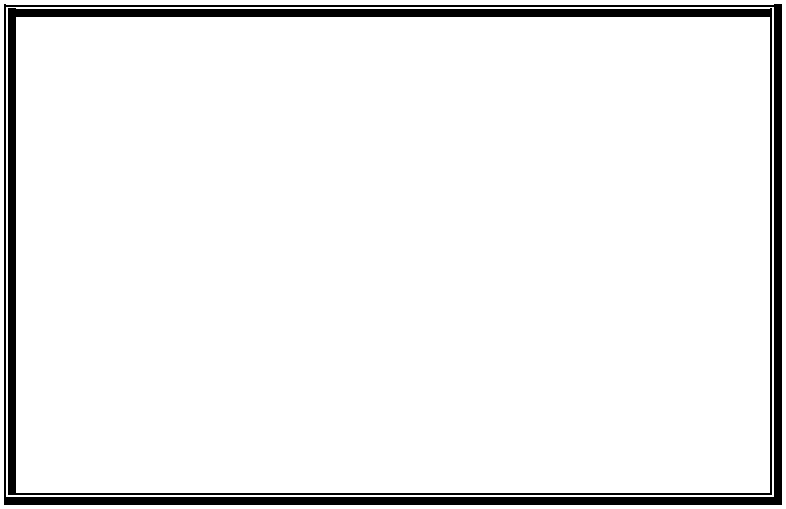

Figure (٤.١) Linear and Quadratic Isoparamatric Solid Element [٣] .

Standard interpolation functions are used in the present formulation . Isoparametric finite element are highly effective in practice , although for linear problems a considerable proportion of the total computational effort is often absorbed in the numerical integration of the stiffness matrix coefficients . It is thus very important to choose suitable integration schemes that are both accurate and computationally efficient [٢٥] .

For nonlinear problems the previous observation is even more critical since evaluation of the stiffness matrix occurs frequently . The integration points are also the sampling points for the stresses and material state determination . These points are used in the evaluation of the internal resisting forces . The use of few hand , the use of more stress sampling points provides more complete information a bout the material state throughout the element . Clearly , a compromise is to be sought .

٤.٣.١.١ Shape Functions

The starting point for stiffness matrix derivation is an element displacement field . In the ٣-D isoparametric finite element formulations , the displacement components are expressed by polynomials in the (x,y,z) plane . the main concept here is to define the displacement field within its boundary in terms of displacement values at the nodes . It is convenient to express the shape functions in terms of the non – dimensional co-ordinate element (ξ , η , τ) which varies from -١ to +١ over the element for standard local co-ordinate , Figure (٤.٢) .

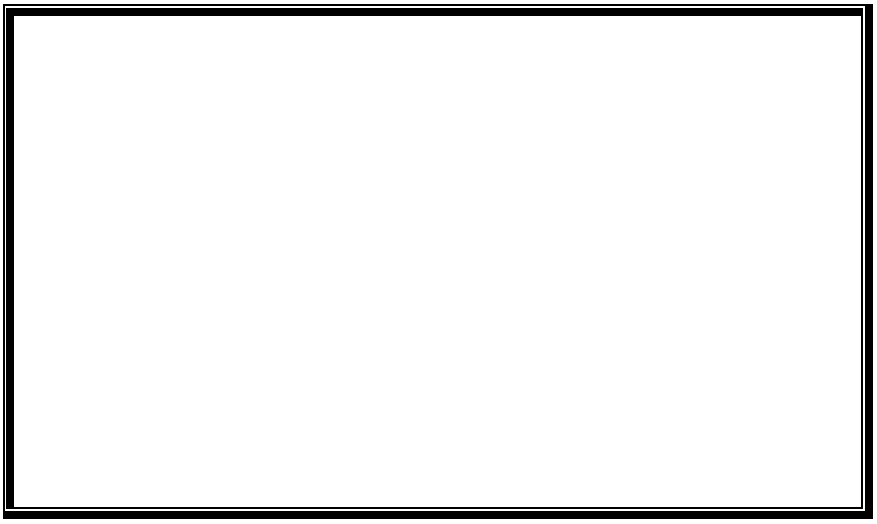

Figure (٤.٢) Non – Dimensional Co – ordinate Element (ξ , η , τ) [١٥] .

Displacement components at a particular point P(ξ , η , τ) are defined using the nodal values at each nodes and the quadratic shape functions such that :

$$U(\xi , \eta , \tau) = \sum^{n} N_i(\xi , \eta , \tau)\, u_i \qquad (٤.١a)$$

$$V(\xi, \eta, \tau) = \sum_{i=1}^{n} N_i(\xi, \eta, \tau)\, v_i \qquad (٤.١b)$$

$$W(\xi, \eta, \tau) = \sum_{i=1}^{n} N_i(\xi, \eta, \tau)\, w_i \qquad (٤.١c)$$

where (n) is a number of nodes per element and $N_i(\xi, \eta, \tau)$ is the shape function at the i-th node and ui ,vi and wi are the corresponding nodal displacements . The shape function of the quadratic eight or twenty node brick element are shown in Table (٤.١) [٤٣] .

Table (٤.١) Shape Functions of the Quadratic ٨ or ٢٠ – node Brick Element (Cook) ١٩٧٤ [٤٣] .

In the isoparametric group of elements , the shape functions are also used to define the geometry of the element . Therefore , the Cartesian coordinate values of any point $P(\xi, \eta, \tau)$ within the element may be defined as :

$$X(\xi, \eta, \tau) = \sum_{i=1}^{n} N_i(\xi, \eta, \tau)\, x_i \qquad (٤.٢a)$$

$$Y(\xi, \eta, \tau) = \sum_{i=1}^{n} N_i(\xi, \eta, \tau)\, y_i \qquad (٤.٢b)$$

$$Z(\xi, \eta, \tau) = \sum_{i=}^{n} N_i(\xi, \eta, \tau)\, z_i \qquad (٤.٢c)$$

where xi , yi and zi are the global coordinate of the node (i) and x,y and z are the coordinates at any point .

٤.٣.١.٢ Stresses and Strain Fields

Since the geometrical nonlinearities are not considered in the present work , displacement gradients remain small throughout the loading process and hence the engineering components of strain can be expressed in terms of the first partial derivatives of the displacement components . Therefore , the linearized strain – displacement relationships may be written as follows [١٥] :

$$\{\varepsilon\} = \begin{Bmatrix} \varepsilon_x \\ \varepsilon_y \\ \varepsilon_z \\ \gamma_{xy} \\ \gamma_{yz} \\ \gamma_{zx} \end{Bmatrix} = \begin{Bmatrix} \partial u/\partial x \\ \partial v/\partial y \\ \partial w/\partial z \\ \partial u/\partial y + \partial v/\partial x \\ \partial v/\partial z + \partial w/\partial y \\ \partial w/\partial x + \partial u/\partial z \end{Bmatrix} = \sum_{i=1}^{n} \begin{bmatrix} \partial Ni/\partial x & 0 & 0 \\ 0 & \partial Ni/\partial y & 0 \\ 0 & 0 & \partial Ni/\partial z \\ \partial Ni/\partial y & \partial Ni/\partial x & 0 \\ 0 & \partial Ni/\partial z & \partial Ni/\partial y \\ \partial Ni/\partial x & 0 & \partial Ni/\partial z \end{bmatrix} \begin{Bmatrix} u \\ v \\ w \end{Bmatrix} \quad \text{.....(٤.٣)}$$

$$\{a\}^e$$

$$[B]$$

Where ; $[B]$ is the strain – displacement matrix .

$$\{\varepsilon\} = \{\varepsilon_e\} + \{\varepsilon_{vp}\} \quad \text{.....(٤.٤)}$$

where ; $\{\varepsilon_e\}$ is the elastic strain part .

$\{\varepsilon_{vp}\}$ is the viscoplastic strain part .

Since the shape function (N_i) are function of the local coordinates rather than Cartesian coordinates a relationship needs to be established between the derivatives in the two coordinates systems . By using the **Chain** rule , the partial differential relation can be expressed in matrix form as [١] :

$$\begin{matrix} \partial Ni/\partial \xi \\ \partial Ni/\partial \eta \\ \partial Ni/\partial \tau \end{matrix} = \begin{matrix} \partial x/\partial \xi & \partial y/\partial \xi & \partial z/\partial \xi \\ \partial x/\partial \eta & \partial y/\partial \eta & \partial z/\partial \eta \\ \partial x/\partial \tau & \partial y/\partial \tau & \partial z/\partial \tau \end{matrix} \begin{matrix} \partial Ni/\partial x \\ \partial Ni/\partial y \\ \partial Ni/\partial z \end{matrix} \quad \text{.....} \quad (٤.٥)$$

$$[J]$$

Where ; $[J]$ is the **Jacobian** matrix and the element of this matrix can be obtained by differentiation of equation (٤.٢) .
The **Jacobian** matrix can be expressed as [١٥]:

$$[J] = \begin{matrix} \sum_{i=1}^{n}(\partial Ni/\partial \xi)\, x_i & \sum_{i=1}^{n}(\partial Ni/\partial \xi)\, y_i & \sum_{i=1}^{n}(\partial Ni/\partial \xi)\, z_i \\ \sum_{i=1}^{n}(\partial Ni/\partial \eta)\, x_i & \sum_{i=1}^{n}(\partial Ni/\partial \eta)\, y_i & \sum_{i=1}^{n}(\partial Ni/\partial \eta)\, z_i \\ \sum_{i=1}^{n}(\partial Ni/\partial \tau)\, x_i & \sum_{i=1}^{n}(\partial Ni/\partial \tau)\, y_i & \sum_{i=1}^{n}(\partial Ni/\partial \tau)\, z_i \end{matrix} \quad \text{.....} \quad (٤.٦)$$

Then the derives of the shape function with respect to Cartesian coordinates can obtain as [١٥] :

$$\begin{matrix} \partial Ni/\partial x \\ \partial Ni/\partial y \\ \partial Ni/\partial z \end{matrix} = [J]^{-1} \begin{matrix} \partial Ni/\partial \xi \\ \partial Ni/\partial \eta \\ \partial Ni/\partial \tau \end{matrix} \quad \text{.....} \quad (٤.٧)$$

Where ; $[J]^{-1}$ is the inverse of **Jacobian** matrix given by :

$$[J]^{-1} = \begin{matrix} \partial\xi/\partial x & \partial\eta/\partial x & \partial\tau/\partial x \\ \partial\xi/\partial y & \partial\eta/\partial y & \partial\tau/\partial y \\ \partial\xi/\partial z & \partial\eta/\partial z & \partial\tau/\partial z \end{matrix} \quad \text{.....} \quad (٤.٨)$$

As $[J] * [J]^{-1} = [J]^{-1} * [J] = [I]$ (unite matrix)

Three shear and three normal elastic stresses , at each **Gaussian** point , are calculated using the constitutive relation ;

$$\{\sigma\} = \begin{matrix} \sigma_x \\ \sigma_y \\ \sigma_z \\ \tau_{xy} \\ \tau_{yz} \\ \tau_{zx} \end{matrix} \quad \text{.....} \quad (٤.٩)$$

and the stresses – strain relationship is represented as :

$$\{\sigma\} = [D] * \{\varepsilon\} \quad \text{.....} \quad (٤.١٠)$$

Where ; $[D]$ is the elasticity matrix . Designation of stresses components shown in Figure (٤.٣).

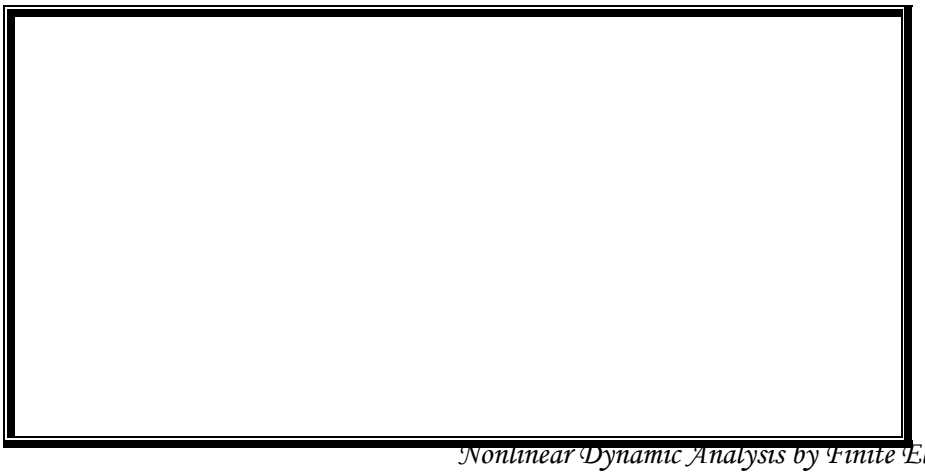

Figure (٤.٣) Designation of Stresses Components [١٥] .

Using the elastic stresses to check for cracking and to modify these stresses to real viscoplastic stresses at each **Gaussian** point , is adopted . Using the **Gaussian** product rules , the stiffness matrix is obtained :

$$[K] = \int_{-1}^{1}\int_{-1}^{1}\int_{-1}^{1} [B]^{T} [D] [B] |J| d\xi\, d\eta\, d\tau \qquad \text{(٤.١١a)}$$

Define $T = [B]^{T} [D] [B] |J|$

Where ; $|J|$ is the determinant of **Jacobian** matrix .

$$\text{Then } [K] = \sum_{p=1}^{NGAUSS} \sum_{q=1}^{NGAUSS} \sum_{L=1}^{NGAUSS} T(\xi_p, \eta_q, \tau_L)\, w_p . w_q . w_L \qquad \text{(٤.١١b)}$$

Where ; w_p , w_q and w_L are the weighted values of the numerical integration , **NGAUSS** is the number of **Gaussian** points .
The ٢*٢*٢ and ٣*٣*٣ **Gaussian** product rules exactly integrate the stiffness matrix of the eight and twenty noded elements respectively , reduced integration is here defined as the use of ١*١*١ and ٢*٢*٢ for eight and twenty noded elements respectively . The distribution of the sampling point over the volume of the ٢٠ – nodded element can be seen in Figure (٤.٤) . In the ٨ – noded element the sampling points are located at the centers of the six faces [٤٤] .

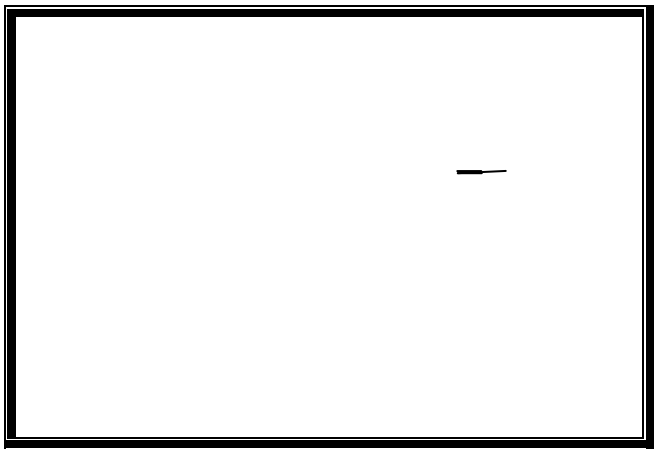

Figure (٤.٤) Three - Dimensional Concrete Element with ٢٠ nodes [٤٤] .

٤.٣.١.٣ Formulation of Load Matrix

External nodal forces have three components in x , y and z which are F_{xi} , F_{yi} and F_{zi} respectively . Gravity loading is treated as consistent nodal forces . For node i of an element , the forces are ;

$$\begin{matrix} F_x \\ F_y \\ F_z \end{matrix} = \int_V [N] \quad \rho . g \quad \begin{matrix} f_1 \\ f_2 \\ f_3 \end{matrix} \quad . \, d_v \qquad \text{(٤.١٢a)}$$

Where ; v is the element volume , g is the gravity constant ; f_1 , f_2 and f_3 are x , y and z components of gravity direction vector , which are usually ٠ , ٠ and -١ respectively ; so that :

$$F_{zi} = -\int_{-1}^{1}\int_{-1}^{1}\int_{-1}^{1} \rho . g \; [N]^T \, d\xi \, d\eta \, d\tau \qquad \text{(٤.١٢b)}$$

$$F_z = - \rho . g \sum_{p=1}^{NGAUSS} \sum_{q=1}^{NGAUSS} \sum_{L=1}^{NGAUSS} [N(\xi_p , \eta_q , \tau_L)]^T \; w_p . w_q . w_L \qquad \text{(٤.١٢c)}$$

only linearly distributed in x , y and z face loadings are used here in – Numerical integration is taken on the loaded element face area A(c) , to fined F_{xi} , F_{yi} and F_{zi} [٣].

٤.٣.٢ Steel Layer

Steel equivalent layer thickness (t_{sx}) is taken as (ρ_x . t) where ρ_x is the reinforcement ratio in the direction of the local element x – axis and (t) is the total element thickness . Each set of reinforcing bars is smeared as a two – dimensional membrane of equivalent thickness . The contribution of the bar is added to that of the solid concrete [٣] .

$$[K] = [K_c] + [K_s] \qquad \text{(٤.١٣)}$$

Where ; $[K]$ is the total stiffness matrix of the element , $[K_c]$ and $[K_s]$ are the concrete and steel stiffness matrices , respectively .

Using the **Gauss – Legendre** quadrature numerical integration scheme , the steel membrane matrix linking node (i) and (j) is obtained :

$$[K_s] = \int_{-1}^{1}\int_{-1}^{1} [B_s]^T [D_s] [B_s] \, |J| \, d\xi \, d\eta \qquad (٤.١٤a)$$

Define $T_s = [B_s]^T [D_s] [B_s] \, |J_s|$

Then $$[K_s] = \sum_{p=1}^{NGASS} \sum_{q=1}^{NGASS} T_s(\xi_p, \eta_q) \, w_p . w_q \qquad (٤.١٤b)$$

where NGASS is the number of **Gaussian** points of steel membrane . $[D_s]$ is the stresses – strain relation matrix of steel membrane .

٤.٤ Dynamic Equilibrium Equations in Semi – Discrete Form

The nonlinear dynamic equilibrium equations can be written in semi – discrete form as :

$$[M] \{\ddot{U}\} + [C] \{\dot{U}\} + [K] \{U\} = \{F\} - \{R\} \qquad (٤.١٥)$$

where ; $\{U\}$, $\{\dot{U}\}$ and $\{\ddot{U}\}$ are vectors of nodal displacement , velocities and acceleration respectively ,

$[M]$ and $[C]$ are the mass and damping matrices ,

$\{F\}$ is the vector of external applied forces and

$\{R\}$ is the vector of internal resisting forces .

٤.٤.١ Mass Matrix Formulation

Two alternative formulations of the mass matrix exist in literature , these are :

a – Lumped Mass Matrix

In this approach , the idealization of the mass properties of the system are separated from elastic properties . Equivalent concentrated masses are placed at the nodal points to represent the inertia forces in the direction of assumed element degrees of freedom . These masses correspond to both translation and rotational inertia of the element displacements . The resulting mass matrix is purely diagonal[٣٨] .

b – Consistent Mass Matrix

In this approach , the mass coefficients are computed using the same stiffness interpolation function and the resulting matrix called consistent mass matrix . The dynamic analysis of a consistent mass system generally requires considerably more computational effort than a lumped mass system does [٩] . The principle advantages of consistent mass are the more accurate mode shapes and frequencies which are proven upper bounds . In most applications , advantages of lumped masses are of overriding consideration [٣٠] . **Ghosh** and **Wilson** [٣٨] suggested that the diagonal mass matrix may be obtained from the full mass matrix by adding the off – diagonal elements to the appropriate diagonal elements . **Cook** [٢٤] applied this concept on element whose translational d.o.f. are mutually parallel . Heindicated that the consistent mass matrix was more occurate for flexural problems , The global mass and damping matrices and defined as :

$$[M] = \int_V [N]^T \rho \ [N] \ d_{v.} \qquad \text{(٣.١٦a)}$$

$$\text{So } [M] = \int_{-١}^{١}\int_{-١}^{١}\int_{-١}^{١} \rho [N]^T [N] \ |J| \ d\xi \, d\eta \, d\tau \qquad \text{(٤.١٦b)}$$

$$\text{Define } T = \rho \ [N]^T [N] \ |J|$$

$$[M] = \sum_{p=١}^{NGAUSS} \sum_{q=١}^{NGAUSS} \sum_{L=١}^{NGAUSS} T(\xi_p, \eta_q, \tau_L) \ w_p . w_q . w_L \qquad \text{(٤.١٦c)}$$

$$[C] = \int_V [N]^T c \ [N] \ d_{v.} \qquad \text{(٤.١٧a)}$$

$$\text{Define } T = c [N]^T [N] \ |J|$$

$$\text{So } [C] = \sum_{p=١}^{NGAUSS} \sum_{q=١}^{NGAUSS} \sum_{L=١}^{NGAUSS} T(\xi_p, \eta_q, \tau_L) \ w_p . w_q . w_L \qquad \text{(٤.١٧b)}$$

where $T(\xi_p, \eta_q, \tau_L) \ w_p . w_q . w_L$ is the transformation matrix , and (c) is the damping parameter . The vector of internal resisting forces $\{R\}$ is given by the expression :

$$\{R\} = \int_V^T [B] \{\sigma\} d_{v.} \quad \text{(٤.١٨)}$$

Where $\{\sigma\}$ is the vector of total stresses

٤.٤.٢ Modeling of Damping

The damping parameter $[C]$ appearing in equation (٤.١٧a) is not usually known ,so a different procedure has to be used to construct the C matrix . The total damping in the structure is assumed to be a sum of the damping of the individual modes present in the system response . If two modes are considered then so – called **Rayleigh** damping is a linear combination of the mass and stiffness matrices so that :

$$[C] = \gamma_{.} [M] + \gamma_{١} [K] \quad \text{(٤.١٩)}$$

Where ; $\gamma_{.}$ and $\gamma_{١}$ are constants . Equation (٤.١٩) for evaluating the damping matrix is adopted . This matrix has the same structure as the stiffness matrix , so it is in a banded form .

٤.٥ Nonlinear Solution Technique

Nonlinear problems is solid mechanics are classified into two forms , first nonlinearity due to strain – displacement relationship which is geometric nonlinearity , and secondly nonlinearity due to nonlinear stresses – strain relationship which is material nonlinearity . In the present study , only the second form is taken into consideration . The solution of nonlinear problems by the finite element method is usually attempted by one of three basic technique [٩٣] .

٤.٥.١ General

a – Incremental Procedures

The basis of the incremental or piecewise linear procedure is the subdivision of the load into many small partial loads or incremental . The stiffness matrix may take different values during differential load increments . The displacement increments are accumulated to give the total displacement at any stage of loading , and the incremental process is repeated until the total load has been reached .

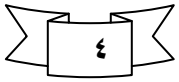

b – Iterative Procedures

The iterative procedure is a sequence of calculations in which the body or the structure is fully loaded in each iteration . Different approaches are updated , the variable stiffness method , while in others a constant linear matrix is used throughout requiring only a single matrix inversion .

c – Mixed Procedures

The mixed procedures utilize a combination of the incremental and iterative schemes . The load is applied incrementally , but after each increment successive iterations are performed . This method yields higher accuracy but with a large cost of computational effort .This procedure is adopted in the present study .

٤.٥.٢ Direct Integration Methods

In direct integration methods , Equation (٤.١٥) is integrated by using a numerical step by – step procedure , the term (direct) meaning that prior to the numerical integration , no transformation of the equations into different forms is carried out . The direct integration is based on two ideas . First , instead of satisfying Equation (٤.١٥) at any time (t) , it is aimed to satisfy this equation only at discrete time intervals (Δt) a part . The second idea on which a direct integration method is based is that a variation of displacements , velocities and accelerations with in each time interval (Δt) is assumed . It is the form of this assumption , that determines the accuracy , stability and efficiency of each scheme [٢٢] .

Direct integration methods are generally , divided into :

a – Explicit integration algorithm , in which the solution at time ($t+\Delta t$) is based on the equilibrium conditions at time (t) . They require little computer storage and are inexpensive per time step . These algorithms are conditionally stable and need strict limits to evaluate the time step size . The most popular of these method is the central difference method [٢٢,٢٩,٤٤] .

b – Implicit integration algorithm , in which equilibrium at time ($t+\Delta t$) is imposed to obtain the corresponding solution . These method are usually unconditionally stable , permitting larger time step . However , the storage required and the cost per step is high because it is necessary to factories the stiffness matrix . Some of these methods are **Newmark** method , **Houbolt** and **Wilson** – θ method [٢٢,٤٤,٦٩] .

٤.٥.٢.١ The Newmark Method The **Newmark** method , adopted in this work [٦٧] , is an extension of the linear acceleration method . The dynamic equilibrium equation is line arised and written at time (t_{n+1}) as :

$$[M]\{\ddot{U}_{n+1}\} + [C]\{\dot{U}_{n+1}\} + [K]\{U_{n+1}\} = \{F_{n+1}\} \quad \text{.....} \quad (٤.٢٠)$$

The following assumption on the variation of displacement and velocities are made within atypical time step ;

$$\{U_{n+1}\} = \{U_n\} + \Delta t\{\dot{U}_n\} + ((1-2\beta)\{\ddot{U}_n\} + 2\beta\{\ddot{U}_{n+1}\})\Delta t^2/2 \quad \text{.....} \quad (٤.٢١a)$$

$$\{\dot{U}_{n+1}\} = \{\dot{U}_n\} + \Delta t((1-\delta)\{\ddot{U}_n\} + \delta\{\ddot{U}_{n+1}\}) \quad \text{.....} \quad (٤.٢١b)$$

where ; $\{U_n\}$, $\{\dot{U}_n\}$ and $\{\ddot{U}_n\}$ are values of displacement , velocity and acceleration known at time (t) . Parameters β and δ control the stability and accuracy of the method . When β equals (١/٦) and δ equals (١/٢) , relation (٤.٢١) corresponds to the linear acceleration method . Newmark method was originally proposed as an unconditionally stable scheme . The constant – average acceleration method (also cold trapezoidal rule) , in which case δ equals (١/٢) and β equals (١/٤) are adopted in the present study .

٤.٥.٢.٢ Computational Algorithm Form of Newmark's Method

In the present study the unconditionally stable implicit scheme such as Newmark method which permit the use of large time steps , is adopted . The following steps describe the predictor – corrector form of Newmark scheme for the integration of the system equations which govern nonlinear transient dynamic problems [٦٩] .

١ – Set iteration counter i = ١, for (m+١) time step .

٢ – Begin predictor phase as set :

$$\{U^i_{m+1}\} = \{U^{\wedge}_{m+1}\} = \{U_m\} + \Delta t\{\dot{U}_m\} + \Delta t^2(1-2\beta)\{\ddot{U}_m\}/2 \quad \text{.....} \quad (٤.٢٢a)$$

$$\{U^{i}_{m+1}\}=\{U^{\wedge}_{m+1}\}=\{U_m\} + \Delta t\,(1-\delta)\{\dot{U}_m\} \quad \text{(٤.٢٢b)}$$

$$\{\ddot{U}^{i}_{m+1}\} = [\{U^{i}_{m+1}\}-\{U^{\wedge}_{m+1}\}] / (\Delta t^{2}\beta) \quad \text{(٤.٢٢c)}$$

٣ – Evaluate residual forces :

$$\{\psi^{i}_{m+1}\}=\{F_{m+1}\} - [M]\{\ddot{U}^{i}_{m+1}\} - R^{i-1}_{m+1} \quad \text{(٤.٢٣)}$$

$$R^{i-1}_{m+1} = \int_{v} \beta\, \sigma^{i-1}_{m+1}\, dv. \quad \text{(٤.٢٤)}$$

٤-The effective stiffness matrix is :

$$[K^{*}] = [M] / (\Delta t^{2}\beta) + K \quad \text{(٤.٢٥)}$$

٥ – Factorize , forward reduction and back substitute as required to solve

$$[K^{*}]\{\Delta U^{i}\} = \{\psi^{i}\} \quad \text{(٤.٢٦)}$$

٦ – Find the corrector phase

$$\{U^{i}_{m+1}\} = \{U^{i}_{m+1}\} + \{\Delta U^{i}\} \quad \text{(٤.٢٧a)}$$

$$\{\ddot{U}^{i}_{m+1}\} =[\{U^{i}_{m+1}\} - \{U^{\wedge}_{m+1}\}] / (\Delta t^{2}\beta) \quad \text{(٤.٢٧b)}$$

$$\{\dot{U}^{i}_{m+1}\} = \{\dot{U}^{\wedge}_{m+1}\} + \Delta t\,\delta\{\ddot{U}^{i}_{m+1}\} \quad \text{(٤.٢٧c)}$$

٧- If ΔU^{i} do not satisfy the convergence condition , set i =i+١ and go to step (٣) .

٨ – Set :

$$\{U_{m+1}\} =\{U^{i}_{m+1}\} \quad \text{(٤.٢٨a)}$$

$$\{\dot{U}_{m+1}\} = \{\dot{U}^{i}_{m+1}\} \quad \text{(٤.٢٨b)}$$

$\ddot{U}$ $\ddot{U}$

$$\{U_{m+1}\} = \{U^{i}_{m+1}\} \qquad (٤.٢٨c)$$

Then use the above values for the next time step . The vectors $\{\hat{U}_{m+1}\}$ and $\{\hat{U}_{m+1}\}$ are predictor vectors ; $\{U_{m+1}\}$ and $\{U_{m+1}\}$ are corrector vectors .

٤.٥.٣ Selection of the Time Step Size for Viscoplastic Model

As mentioned in the previous chapter , the viscoplastic flow rule is valid for all time (t) , as :

$$\dot{\varepsilon}_{vp} = \gamma(\dot{\varepsilon}_{v}) \langle \phi(F.) \rangle n \qquad (٤.٢٩)$$

In a step – by – step numerical procedure this relationship will only be satisfied for discrete time stations (Δt) a part . The viscoplastic strain is :

$$\bar{\varepsilon}_{vp} = \int \dot{\varepsilon}_{vp}\, dt \qquad (٤.٣٠)$$

The viscoplastic strain increment ${}_{n}\dot{\varepsilon}_{vp}$ occurring in a time interval $\Delta t_n = t_{n+1} - t_n$ using an implicit time stepping scheme , is defined as :

$${}_{n}\dot{\varepsilon}_{vp} = [\,(1-k_o)\ {}_{n}\dot{\varepsilon}_{vp} + k_o\ {}_{n+1}\dot{\varepsilon}_{vp}\,] \qquad (٤.٣١)$$

so the viscoplastic strain can be approximated numerically as :

$${}_{n+1}\varepsilon_{vp} = {}_{n}\varepsilon_{vp} + {}_{n}\dot{\varepsilon}_{vp} \cdot \Delta t_n \qquad (٤.٣٢)$$

for $k_o = 0$, the strain increment is determined from condition at time (t_n) , this is the **Euler's** time integration scheme . For $k_o = 1$, the strain increment is determined at end of the time interval , this is the fully – implicit scheme [٢] . Euler integration has been found computationally efficient for quasi – static problems such as creep . The stability limit for Equation (٤.٣٢) depends on the specific form of the viscoplastic potential used in the flow rule . **Cormeau** derived the following limiting time intervals for associated viscoplasticity , a linear flow function , and an explicit time integration :

For **Tresca** $\Delta t \le (1+\upsilon)\,\sigma_o / \gamma E$ (٤.٣٣a)

Misses $\Delta t \le 4(1+\upsilon)\,\sigma_o / 3\gamma E$ (٤.٣٣b)

Mohr – Coulomb $\Delta t \le 4(1+\upsilon)(1-2\upsilon) / \gamma E\,(1-2\upsilon+\sin^2\varphi)$ (٤.٣٣c)

Where ; σ_o = ٠.٣ F_c , φ is the angle of friction , υ is Poisson's ratio , E is **Young's** modulus and γ is the fluidity coefficient . The time step length between any two interval is limited to :

$$\Delta t_{n+1} \leq f \cdot \Delta t_n \qquad \text{(٤.٣٤)}$$

where , f is a constant equals ١.٥

In dynamic analysis , if an explicit integration scheme is used then the stability limit for step – by – step integration of the equation of motion will normally govern the choice of the time step length . Implicit schemes are usually unconditionally stable , but the time step size is limited by accuracy considerations . In particular , when cracking is involved , the time step must be selected so that cracks spread progressively throughout the structure . If a large number of cracks are formed in the same interval , considerable difficulties in convergence may be encountered . So the time step size with implicit algorithms should be chosen to limit the speed at which the crack spreads .

٤.٥.٤ Convergence Criteria

In solving the nonlinear equilibrium equations by iterative method , the convergence at the end of an iteration can be measured by two criteria . The first criteria is the magnitude by which equilibrium is violated . This can be measured by the magnitude of the unbalanced loads . The second criterion is the accuracy of the total displacement . This can be measured by the magnitudes of additional displacement increments . For this study , the convergence criterion is adopted

$$\left| \psi^i_t \right| / \left| \psi^1_t \right| \leq \varepsilon$$

where ; ψ^i_t and ψ^1_t are the vectors of residual forces for the i–th and first iteration of time step (t) respectively . The tolerance (ε) is equal ٠.٠٥ . In addition to the convergence tolerances described above , a ceiling is provided to limit the number of iterations performed for each load step in case convergence tolerances provided are too stringent [٥٤] .

٤.٦ Computer Program for Dynamic Analysis

As apart of this work , a computer program **DARC٣** (three dimensional , nonlinear , dynamic analysis) from **Hinton**[٤٤] used to solved the examples in this research .

The program is coded in **FORTRAN – ٧٧** and has been tested on the personal computer, of the civil engineering department . The flow chart of this program is given in Figure (٤.٥) . This program is used to solve two types of structural material: steel and reinforced concrete ; consists of a main program and fifty one subroutines .In the present study , the **Fortran Power Station ٤.٠** compiler produced by Microsoft incorporation was used to operate the program under PC Pentium IIII with **Intel MMX ١.٨٠ GHZ** processor and **٢٥٦ MB RAM**

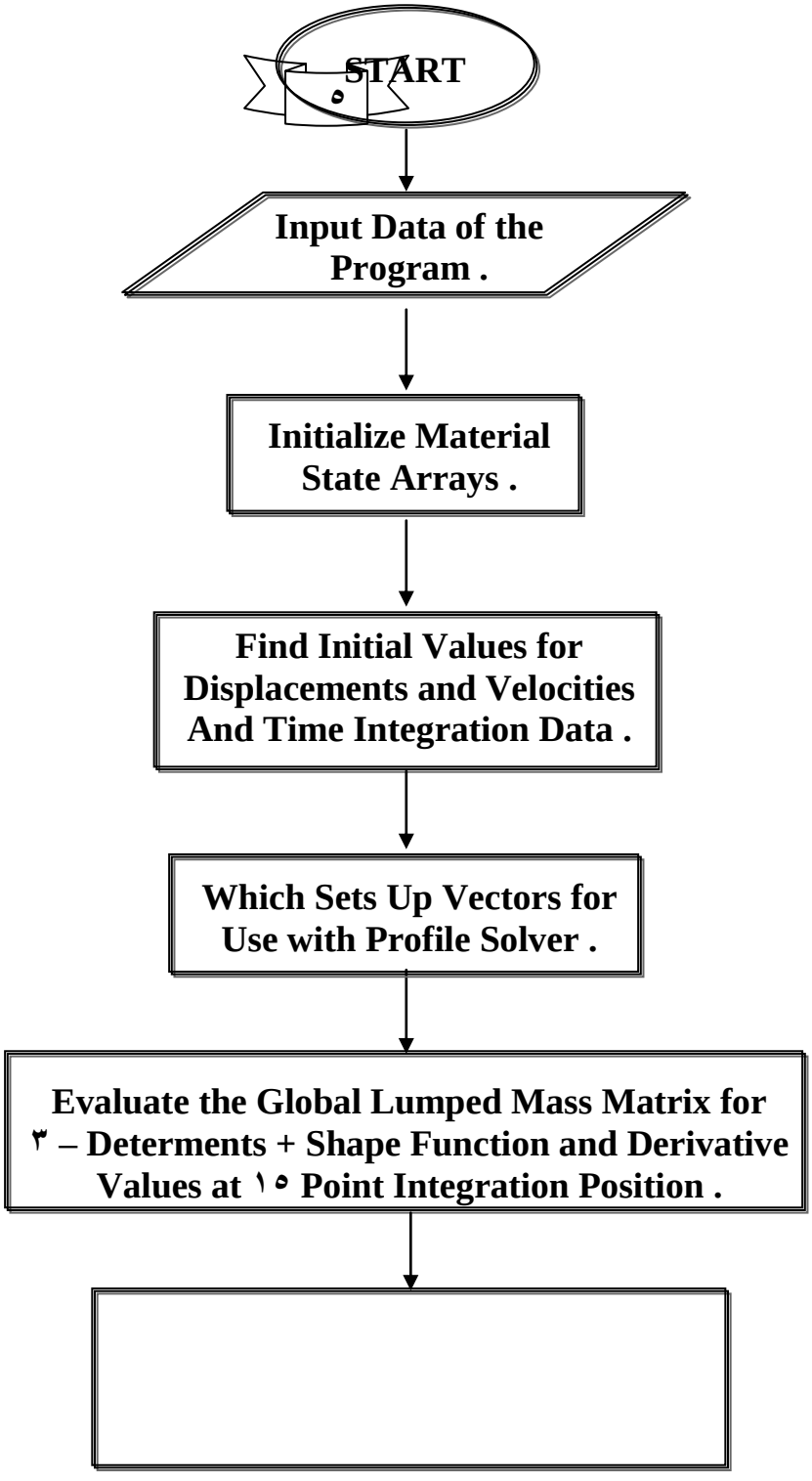

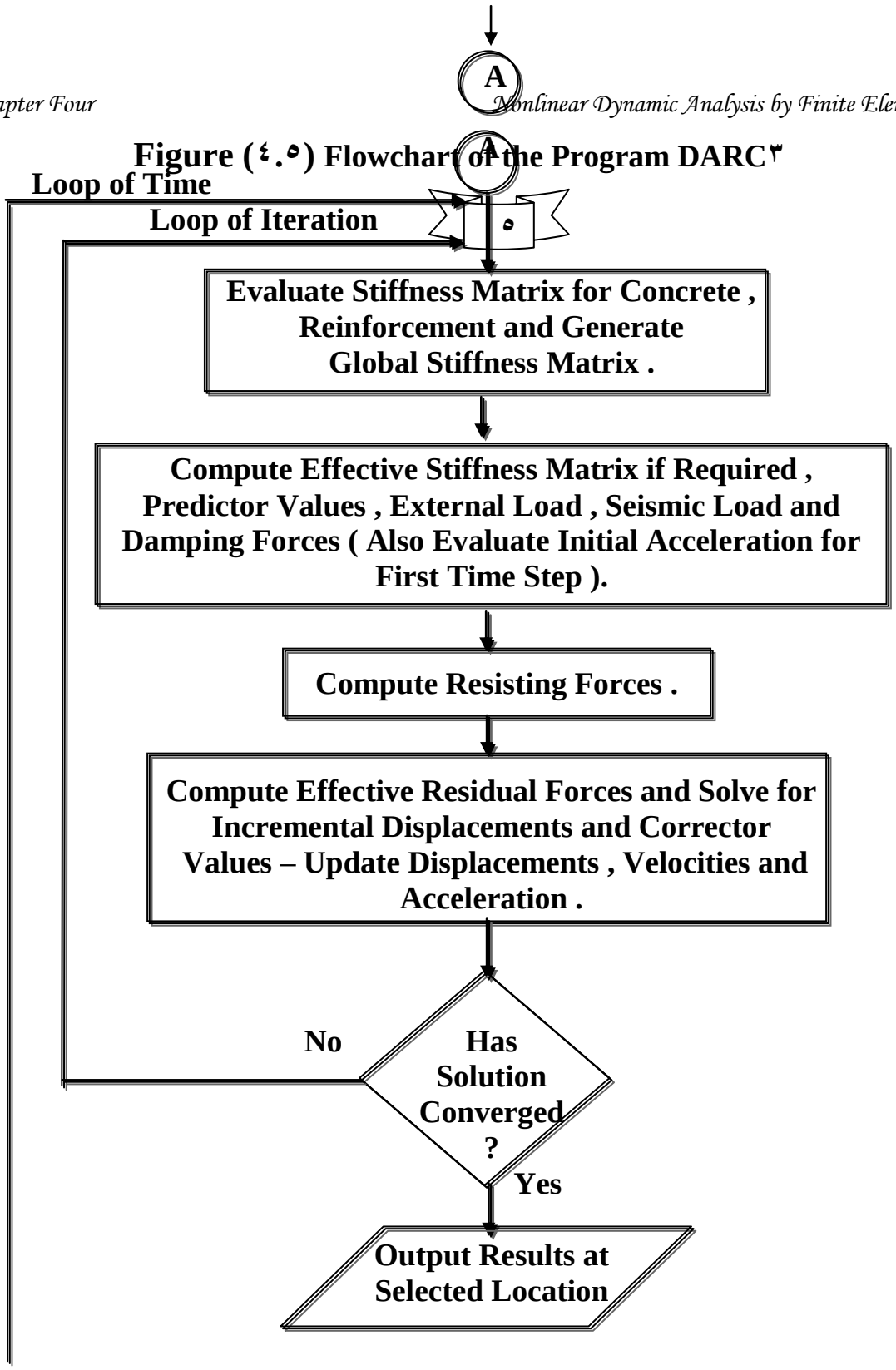

Figure (٤.٥) Flowchart of the Program DARC٣

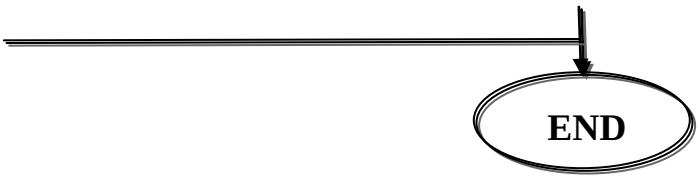

Figure (٤.٥) Continue

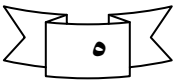

CHAPTER FIVE

NUMERICAL APPLICATION AND PARAMETRIC STUDY

٥.١ General

This chapter deals with examples analyzed numerically by the computer program **DARC٣**[٤٤] (three dimensional nonlinear dynamic analysis for reinforced concrete structures) . These examples can be classified into two main groups . The first group as verification examples used to prove the accuracy of numerical models that simulate the behavior of arch structures .

The examples also serve as a means to check the validity of the material model used , and to demonstrate the applicability and capability of the analysis method adopted in this study to a variety of three dimensional reinforced concrete structures . It is important to mention that this theoretical study has approximation in nature due to different factors mainly :

١- Approximation in the material modeling of concrete and steel
٢- Approximation inherent in the finite element modeling technique
٣- Approximation introduced due to the type of procedure used in solving the nonlinear system of equations in dynamic analyses
٤- Approximation in the integration functions used in this numerical analysis

The main results obtained by the solution introduced by this study are the time – deflection responses , time – stresses in Gauss point and time – shear stresses in Gauss point .

٥.٢ Numerical Applications

٥.٢.١ Semi–Circular Arch Subjected to Step Loading

The clamped semi – circular arch which having cross section as in Figure (٥-١) subjected to a central concentrated load applied as a step function in time was analyzed by **Noor** and **Knight**[٦٨] using explicit central difference method in addition to **Newmark´s** average acceleration and **Park's** stiffly stable methods . **Ali**[٤] presented a theoretical analysis for estimating in plane the large displacement elastic stability behavior of structures . Four different numerical integration algorithms have been used for solving the equation of motion . System mass properties have been represented using both consistent and lumped mass matrices . He used five elements per half of the arch to solve this problem with time step size equal to (٠.٠٠٠١)sec. and the nonlinear response time history for duration of (٠.٠٧٢ sec.) is found.

In the present study , the three dimensional brick elements are used and elasto – viscoplastic models are adopted for the material .

Due to symmetry , half of the circular arch with five of twenty noded brick elements to idealize the arch , and the center of arch is fixed in x and y direction but it is free in z direction (because the symmetry) to represented this we used the roller at the center of arch , as shown in Figure (٥-١d) . Material properties are given in Table (٥-١) .

For dynamic analysis , a constant time step of (٠.٠٠١ sec.) is used , (٩٠) numbers of time steps , a number of iteration for nonlinear solution is taken equal to (٥٠٠) . The time step used in the analysis can satisfy Equation (٤-٣٣) for viscoplastic model . The deflection at the center of arch versus time is presented in Figure (٥-٢) . The computed deflection agrees qualitatively with those obtained from another analytical solutions in Ref. (٤,٦٨) but the period of vibration of those solutions is elongated when compared with the results obtained from the present study , the different for maximum deflection when compared with maximum deflection from Ref. (٤) equals to (٥.٣٪) , but the maximum deflection obtained from present study equals the maximum deflection for Ref. (٦٨) . This different between the results accurs because the different in analytical method that used to solved this example .

P(t)=٣١٦

R ١٧٠

(a)

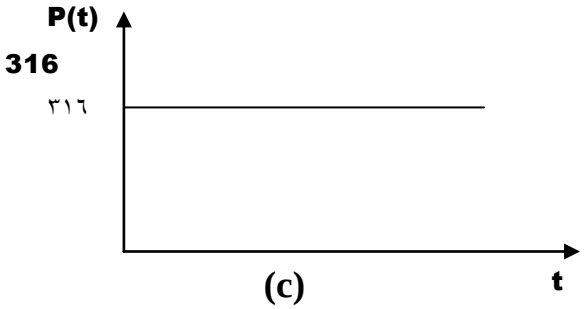

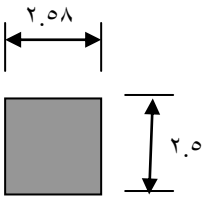

(c) **(b)**

p(t)/٣

P(t)/١ P(t)/١
٢ ٢

١

٢

٣

٤

٥

(d)

Figure (٥-١) Semi – Circular Arch Subjected to Step Loading.

(a) geometry and loading of arch (b) cross section (c) load – time relation
(d) finite element idealization and numbering of half of the arch

Table (٥-١) Material Properties and Additional Parameters [٤] .

Note:
All Load in kg
All Dimension in cm

٨

U=V=W=٠

Material Property and Additional Parameters	Symbol , unit	Value
Aluminum — Young's Modulus	E_a (kg/cm^2)	٧٠٣٤٠٠
Yield Stresses	F_y (kg/cm^2)	٤٠٠
Mass Density	ρ (kg.sec^2/cm^4)	٠.٨١٦E-٠٥
Poisson's Ratio	ψ	٠.٣٠٨
Newmark's Parameter	δ	٠.٥
	β	٠.٢٥

Figure (٥-٢) Load – Displacement in Z - Direction Curve at A center of the Clamped Semi – Circular Arch Under Dynamic Load .

٥.٢.٢ A clamped Circular Arch Subjected to Uniformly Distributed Normal Load

A clamped circular arch which having cross section and reinforcement steel as in Figure (٥-٣) subjected to uniformly distributed normal load (١kg/cm^{٢}) with triangular load – time function . The material properties of concrete and steel and addition parameters are shown in Table (٥-٢).

Tene and **Epstein** [٨٢] analyzed this problem by linear theory to find the elastic stress and deflection for this problem . The effects of transverse shear deformation and rotary inertia were first introduced in the theory of straight beam by Timoshenko , but they didn't take the effective of damping in their studying . The numerical solution is obtained by Houbolt´s method and by the finite differences and they used the time interval equals to (٠.٠١) . The number of location differences for half the arch was (٤١) .

AL – Maroof [٦] analyzed this problem by three dimensional elements based on the linear theory by the finite element method to get the variation of displacements and forces with time . No damping and damping ratios ($\gamma_{٠}$=٢.٦, $\gamma_{١}$=٠.٠٠٣٨٤٦) is considered in the arch . In both cases the arch is discritized by ١٠ curved elements . Also the numerical results obtained by the method of characteristic in Ref. [٧] are compared with those obtained by Tene [٨٢] the agreement between the two solution is encouraging .

In the present study , due to symmetry , half of the arch with five of twenty nodded brick elements , and the center of arch is fixed in x and y direction but it is free in z – direction , for represented this we used the roller at the center of arch, as shown in Figure (٥-٣)(d) . The steel reinforcement by a four layers two of them represent a longitudinal top and bottom reinforcement with thickness equal to (٠.١٦١)cm for each and the others represent the lateral ties with thickness equal to (٠.٠٥٦٥)cm for each and rotational angle equal to (٩٠^{o}) from the x-axis . For dynamic analysis , a constant time step of (٠.٠١)sec. is used , a

number of time steps is (٦٠) , a number of iteration for nonlinear solution is taken equal to (٥٠٠) .

The example is solved twice No damping is considered and with damping ratios (γ_0 =٢.٦ , γ_1 =٠.٠٠٣٨٤٦) and the results are compared with those obtained in Ref. (٦,٨٢) when solved the same example . Good agreement is found with these solutions . From Figures (٥-٤) , (٥-٥) and (٥-٦) , for central deflection without damping , the maximum different found equal to (٣٠٪ and ١٠٪) when the results compared with Ref. (٨٢,٦) respectively . But for central deflection with damping the maximum different is equal to (٢٠.٦٪) when the results compared with Ref.(٦) . The maximum different between central deflection with and without damping that obtained from the present study equal to (٦٠.٢٩٪) .

From Figure (٥-٧) , (٥-٨) and (٥-٩) we obtained that for tangential deflection at (α=٦٧.٥°) without damping the maximum different equals to (٣٠٪ and ٢٧٪) when the results compared with Ref. (٦,٨٢) respectively . But for tangential deflection at (α=٦٧.٥°) with damping the maximum different equals to (٣٠.٧٪) when the results compared with Ref. (٦) . The maximum different for tangential deflection at (α=٦٧.٥°) with and without damping obtained from the present study is equal to (٦٠٪) .

Figure (٥-١٠) shows the stresses in x – direction at arch's center (**Gauss** point (٣)) and the results are comparing with the results from Ref. (٨٢) and we found that the maximum different is equal to (٢٠٪) . That different between the results because Ref. (٨٢) solved this example by linear theory and two dimensional finite differences is used in the analysis but Ref. (٦) solved the same example by linear theory and three dimensional curved elements is used in the analysis .

Also we study the effective of the damping on shear stresses at the center of supported (**Gauss** point (٦٢)) and at the center line of beginning of element No. ٥ (**Gauss** point (٦٣)) because they are critical section for the shear stresses , as shown in Figures from (٥-١١) to (٥-١٦) and we obtained that the damping reduced the deflection , stresses and shear stresses because the damping is one from the characteristic of materials and it reduced the influence of external forces as shown in Equation (٤-١٥) . The maximum different between the shear stresses without and with damping at **Gauss** point (٦٢) is equal to (٧٩.٦٪ , ٧٧.٨٪ and ٦٠٪) for xz , yz and xy plane respectively , but this different at **Gauss** point (٦٣) equals to (٥٣.٨٪ , ٦٦.٧٪ and ٥٠٪) for xz , yz and xy plane respectively . The effect of damping on the shear stresses at **Gauss** point (٦٢) is greater than this effect on the shear stresses at **Gauss** point (٦٣) because the influence of supported on **Gauss** point (٦٢) .

Table (٥-٢) Material Properties and Additional Parameters [٨٢] .

	Material Properties and Additional Parameter	Symbol , unit	Value
Concrete	Young's Modulus	E_C (kg/cm^2)	٢٠٠٠٠٠
	Compressive Strength	F_c (kg/cm^2)	٣٠٠
	Tensile Strength	F_t (kg/cm^2)	٤٨
	Poisson's Ratio	ψ	٠.١٦
	Ultimate Compressive Strain	ε_{cu}	٠.٠٠٣٥
	Fracture Energy	G_f (kg/cm)	٠.١٥٣
	Yield Surface Function	α_c	١٠
	Mass Density	ρ_c (kg.sec^2/cm^4)	٠.٢٤E-٠٥
	Fluidity Parameter	a_0	٠.٣٠٥٥
		a_1	٠.٧٦
	Failure Surface Function	β_0	١.٨٤
		β_1	١.٠٩
Steel	Young's Modulus	E_S (kg/cm^2)	٢٠٠٠٠٠٠
	Yield Stresses	F_y (kg/cm^2)	٣٥٠٠
	Mass Density	ρ_s (kg.sec^2/cm^4)	١٤
	Poisson's Ratio	ψ	٠.٢
Newmark's Parameters		δ	٠.٥
		β	٠.٢٥

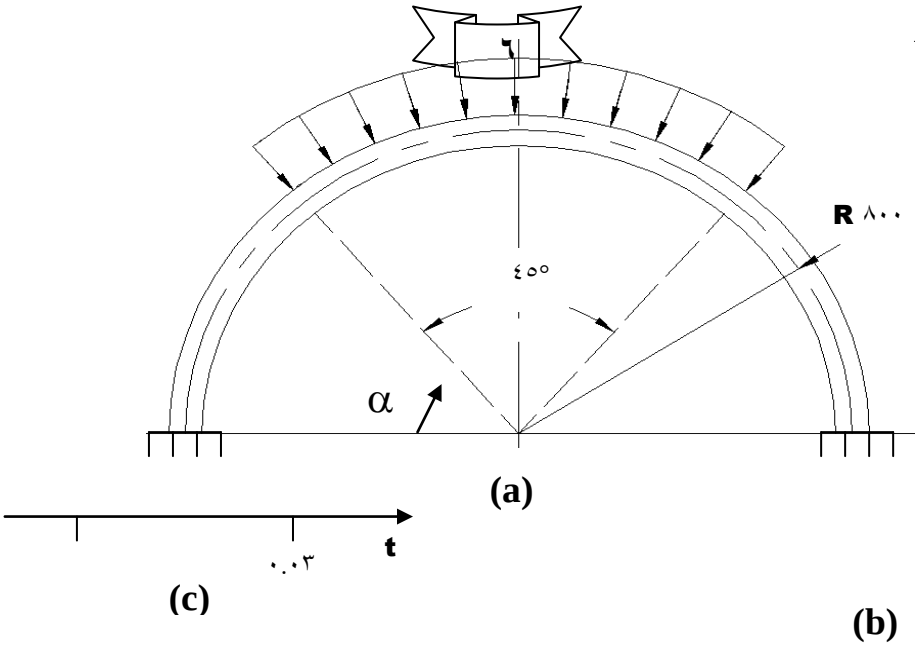

(a) geometry and loading of arch (b) cross section . (c) load – time relation
(d) finite element idealization and numbering of half of the arch

Figure (٥-٣) Circular Arch Under Triangular Normal Load

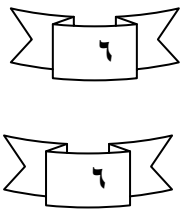

Figure (٥-٤) Time – Displacement in Z - Direction Response for Dynamic Response of the Circular Arch at (α = ٩٠°).

Figure (٥-٥) Time – Displacement in Z - Direction Response for Dynamic Response of the Circular Arch Without Damping at (α = ٩٠°).

Figure (٥-٦) Time – Displacement in Z - Direction Response for Dynamic Response of the Circular Arch With Damping at (α = ٩٠°).

Figure (٥-٧) Time – Tangential Displacement Response for Dynamic Response of the Circular Arch at (α = ٢٢.٥°).

Figure (٥-٨) Time – Tangential Displacement Response for Dynamic Response of the Circular Arch Without Damping at (α = ٦٧.٥°).

Figure (٥-٩) Time – Tangential Displacement Response for Dynamic Response of the Circular Arch With Damping at (α = ٦٧.٥°).

Figure (٥-١٠) Time – Stresses in X – Direction Response of the Circular Arch Without Damping at Gauss Point (3).

Figure (٥-١١) Time –Shear in XZ - Plane Stresses Response of the Circular Arch at Gauss Point (62)

Figure (٥-١٢) Time –Shear Stresses in YZ – Plane Response of the Circular Arch at Gauss Point (62).

Figure (٥-١٣) Time –Shear Stresses in XY - Plane Response of the Circular Arch at Gauss Point (62).

Figure (٥-١٤) Time –Shear Stresses in XZ - Plane Response of the Circular Arch at Gauss Point (٦٣).

Figure (٥-١٥) Time –Shear Stresses in YZ - Plane Response of the Circular Arch at Gauss Point (٦٣).

Figure (٥-١٦) Time –Shear Stresses in XY – Plane Response of the Circular Arch at Gauss Point (٦٣).

Chapter Five *Numerical Application and Parametric Study*

٥.٣ Parametric Study

٦

٥.٣.١ Effect the Subtended Angle on Curved Cantilever Arch

A curved cantilever reinforced by the use of the equation in Ref. (٨٥) is studied in this example with three subtended angles and the radius is

constant , the cross – section , reinforcement steel and load – time relation as shown in Figure (٥-١٧) .

Just [٥٢] solved this structure without reinforcement steel (plain concrete) and under static load .Idealized the arch with five of eight noded brick elements , as shown in Figure (٥-١٧)(d) . Longitudinal top and bottom reinforcement represented with thickness equals to (٠.١٨٦)cm for each layer , two lateral ties layers represented with thickness equals to (٠.٠٥)cm for each layer and rotational angle equals to (٩٠°) from the x – axis . Concrete and steel properties and additional material parameters are given in Table (٥ -٣) . For dynamic analysis , a constant time step of (٠.٠٥ sec.) is used , (٦٠) numbers of time steps , a number of iteration for nonlinear solution is taken equal to (٥٠٠) .

From the result it was found that when the subtended angle for curved beam increased the deflection at free end increased too but at small time the deflection in y – direction at free ends is inverse proportion with $\mathcal{B}$ as shown in Figure (٥-٢٠) . Figure (٥-١٨) shows that when ($\mathcal{B}$ =٩٠°,٦٠° and ٣٠°) the maximum deflections in x- direction is equal to (-١١.٩,-٤ and -١.٢)cm respectively , but in z – direction it is equal to (-١٨,-١٠ and -١)cm respectively , see Figure (٥-١٩) . At y – direction the maximum deflection for the free end equal to (٠.٢٤,٠.٢٨ and -٠.٠٧)cm for ($\mathcal{B}$ =٩٠°,٦٠° and ٣٠°) respectively . Figure (٥-٢١) shows that the maximum value of stresses in y– direction at **Gauss** point (٦) for ($\mathcal{B}$ =٣٠°) is (-٠.٠٠٣٢)kg/cm^{٢} and it is greater than the maximum value for ($\mathcal{B}$ =٦٠°) that is equal to (-٠.٠٠٢٤)kg/cm^{٢} because the influence of Poisson's ratio that causes the stresses in y – direction , but for ($\mathcal{B}$ =٩٠°) the maximum stresses in y – direction at **Gauss** point (٦) is equal to (-٠.٠١٠٢)kg/cm^{٢} and it is greater than the maximum stresses for ($\mathcal{B}$ =٣٠° and ٦٠°) .

Figure (٥-٢٢) shows that if the subtended angle increases the maximum value of compressive normal stresses in the x- direction at **Gauss** point (٦) increased also , and for ($\mathcal{B}$ =٩٠°,٦٠° and ٣٠°) it is equal to (-٠.٠٩٨,-٠.٠٥ and -٠.٠٤٣) kg/cm^{٢} respectively and when the subtended angle increased the stresses in z– direction at **Gauss** point (٦) increased also , see Figure (٥-٢٣) , with maximum stresses for ($\mathcal{B}$ =٩٠°,٦٠° and ٣٠°) is equal to (٠.٠٦٧,٠.٠٤٤ and -٠.٠٤) kg/cm^{٢} respectively . We also obtained the stresses in x , y and z – direction at the end face of element No. (١) (at **Gauss** point (٥)) , in x- direction the

maximum stresses at this point is equal to (٠.١٩,٠.١ and ٠.١١٥)kg/cm^{٢} for ($\mathcal{B}$ =٩٠°,٦٠° and ٣٠°) respectively , as shown in Figure (٥-٢٤) , but Figure (٥-٢٥)
shows that in z – direction its equal to (-٠.١٣٥,-٠.١١ and -٠.٠٧٥)kg/cm^{٢} for ($\mathcal{B}$ =٩٠°,٦٠° and ٣٠°) respectively .

Figure (٥-٢٦) shows the maximum stresses at **Gauss** point (٥) in y – direction which is equal to (٠.٠٢,٠.٠٠٥١ and ٠.٠٠٦٦)kg/cm^{٢} for ($\mathcal{B}$=٩٠°,٦٠° and ٣٠°) respectively and from the result we obtained that the maximum stresses in all direction at **Gauss** point (٥) is greater than the maximum stresses at **Gauss** point (٦) (near the free end of arch) .

Figure (٥-٢٧) shows that when $\mathcal{B}$ increases the maximum shear stresses in xz – plane at supported **Gauss** point (٣٠) will decrease and at ($\mathcal{B}$=٩٠°) its equal to (٠) because the plane at supported becomes horizontally , but the maximum stresses in xz – plane for ($\mathcal{B}$ =٦٠° and ٣٠°) is equal to (-٠.٠٠٣٧ and ٠.٠٠٤)kg/cm^{٢} respectively . Figure (٥-٢٨) shows that the maximum shear stresses for **Gauss** point (٣٠) in yz – plane for ($\mathcal{B}$=٩٠°) is (-٠.٠٠١٨) kg/cm^{٢} and it is lower than it is when we used ($\mathcal{B}$=٣٠°) which is equal to (-٠.٠٠٢٤)kg/cm^{٢} , but in this plane for ($\mathcal{B}$=٦٠°) it is equal to (٠.٠٠٦٨) kg/cm^{٢} and it is greater than it is for ($\mathcal{B}$=٩٠°and ٣٠°) .The maximum shear stresses for **Gauss** point (٣٠) in xy – plane for ($\mathcal{B}$ =٩٠°) is equal to (-٥)kg/cm^{٢} and it is greater than when we used ($\mathcal{B}$ =٦٠°) which is equal to (-٢)kg/cm^{٢} but the maximum shear stresses at **Gauss** point (٣٠) in this plane is positive and equals to (٣.٢)kg/cm^{٢} for (B =٣٠°) as shown in Figure (٥-٢٩). From the results , ($\mathcal{B}$ =٣٠°) is the best angle for practical applications because always the minimum deflections and minimum stresses for the arch occur when subtended angle is equal to (٣٠°) .

Table (٥-٣) Material Properties and Additional Parameters .

	Material Properties and Additional Parameter	Symbol , unit	Value
Concrete	Young's Modulus	E_C (kg/cm^2)	٢٨٥٠٠٠
	Compressive Strength	F_c (kg/cm^2)	٣٠٠
	Tensile Strength	F_t (kg/cm^2)	٤٦
	Poisson's Ratio	ψ	٠.١٥
	Ultimate Compressive Strain	ε_{cu}	٠.٠٠٣٥
	Fracture Energy	G_f (kg/cm)	٠.١٥٣
	Yield Surface Function	α_c	١٠
	Mass Density	ρ_c (kg.sec^2/cm^4)	٠.٢٤٥E-٠٥
	Fluidity Parameter	$a_.$	٠.٣٠٥٥
		$a_,$	٠.٧٦
	Failure Surface Function	$\beta_.$	١.٨٤
		$\beta_,$	١.٠٩
Steel	Young's Modulus	E_S (kg/cm^2)	٢٠٠٠٠٠٠
	Yield Stresses	F_y (kg/cm^2)	٤١٤٠
	Mass Density	ρ_s (kg.sec^2/cm^4)	١٤
	Poisson's Ratio	ψ	٠.١٩
Newmark's Parameters		δ	٠.٥
		β	٠.٢٥

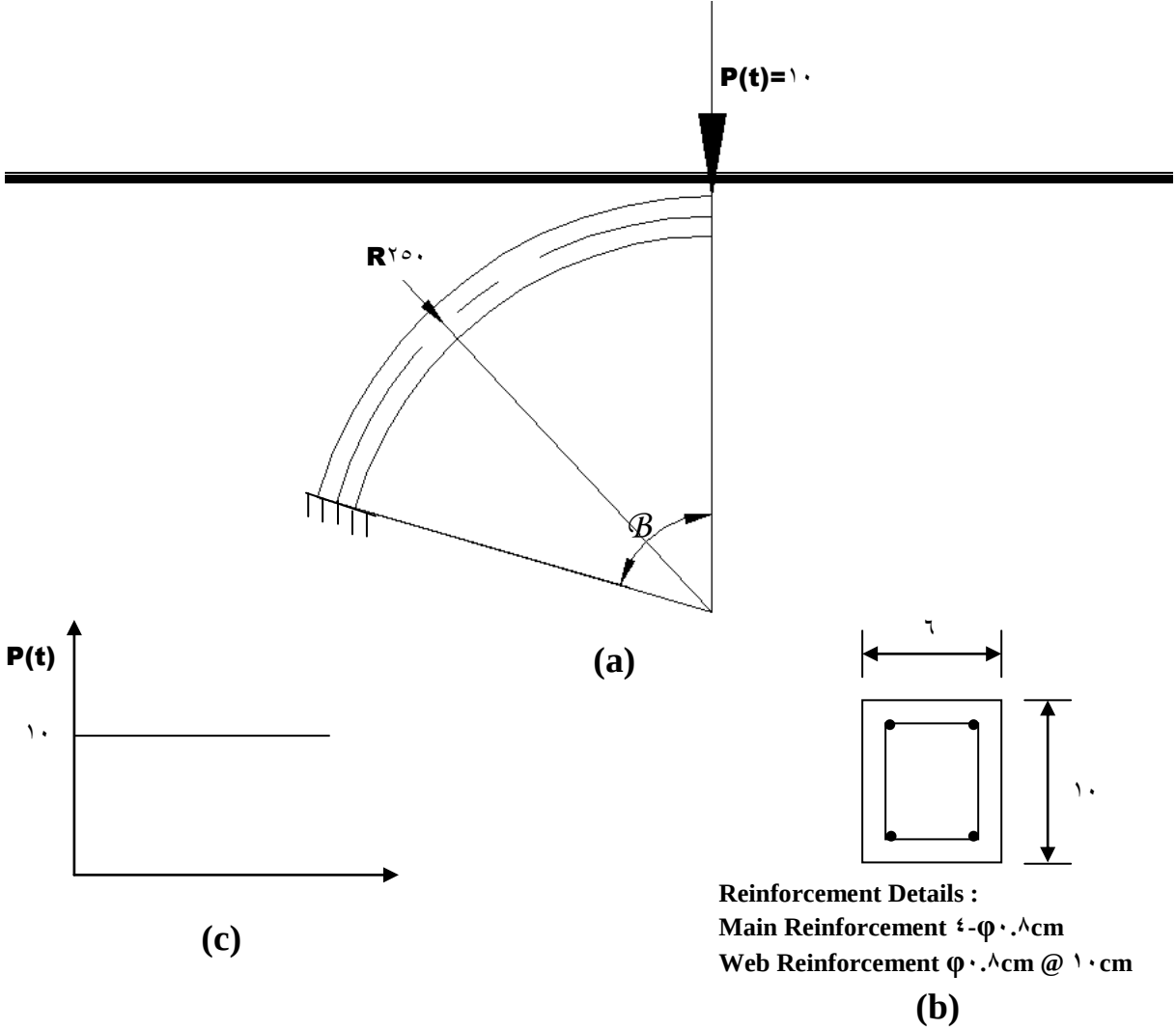

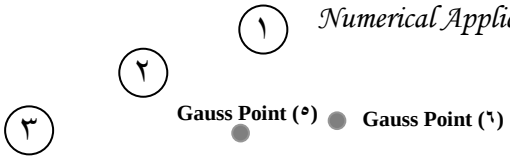

Figure (٥-١٨) Time – Displacement in X - Direction Response at Free End for Curved Cantilever with Three Subtended Angles.

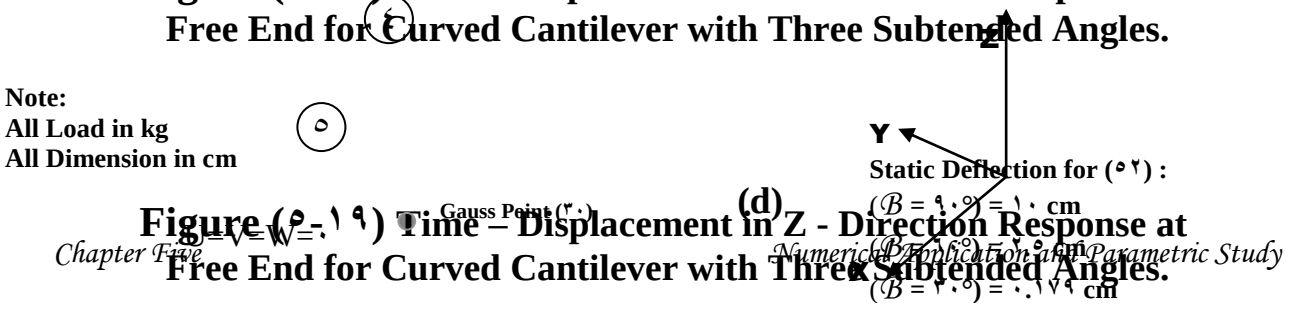

Figure (٥-١٩) Time – Displacement in Z - Direction Response at Free End for Curved Cantilever with Three Subtended Angles.

(a) geometry and loading of arch (b) cross section (c) load – time relation
(d) finite element idealization and numbering of the arch

Figure (٥-٢٠) Curved Cantilever with Three Subtended Angles

Figure (٥-٢١) Time – Displacement in Y - Direction Response at Free End for Curved Cantilever with Three Subtended Angles.

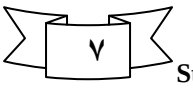

Static Displacement for (٥٢) :
(ℬ = ٩٠°) = ١٠ cm
(ℬ = ٦٠°) = ٢.٥ cm
(ℬ = ٣٠°) = ٠.١٧٩ cm

Figure (٥-٢١) Time – Stresses in Y - Direction Response at Gauss

Point (٦) for Curved Cantilever with Three Subtended Angles.

Figure (٥-٢٢) Time – Stresses in X - Direction Response at Gauss Point (٦) for Curved Cantilever with Three Subtended Angles.

Figure (٥-٢٣) Time – Stresses in X - Direction Response at Gauss Point (٦) for Curved Cantilever with Three Subtended Angles.

Figure (٥-٢٤) Time – Stresses in X - Direction Response at Gauss Point (٥) For Curved Cantilever with Three Subtended Angles.

Figure (٥-٢٥) Time – Stresses in Z - Direction Response at Gauss Point (٥) For Curved Cantilever with Three Subtended Angles.

Figure (٥-٢٦) Time – Stresses in Y - Direction Response at Gauss Point (٥)For Curved Cantilever with Three Subtended Angles.

Figure (٥-٢٧) Time – Shear Stresses in XZ – Plane Response at Gauss Point (٣٠) For Curved Cantilever with Three Subtended Angles.

Figure (٥-٢٨) Time – Shear Stresses in YZ - Plane Response at Gauss Point(٣٠) For Curved Cantilever with Three Subtended Angles.

Figure (٥-٢٩) Time – Shear Stresses in XY - Plane Response at Gauss Point(٣٠) For Curved Cantilever with Three Subtended Angles.

٥.٣.٢ Non- Prismatic Reinforced Concrete Clamped Circular Arch Structure with Subtended Angle (١٧٠°)

In this example, two cases of clamped circular arch structure was studied with subtended angle (١٧٠°) discontinuity varying cross – section is analyzed to fined the best case for the practical using . Figures (٥-٣٠a) and (٥-٣٠b) show that h./h=٠.٨, h./h=١.٢٥ for case (١) and case (٢) respectively . We used the method in Ref. (٨٥) for design this arch structure . Due to symmetry , half of the arch with five of twenty noded brick elements for the two case , as shown in Figures (٥-٣٠a) and (٥-٣٠b) .

The steel reinforcement is represented by four layers for each case . Two of them representing the longitudinal top and bottom reinforcement with thickness equals to (٠.١٠٣٧cm) for each layers , the others represent the lateral ties with thickness equals to (٠.٠٢٥٧)cm for each and with a rotational angle of (٩٠°) from the local x- axis .The material properties and the model parameters for concrete and steel as shown in Table (٥-٤) .

For dynamic analysis , a constant time step of (٠.٠٠٠٥)sec. is used , (١٠٠) numbers of time steps , a number of iteration for nonlinear solution is taken equals to (٥٠٠) .

Figure (٥-٣١) shows central deflection versus time for the two cases and from the result for case (١) the period of vibration is elongated than case (٢) and the maximum different between the two cases is equal to (٦٠٪) . The deflection in x , y and z – direction at (α=٤٢.٥°) is represented in Figures (٥-٣٢) , (٥-٣٣) and (٥-٣٤) respectively , and these deflection for case (١) is greater than it is for case (٢) and it is found that the maximum different is equal to (٦٥٪) , (٣٣.٣٣٪) and (٦٢.٢٢٪) for x ,y and z- direction respectively . Figures (٥-٣٥) , (٥-٣٦) and (٥-٣٧) show the stresses in x , y and z – direction at **Gauss** point (٣) for case (١) and (٢) , the maximum different between the two case is equal to (٥٤٪ , ٦٠٪ and ٤٨٪) for x , y and z –direction .

The stresses in x , y and z – direction at the end face of element No. (١) (near the arch's center) (**Gauss** point (٢)) for case (١) and (٢) is obtained also , and the maximum different between the two case is equal to (٢٩.٢٪ , ٧٦.٨٪ and ٥٥.٨٣٪) for x , y and z – direction respectively , as shown in Figures (٥-٣٨) , (٥-٣٩) and (٥-٤٠) . But Figures (٥-٤١) , (٥-٤٢) and (٥-٤٣) show the stresses in x , y and z – direction for the arch at **Gauss** point (٣١) (α=٤٢.٥°) for case (١) and (٢) because the change of sections at this positions , and the maximum different between the two case is equal to (٦٥٪ , ٦٠٪ and ٥٨.٣٣٪) for x , y and z – direction respectively .

From the results of stresses with time , it is found that always the maximum stresses is at (t=٠.٠٠٢٥)sec. , therefore we draw the stresses in x , y and z – direction along the arch structure at this time . We found also that when (α=٤٢.٥°) the stresses is change suddenly because of the variation of cross–

	Material Properties and Additional Parameter	Symbol , unit	

section .

Figure (٥-٤٤) shows the stresses along the arch in y – direction with maximum values for case (١) and (٢) equals to (٠.٠٠٤ and -٠.٠٠٤١)kg/cm^{٢} respectively . Figure (٥-٤٥) shows the stresses along the arch in x – direction , before (α=٤٢.٥°) the stresses for case (١) is less than it is for case (٢) and the maximum value for case (١) and (٢) is equal to (-٠.١٠٩ and -٠.١٣٢)kg/cm^{٢} respectively , but the stresses in z – direction at (t=٠.٠٠٢٥)sec. for case (١) and before (α=٢٩°) is lower than it is for case (٢) but at (α=٢٩°) the inverse is happened , as shown in Figure (٥-٤٦) and the maximum stresses in z – direction at this time along the arch for case (١) and (٢) is equal to (-٠.١١ and ٠.٠٨٥)kg/cm^{٢} respectively . From the results we obtained that case (٢) is the best because it gives less deflection from case (١) .

Concrete	**Young's Modulus**	**E_C (kg/cm^2)**	٢٢٥٠٠٠
	Compressive Strength	**F_c (kg/cm^2)**	٢١٠
	Tensile Strength	**F_t (kg/cm^2)**	٣٢
	Poisson's Ratio	ψ	٠.١٥
	Ultimate Compressive Strain	ε_{cu}	٠.٠٠٣٩
	Fracture Energy	**G_f (kg/cm)**	٠.١٥٣
	Yield Surface Function	α_c	١٠
	Mass Density	ρ_c **(kg.sec^2/cm^4)**	٠.٢٣٥E-٠٥
	Fluidity Parameter	a_0	٠.٣٠٥٥
		a_1	٠.٧٦
	Failure Surface Function	β_0	١.٨٤
		β_1	١.٠٩
Steel	**Young's Modulus**	**E_S (kg/cm^2)**	٢٠٠٠٠٠٠
	Yield Stresses	**F_y (kg/cm^2)**	٤١٤٠
	Mass Density	ρ_s **(kg.sec^2/cm^4)**	١٤
	Poisson's Ratio	ψ	٠.٢
Newmark's Parameters		δ	٠.٥
		β	٠.٢٥

Table (٥-٤) Material Properties and Additional Parameters.

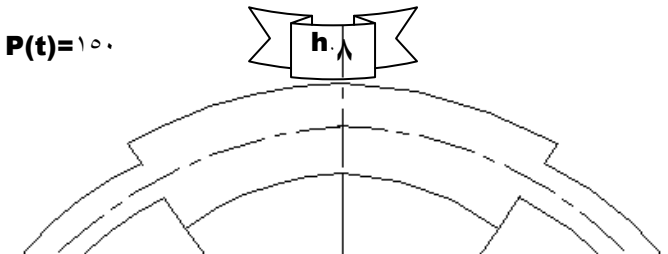

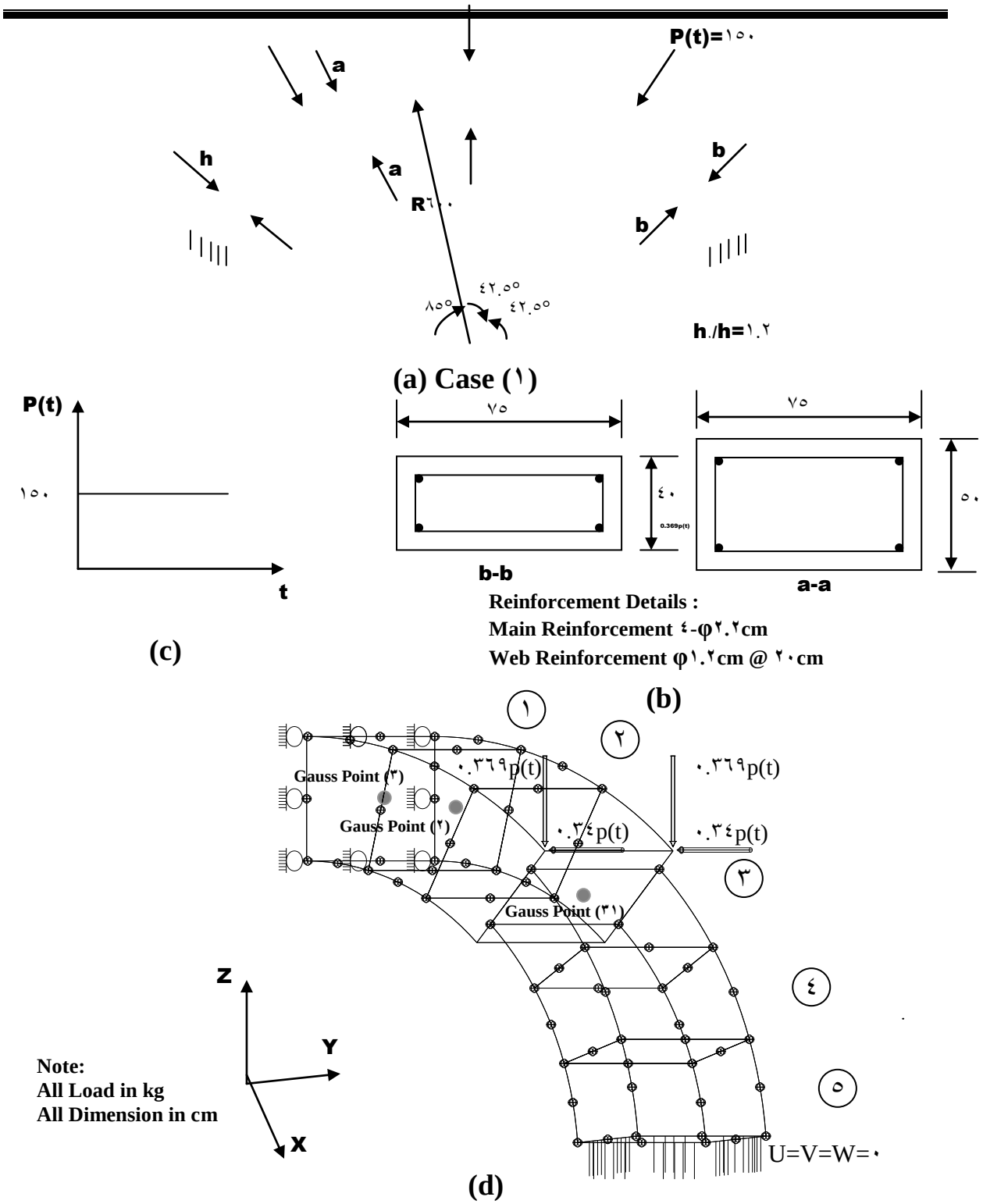

(a) geometry and loading of arch (b) cross section (c) load – time relation
(d) finite element idealization and numbering of half of the arch

Figure (٥-٣٠a) Non-prismatic Clamped Circular Arch Structure with Subtended Angle ١٧٠٥ (Case ١)

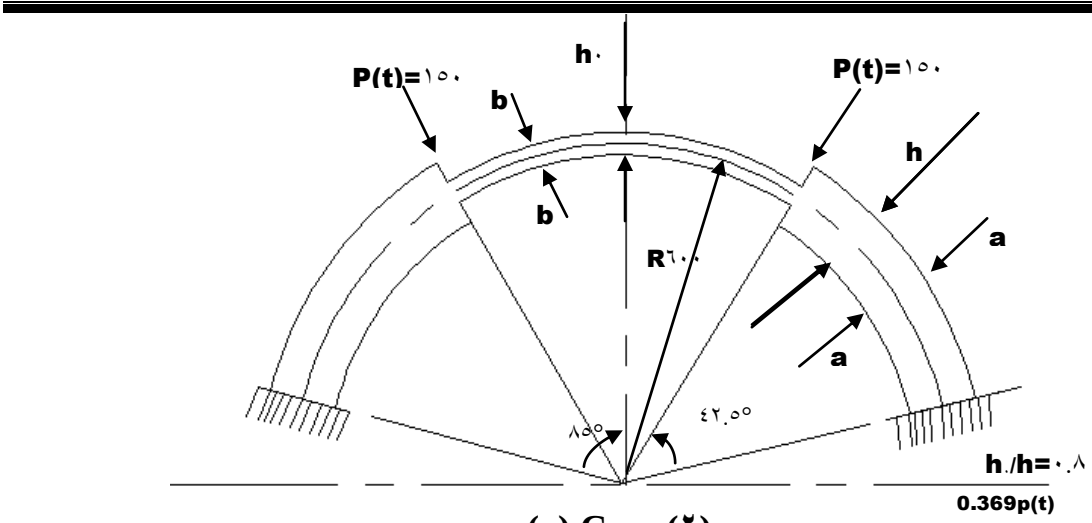

(a) Case (٢)

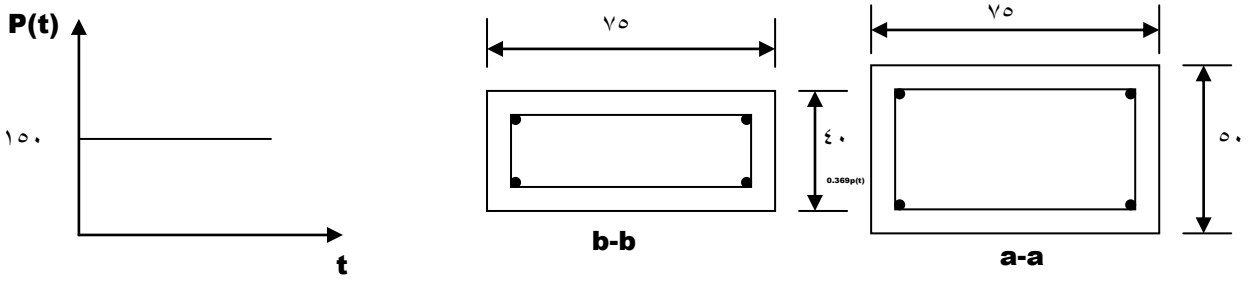

(c)

Reinforcement Details :
Main Reinforcement ٤-φ٢.٢cm
Web Reinforcement φ١.٢cm @ ٢٠cm

(b)

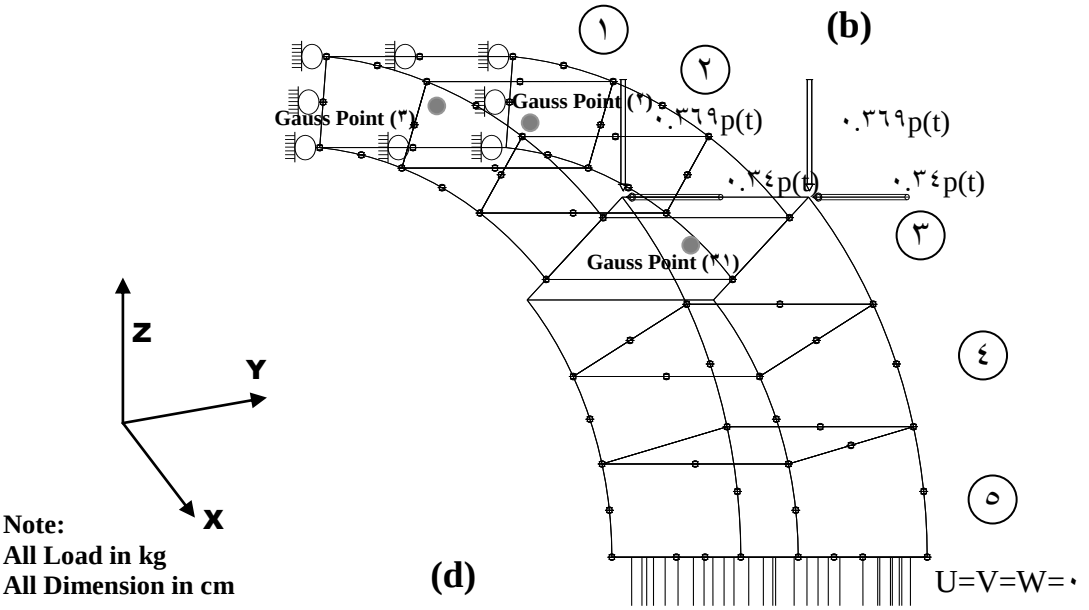

Note:
All Load in kg
All Dimension in cm

(d)

(a) geometry and loading of arch (b) cross section (c) load – time relation
(d) finite element idealization and numbering of half of the arch

Figure (٥-٣٠b) Non-prismatic Clamped Circular Arch Structure with Subtended Angle ١٧٠° (Case ٢)

Figure (٥-٣١) Time – Displacement in Z - Direction Response Of the Center of Circular Arch.

Figure (٥-٣٢) Time – Displacement in Z - Direction Response of the Circular Arch at (α=٤٢.٥°).

Figure (٥-٣٣) Time – Displacement in X - Direction Response of The Circular Arch at (α=٤٢.٥°).

Figure (٥-٣٤) Time – Displacement in Y - Direction Response of The Circular Arch at (α=٤٢.٥°).

Figure (٥-٣٥) Time – Stresses in x - Direction Response of The Circular Arch at Gauss point (٣).

Figure (٥-٣٦) Time – Stresses in Z - Direction Response of The Circular Arch at Gauss point (٣).

Figure (٥-٣٧) Time – Stresses in Y - Direction Response of The Circular Arch at Gauss point (٣).

Figure (٥-٣٨) Time – Stresses in Y - Direction Response of The Circular Arch at Gauss Point (٢).

Figure (٥-٣٩) Time – Stresses in X - Direction Response of The Circular Arch at Gauss Point (٢).

Figure (٥-٤٠) Time – Stresses in Z - Direction Response of The Circular Arch at Gauss Point (٢).

Figure (٥-٤١) Time – Stresses in X - Direction Response of The Circular Arch at Gauss point (٣١) .

Figure (٥-٤٢) Time – Stresses in Z – Direction Response of The Circular Arch at Gauss point (٣١) .

Figure (٥-٤٣) Time – Stresses in Y - Direction Response of The Circular Arch at Gauss point (٣١) .

α **(Degree)**

Figure (٥-٤٤) The Stresses in Y - Direction Along the Arch at (t=٠.٠٠٢٥ sec.).

α **(Degree)**

Figure (٥-٤٥) The Stresses in X - Direction Along the Arch at (t=٠.٠٠٢٥ sec.).

α **(Degree)**

Figure(٥-٤٦) The Stresses in Z - Direction Along the Arch at (t=٠.٠٠٢٥ sec.).

٥.٣.٣ Simply Supported Reinforced Concrete Arch Structure Under A concentrated Load

In this example , we study the effect of number of elements , initial displacement at hinge and width of cross section on a simply reinforcement concrete arch structure which has a cross section with reinforcement steel as shown in Figure (٥-٤٧) , is tested under a concentrated load equals to (١٥٠٠٠ kg) with step load – time function .We used the method in Ref. (٨٥) to design this structure . The cross sectional area is reinforcement by four layers . Two of which representing the longitudinal top and bottom reinforcement with thickness (٠.٢٣٦cm) for each layer , the others represent the lateral ties with thickness (٠.٠١٦٨cm) for each layer and with a rotational angle of (٩٠°) from the local x – axis . Concrete and steel properties and additional material parameters are given in Table (٥-٥) . Due to symmetry , half of the structure divided to five, six, seven, eight, and nine elements with eight nodded brick elements , for the example seven of eight noded brick elements shown in Figure (٥-٤٧d). For dynamic analysis , a constant time step of (٠.٠٥ sec.) is used , (٦٠) numbers of time steps , a number of iteration for nonlinear solution is taken equals to (٥٠٠) .

Figure (٥-٤٨) shown the effect of the number of elements on the central deflection , but this effect on the stresses of top face of arch's center (**Gauss** point (٤)) shows in Figures (٥-٥٥) , (٥-٥٦) and (٥-٦٧) , are studied in this example . From the results, we obtained that when the number of elements increased the convergence and values of results increased .

Figure (٥-٤٩) shows the effect of width for cross section on the center deflection at a number of elements equals to (٩) , the maximum deflection at (b = ٥٠)cm is equal to (١.٥٥)cm downward but at (b= ٤٠)cm it is equal to (١.٩)cm downward that shows the maximum different equals to (١٨.٤٢٪) . Figure (٥-٥١) shows the effect of time step on central deflection , we found when the time step decreases the curve becomes more smoothing . Also we studied the effect of initial displacement at hinge in x – direction on central deflection for five , six and seven elements . From the results we found the initial displacement causes vibration in deflection and when the number of elements increase the vibration of central deflection decreases , as shown in Figures (٥-٥٢) , (٥-٥٣) and (٥-٥٤) . The maximum central deflection with initial displacement equals to (-٠.٧٦,-١.٠٣ and -١.٤٥)cm for ٥,٦ and ٧ elements respectively .

We studied here the change between the arch when we used reinforced and plain concrete for a number of elements equals to ٩ on the central deflection , as shown in Figure (٥-٥٠) , and on the stresses in x , y and z – direction at the face of the side of element No. (١) (Gauss point (١ or ٢) near the center of arch) ,
as shown in Figures (٥-٦١) , (٥-٦٢) and (٥-٦٣) , from the results we obtained

in plain concrete the deflection increase and the maximum value is equal to (-١.٥,-١.٦٢)cm for reinforced and plain concrete arch respectively and the maximum different is equal to (٧.٤٪) , this different is small because of the membrane action in the arch . But the maximum stresses in x – direction at **Gauss** point (١or٢) for reinforced and plain concrete arch equals to (-١٠,-٦.٨) kg/cm^{٢} respectively , but in y – direction for reinforced and plain concrete it is equal to (-١.٣, and -١.١)kg/cm^{٢} respectively , and in z – direction the maximum stresses at **Gauss** point (١or٢) for reinforced concrete arch is equal to the maximum stresses for plain concrete arch (٣.٨)kg/cm^{٢} .

We also compared the compressive stresses of the top face at (Gauss point (٤)) and tensile stresses of the bottom face at (Gauss point (٣)) of element No. (١) (near the center of arch) in x , y and z – direction for number of element = ٩ , as shown in Figures (٥-٥٨) , (٥-٥٩) and (٥-٦٠) , from the results we found that the maximum tensile stresses at **Gauss** point (٣) is equal to (١٦٠,١٧ and ٢٨)kg/cm^{٢} for x,y and z – direction respectively and it is greater than the maximum compressive stresses at **Gauss** point (٤) that is equal to (١٥٨,١٧ and ٢٧)kg/cm^{٢} for x,y and z – direction respectively .

Table (٥-٥) Material Properties and Additional Parameters .

	Material Properties and Additional Parameter	**Symbol , unit**	

Concrete	**Young's Modulus**	**E_C (kg/cm^2)**	٢٨٤٠٠٠
	Compressive Strength	**F_c (kg/cm^2)**	٣٦٦
	Tensile Strength	**F_t (kg/cm^2)**	٤٦
	Poisson's Ratio	ψ	٠.١٥
	Ultimate Compressive Strain	ε_{cu}	٠.٠٠٤
	Fracture Energy	**G_f (kg/cm)**	٠.١٥٣
	Yield Surface Function	α_c	١٠
	Mass Density	ρ_c **(kg.sec^2/cm^4)**	٠.٢٤٥E-٠٥
	Fluidity Parameter	a_0	٠.٣٠٥٥
		a_1	٠.٧٦
	Failure Surface Function	β_0	١.٨٤
		β_1	١.٠٩
Steel	**Young's Modulus**	**E_S (kg/cm^2)**	٢١٠٠٠٠٠
	Yield Stresses	**F_y (kg/cm^2)**	٤١٤٠
	Mass Density	ρ_s **(kg.sec^2/cm^4)**	١٤
	Poisson's Ratio	ψ	٠.٢
Newmark's Parameters		δ	٠.٥
		β	٠.٢٥

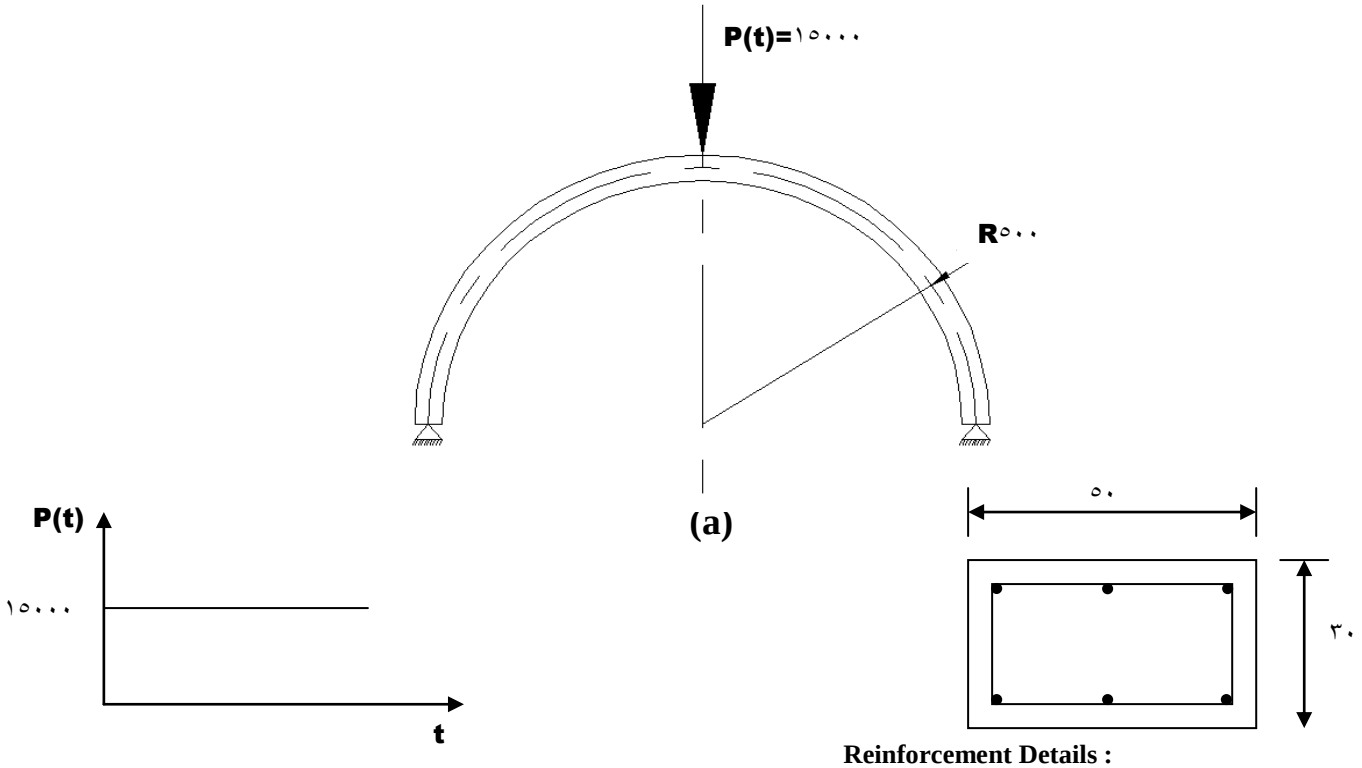

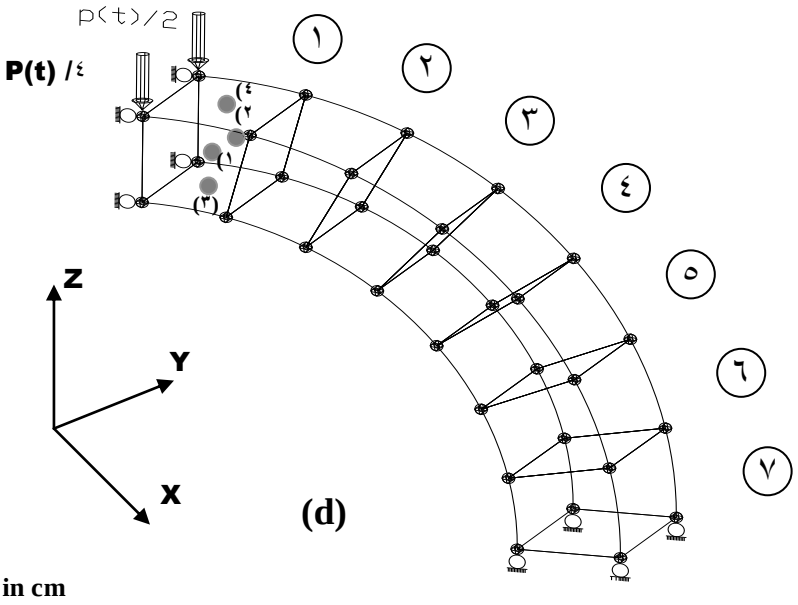

(a) geometry and loading of arch (b) cross section (c) load – time relation
(d) finite element idealization and numbering of half of the arch

Figure (٥-٤٧) Simply Supported Arch Structure Under A Concentrated Load

Figure (٥-٤٨) Effect the Number of Elements on Time – Displacement in Z - Direction Response at Center of Arch.

Figure (٥-٤٩) Effect the Change of Width on Time – Displacement in Z – Direction Response at A center of Arch with Number of Element = ٤٠.

Figure (٥-٥٠) Effect of Reinforcement on Time – Displacement in Z - Direction Response at Center of Arch.

Figure (٥-٥١) Effect of Time – step on Time – Displacement in Z - Direction Response at Center of Arch.

Figure (٥-٥٢) Effect Initial Displacement at Hinge on Time -Displacement in Z - Direction Response at Center of Arch for Number of Element = ٥.

Figure (٥-٥٣) Effect Initial Displacement at Hinge on Time – Displacement in Z - Direction Response at Center of Arch for Number of Element = ٦.

Figure (٥-٥٤) Effect Initial Displacement at Hinge on Time – Displacement in Z - Direction Response at Center of Arch for Number of Element = ٧.

Figure (٥-٥٥) Effect the Number of Elements on Time – Stresses In X – Direction Response of Arch at Gauss Point (٤).

Figure (٥-٥٦) Effect the Number of Elements on Time – Stresses In Z - Direction Response of Arch at Gauss Point (٤).

Figure (٥-٥٧) Effect the Number of Elements on Time – Stresses In Y – Direction Response of Arch at Gauss Point (٤).

Figure (٥-٥٨) Time – Stresses in X – Direction Response of Arch at Gauss Point (٣) and (٤) for Number of Elements = ٩.

Figure (٥-٥٩) Time – Stresses in Z - Direction Response of Arch at Gauss Point (٣) and (٤) for Number of Elements = ٩.

Figure (٥-٦٠) Time – Stresses in Y - Direction Response of Arch at Gauss Point (٣) and (٤) for Number of Elements = ٩.

Figure (٥-٦١) Time – Stresses in Y - Direction Response of Arch at Gauss Point (١) or (٢) for Number of Elements = ٩.

Figure (٥-٦٢) Time – Stresses in X - Direction Response of Arch at Gauss Point (١) or (٢) for Number of Elements = ٩.

Figure (٥-٦٣) Time – Stresses in Z - Direction Response of Arch at Gauss Point (١) or (٢) for Number of Elements = ٩.

٥.٣.٤ Effect of Boundary Conditions on Reinforced Concrete Arch Structures

Four cases of boundary conditions are studied for the reinforcement concrete arch structure under concentrated load at (α=٥٠°) with load – time relation as shown in Figure (٥-٦٤) . The arch with cross – section and reinforcement steel as shown in Figure (٥-٦٤) . Concrete and steel properties and additional parameters are given in Table (٥-٦) . Figure (٥-٦٤)(d) also shows the details of the finite element mesh for the arch with nine of eight noded brick elements . The arch reinforced by a four layers two of which represent a longitudal top and bottom reinforcement with thickness equals to (٠.٥٢٤ cm) for each layer and the others represent the lateral ties with thickness (٠.٠١٦٨ cm) for each layer , and rotational angle equals to (٩٠^{o}) from x – axis . For dynamic analysis , a constant Time steps of (٠.٠١ sec.) is used , (٦٠) numbers of time steps , a number of iteration for nonlinear solution is taken equals to (٥٠٠) .

The deflection and stresses in x ,y and z- direction is studied in this example for various boundary condition . The maximum horizontal deflection under point load at (α=٥٠°)for fixed ends arch is (٠.٨٧)cm as shown in Figure (٥-٦٥) , that is because in this work we assumed that the hinge is free in horizontal direction . The deflection in z and y –direction at (α=٥٠°) for fixed ends arch is lower than it is for hinge ends arch and the maximum difference in z and y –direction is found to be (٦٧.٨٦٪)and (٥٣.٣٣٪) respectively .The deflection in y–direction is caused by Poisson's ratio, these two solutions are plotted in Figure (٥-٦٦) and Figure (٥-٦٧).

In the case of fixed and hinge ends , Figure (٥-٦٩) when the hinge is far from the loading it becomes positive (for right) and equals to (٢.٥)cm . The deflection in z and y – direction at (α=٥٠°) when the hinge is far from loading it is smoothing than the deflection for hinge – fixed ends and the maximum difference is (٤٦.٨٪) and (٤٢.٤٢٪) for z and y – direction respectively , see Figure (٥-٦٨) and (٥-٧٠) .

In this example we found that the deflection along the arch at (t=٠.٣٥٥ sec.) usually represented the maximum deflection for various cases . Figure (٥-٧١) represented hinge ends arch case , the horizontal deflection is negative when α less than (٧٠°) with maximum value equals to (-٢.٥)cm , but at (α=٧٠°)it becomes positive and the maximum value equals to (١.٧)cm and the vertical deflection is negative along the arch with maximum value equals to (-٢.٣)cm . For fixed ends arch , see Figure (٥-٧٢) , the horizontal deflection is positive along the arch with maximum value equals to (٠.٤)cm and the vertical

deflection is negative when α is less than (٩٩°) and the maximum value equals to (٠.٥)cm but at (α=٩٩°) it becomes positive with maximum value (٠.١٢)cm while for fixed – hinge ends arch the horizontal deflection is positive with maximum value equals to (٠.٣)cm but at (α=١٥٥°)it becomes negative and the horizontal deflection at the hinge is very small and equals to (-٠.٤)cm because it is far from loading .

The vertical deflection is negative with maximum value equals to (-٠.٣٦)cm and at (α=٨٥°) it becomes positive with maximum value equals to (٠.١٧)cm , as shown in Figure (٥-٧٣) . while the vertical deflection at hinge – fixed ends becomes positive at (α=١١٩°) with maximum value equals to (-٠.٨٣ and ٠.١)cm , but horizontal deflection in this case is negative when α is less than (٣٨°) with maximum value (-٠.٧)cm and when (α=٣٨°)it becomes positive with maximum value equals to (٠.٤١)cm , as shown in Figure (٥-٧٤) .

The maximum stresses at center of arch therefore we obtained time stresses curve in side face of arch's center in x, y and z direction For all cases as shown in Figures from (٥-٧٥) to (٥-٨٠) . Generally the stresses at **Gauss** point (٢٥ or ٢٦) in z and y direction for hinge ends arch with maximum values equals to (٢.٥ and ٠.٧)kg/cm^{٢} respectively and it is greater than it is for fixed ends arch with maximum values equals to (-١.٧ and ٠.٤٣)kg/cm^{٢} for stresses in z and y – direction respectively ,see Figures (٥-٧٦) and (٥-٧٧) . But the maximum stresses in x – direction for fixed ends arch equals to (-١٨)kg/cm^{٢} and it is greater than it is for hinge ends arch that equal to (-١٣.٥)kg/cm^{٢} , see Figure (٥-٧٥) .

The maximum stresses at **Gauss** point (٢٥ or ٢٦) in y – direction is equal to (-٠.٦٢ and -٠.٦٦)kg/cm^{٢} for hinge – fixed and fixed – hinge ends arch respectively , see Figure (٥-٧٨) , but it is in x – direction equals to (١٤ and -١٨.٣) kg/cm^{٢} for hinge – fixed and fixed – hinge ends arch respectively , see Figure (٥-٧٩) . Figure (٥-٨٠) shows that maximum stresses at **Gauss** point (٢٥ or ٢٦) in z – direction equals to (٢ and ٢.٣)kg/cm^{٢} for hinge – fixed and fixed – hinge ends arch respectively .Figures (٥-٨١) and (٥-٨٢) show the stresses at the lower surface of arch's center at **Gauss** point (٢٧) in x – direction and the maximum value of fixed , hinge , hinge – fixed and fixed – hinge ends arch equals to (-٣٥,٩٠,٨٥ and ٨٦)kg/cm^{٢} respectively .

Figure (٥-٨٣) and (٥-٨٤) show the stresses at the upper surface of arch's center at **Gauss** point (٢٨) in x – direction and the maximum value for fixed , hinge , hinge – fixed and fixed – hinge ends arch equals to (٢٢,-٧٩,-٧٥ and -٧٩) kg/cm^{٢} respectively . Shear stresses in xy – plane versus time obtained at **Gauss** point (٦) (α=٠°) and at **Gauss** point (٥٣) (α=١٨٠°) because the maximum shear stresses at the supported . The maximum shear stresses at **Gauss** point (٦) in xy – plane equals to (٤١,١٠٩,٩٠ and ١٠٨)kg/cm^{٢} fixed , hinge , hinge – fixed and fixed – hinge ends arch respectively , see Figures (٥-٨٥) and (٥-٨٦) . The maximum shear stresses at **Gauss** point (٥٣) in xy – plane equals to (٤٧,-٥٥,-٧٠and -٥٣) kg/cm^{٢} for fixed , hinge , hinge – fixed and fixed – hinge ends arch respectively , see Figure (٥-٨٧) and (٥-٨٨) .

Table (٥-٦) Material Properties and Additional Parameters .

	Material Properties and Additional Parameter	Symbol , unit	Value
	Young's Modulus	EC (kg/cm^{٢})	٢٨٤٠٠٠
	Compressive Strength	Fc (kg/cm^{٢})	٣٦٦
	Tensile Strength	Ft (kg/cm^{٢})	٤٦

Concrete	**Poisson's Ratio**	ψ	٠.١٥
	Ultimate Compressive Strain	ε_{cu}	٠.٠٠٤
	Fracture Energy	G_f (kg/cm)	٠.١٥٣
	Yield Surface Function	α_c	١٠
	Mass Density	ρ_c (kg.sec^2/cm^4)	٠.٢٤٥E-٠٥
	Fluidity Parameter	a_0	٠.٣٠٥٥
		a_1	٠.٧٦
	Failure Surface Function	β_0	١.٨٤
		β_1	١.٠٩
Steel	**Young's Modulus**	E_S (kg/cm^2)	٢١٠٠٠٠٠
	Yield Stresses	F_y (kg/cm^2)	٤١٤٠
	Mass Density	ρ_s (kg.sec^2/cm^4)	١٤
	Poisson's Ratio	ψ	٠.٢
Newmark's Parameters		δ	٠.٥
		β	٠.٢٥

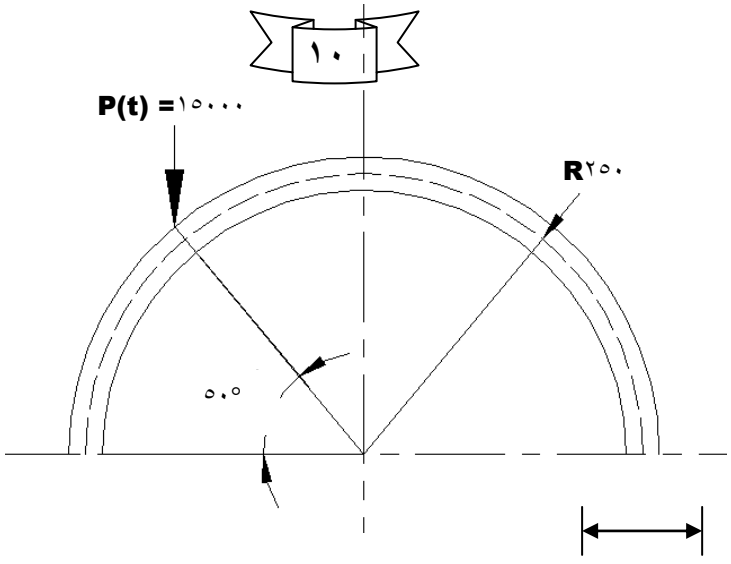

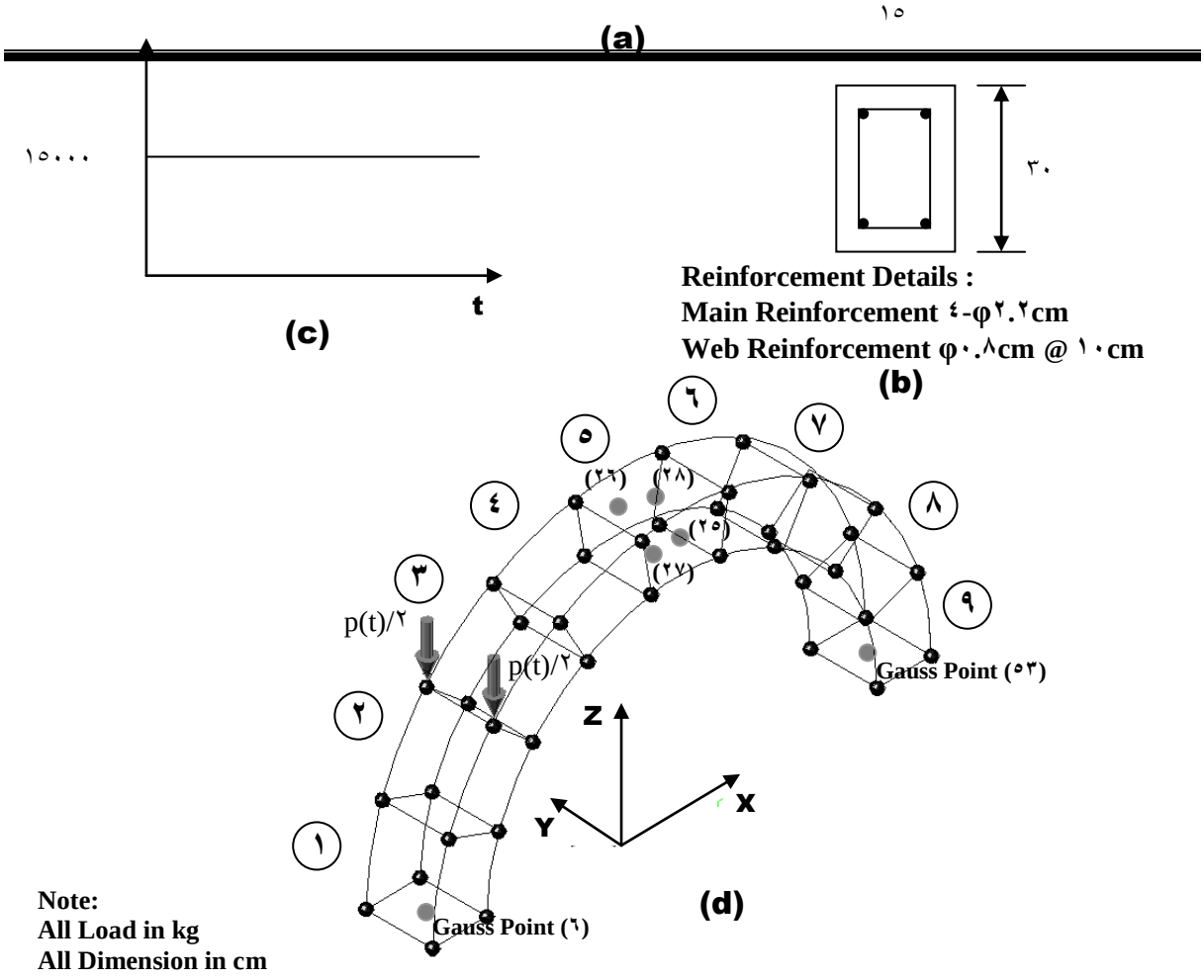

(a) geometry and loading of arch (b) cross section (c) load – time relation
(d) finite element idealization and numbering of half of the arch

Figure (٥-٦٤) Arch Structure with Different Boundary Condition .

Figure (٥-٦٥) Time – Displacement in X – Direction Response at (α=٥٠°) with Various Boundary Condition.

Figure (٥-٦٦) Time – Displacement in Z - Direction Response at (α=٥٠°) with Various Boundary Condition.

Figure (٥-٦٧) Time – Displacement in Y - Direction Response at (α=٥٠°) with Various Boundary Condition.

Figure (٥-٦٨) Time – Displacement in Y - Direction Response at (α=٥٠°) with Various Boundary Condition.

Figure (٥-٦٩) Time – Displacement in X - Direction Response at (α=٥٠°) with Various Boundary Condition.

Figure (٥-٧٠) Time – Displacement in Z - Direction Response at (α=٥٠°) with Various Boundary Condition.

α (Degree)

Figure (٥-٧١) The Displacement Along the Arch Under Dynamic Load with Hinge – Hinge Ends at (t=٠.٣٥ sec.).

α (Degree)

Figure (٥-٧٢) The Displacement Along the Arch Under Dynamic Load with Fixed – Fixed Ends at (t=٠.٣٥ sec.).

α (Degree)

Figure (٥-٧٣) The Displacement Along the Arch Under Dynamic Load with Fixed – Hinge Ends at (t=٠.٣٥sec.).

α (Degree)

Figure (٥-٧٤) The Displacement Along the Arch Under Dynamic Load with Hinge – Fixed Ends at (t=٠.٣٥sec.).

Figure (٥-٧٥) Time – Stresses in X - Direction Response at Gauss Point (٢٥ or ٢٦) With Various Boundary Condition.

Figure (٥-٧٧) Time – Stresses in Y - Direction Response at Gauss Point (٢٥ or ٢٦) With Various Boundary Condition.

Figure (٥-٧٨) Time – Stresses in Y - Direction Response at Gauss Point (٢٥ or ٢٦) With Various Boundary Condition.

Figure (٥-٧٩) Time – Stresses in Z - Direction Response at Gauss Point (٢٥ or ٢٦) With Various Boundary Condition.

Figure (٥-٨٠) Time – Stresses in Z - Direction Response at Gauss Point (٢٥ or ٢٦) With Various Boundary Condition.

Figure (٥-٨١) Time – Stresses in X - Direction Response at Gauss Point (٢٧) With Various Boundary Conditions .

Figure (٥ -٨٢) Time – Stresses in X - Direction Response at Gauss Point (٢٧) With Various Boundary Conditions.

Figure (٥-٨٣) Time – Stresses in X - Direction Response at Gauss Point (٢٨) With Various Boundary Conditions.

Figure (٥-٨٤) Time – Stresses in X - Direction Response at Gauss Point (٢٨) With Various Boundary Conditions.

Figure (٥-٨٥) Time – Shear Stresses in XY - Plane Response at Gauss Point (٦) with Various Boundary Conditions.

Figure (٥-٨٦) Time – Shear Stresses in XY - Plane Response at Gauss Point (٦) with Various Boundary Conditions.

Figure (٥-٨٧) Time – Shear Stresses in XY - Plane Response at Gauss Point (٥٣) with Various Boundary Conditions.

Figure (٥-٨٨) Time – Shear Stresses in XY - Plane Response at Gauss Point (٥٣) with Various Boundary Conditions.

٥.٣.٥ Simply Supported Reinforced Concrete Arch Under Concentrated Load with Harmonic Excitation Load–Time Function

In this example , we study the effect of thickness of reinforced layers , time step and initial displacement on a simply supported arch having cross section and reinforcement steel shown in Figure (٥-٨٩) subjected to concentrated load with harmonic excitation load – time function p(t)=١+sin٠.١t . The material properties of concrete and steel and addition parameters in Table (٥-٧) .

Figure (٥-٨٩)(d) shows the details of the finite elements mesh for all the reinforced concrete arch with seven of eight noded brick elements . The steel reinforcement by a four layers two of them represent a longitudal top and

bottom reinforcement with thickness equals to (٠.٥٢٤)cm for each layer and the others represent the lateral ties with thickness (٠.٠٠٩٤)cm for each layer and rotational angle equal to (٩٠°) from x – axis. For dynamic analysis , a constant time step of (٠.٠١sec.) is used , (١٥٠) numbers of time steps , a number of iteration for nonlinear solution is taken equals to (٥٠٠) .

In this example we studied the effect of thickness layers of main reinforcement on central deflection of this arch ,three cases from reinforcement were analyzed . The first case has main reinforcement with thickness of layers equals to (٠.٥١)cm and (٠.٢١)cm for the second case with maximum different equals to (١٤.٥٪) . Finally , the third case without main reinforcement layers, with the maximum different equals to (١٢.٧٪ and ٢٥.٤٪) with thickness of main reinforcement equals to (٠.٢١ and ٠.٥١)cm respectively . Figure (٥-٩٠) shows that ,the central deflection increases if the thickness of main reinforcement layers decreases . Figure (٥-٩١) shows the effect of change time step on central deflection of arch , if time step decreases central deflection and exactly of solution are increased . The maximum different between time step equals to (٠.٠١ and ٠.٠٠٥)sec. equals to (٢٩.٢٣٪) . We studied the effect of initial displacement at hinge in x – direction on central deflection and the result explained the initial displacement caused vibration in deflection .

Figures (٥-٩٢) and (٥-٩٣) show the difference is between the central deflection without the initial displacement and with the initial displacement equals to (٠.٢,-٠.٢)cm with maximum deflection equals to (٢٩.٦٪ and ٢٧.٥٪) respectively . Figure (٥-٩٤) shows that maximum value of central deflection when the initial displacement (-٠.٢)cm (opposite x – axis direction) is greater than it is when the initial displacement equals to (٠.٢cm) (in x – axis direction) with maximum different equals to (٥٧.٥٪) . When we assumed the initial displacement equals to (٠.٢)cm , the maximum stresses at **Gauss** point (٦) (at the center of arch) equal to (-١٢٣)kg/cm^{٢} but it is equal to (١١٠)kg/cm^{٢} when initial displacement is equal to (-٠.٢)cm , we obtained the maximum different equals to (١٠.٦٪) . But when no initial displacement , maximum stresses at **Gauss** point (٦) equals to (-٨.٥)kg/cm^{٢} as shown in Figures (٥-٩٥) and (٥-٩٦) .

Effect the thickness of main reinforcement layers on the stresses at **Gauss** point (٦) , as shown in Figure (٥-٩٧) . When the thickness of main reinforcement layers decreases the compressive stresses decreases but tensile stresses increases and the difference in compressive and tensile stresses between the reinforcement is equal to (٠.٥١ and ٠.٢١)cm equals to (٢٩٪ and ٦١.٥٪) respectively , but the different between the reinforcement equal to (٠.٢١)cm and no reinforcement is equal to (٣٤٪ and ٥٨.٠٦٪) for compressive and tensile stresses respectively .

Table (٥-٧) Material Properties and Additional Parameters .

	Material Properties and Additional Parameter	Symbol	Value
Concrete	Young's Modulus	E_C (kg/cm^2)	٣٠٠٠٠٠
	Compressive Strength	F_c (kg/cm^2)	٤٢٠
	Tensile Strength	F_t (kg/cm^2)	٢٨
	Poisson's Ratio	ψ	٠.١٥
	Ultimate Compressive Strain	ε_{cu}	٠.٠٠٣
	Fracture Energy	G_f (kg/cm)	٠.١٥٣
	Yield Surface Function	α_c	١٠
	Mass Density	ρ_c (kg.sec^2/cm^4)	٠.٢٤E-٠٥
	Fluidity Parameter	a_0	٠.٣٠٥٥
		a_1	٠.٧٦
	Failure Surface Function	β_0	١.٨٤
		β_1	١.٠٩
Steel	Young's Modulus	E_S (kg/cm^2)	٢٠٠٠٠٠٠
	Yield Stresses	F_y (kg/cm^2)	٣٨٤٠
	Mass Density	ρ_s (kg.sec^2/cm^4)	١٤
	Poisson's Ratio	ψ	٠.٢
Newmark's Parameters		δ	٠.٥
		β	٠.٢٥

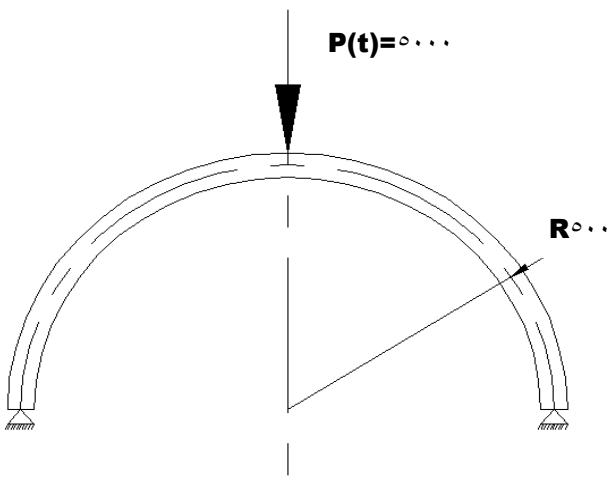

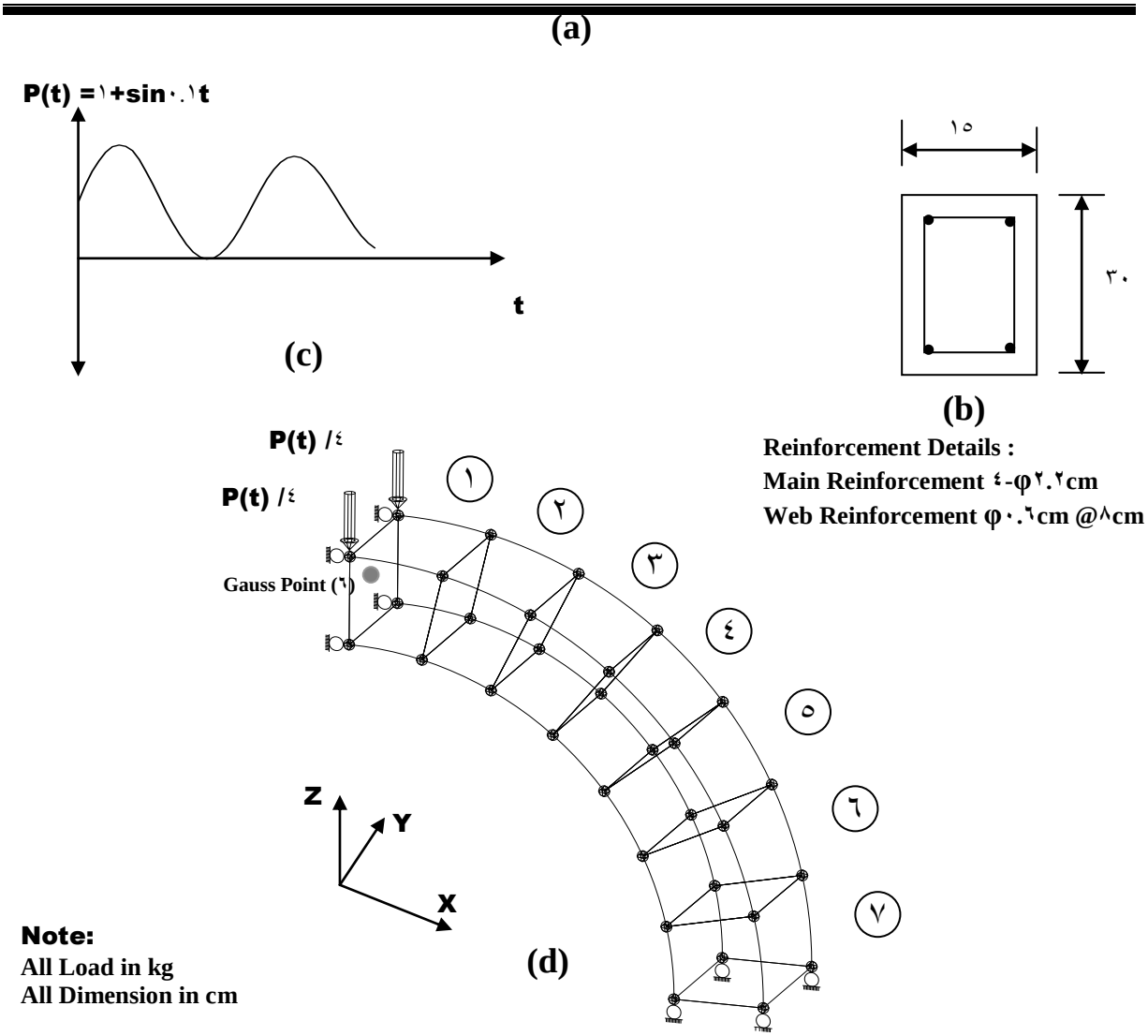

(a) geometry and loading of arch (b) cross section (c) load – time relation
(d) finite element idealization and numbering of half of the arch

Figure (٥-٨٩) Simply Supported Arch Under Concentrated Load with Harmonic Excitation Load – Time Function

Figure (٥-٩٠) Effect the Thickness of Main Reinforcement Layers on Time – Displacement in Z - Direction Response at Center of Arch .

Figure (٥-٩١) Effect the Time Step on Time – Displacement in Z - Direction Response at Center of Arch .

Figure (٥-٩٢) Effect the Initial Displacement in X - Direction on Time – Displacement in Z - Direction Response at Center of Arch .

Figure (٥-٩٣) Effect the Initial Displacement opposite X – Direction on Time – Displacement in Z - Direction Response at Center of Arch .

Figure (٥-٩٤) Effect the Initial Displacement on Time – Displacement in Z - Direction Response at Center of Arch

Figure (٥-٩٥) Time – Stresses in X - Direction Response at Gauss Point (٦) .

Figure (٥-٩٦) Effect the Initial Displacement on Time – Stresses Response at Gauss Point (٦) .

Figure (٥-٩٧) Effect the Thickness of Main Reinforcement Layers on Time – Stresses Response at Gauss Point (٦) .

٥.٣.٦ Reinforced Concrete Clamped Circular Arch Structure of Continuously Varying Cross – Section

In this example, two cases of circular arch structure was studied with continuously varying cross – section . Figures (٥-٩٨a) and (٥-٩٨b) show the geometry , loading and cross-section of arch . Due to symmetry , half of the arch with six of eight noded brick elements for the two case , as shown in Figures (٥-٩٨a) and (٥-٩٨b) .

The steel reinforcement is represented by four layers for each case . Two of them representing the longitudinal top and bottom reinforcement with thickness equals to (٠.٠٩٢٥)cm for each layers , the others represent the lateral ties with thickness equals to (٠.٠٢٥)cm for each and with a rotational angle of (٩٠°) from the local x- axis .The material properties and the model parameters for concrete and steel as shown in Table (٥-٨) .

For dynamic analysis , a constant time step of (٠.٠٠٠٥)sec. is used , (٢٠٠٠) numbers of time steps , a number of iteration for nonlinear solution is taken equals to (٥٠٠) .

The deflection at the center of arch for case(٢) is greater than it's for case(١) , as shown in Figure (٥-٩٩) that because the smaller section at the center of arch in case(٢) .

The displacement at (α=٤٥°) was studied because the two arches have the same section at this angle , the displacement in y-direction for case(٢) is greater than it's for case(١) . But the displacement in z-direction at (α=٤٥°) for case (١) is greater than it's for case(٢) , as shown in Figures (٥-١٠٠),(٥-١٠١) and (٥-١٠٢) .

The stresses in x,y and z-direction at arch´s center (**Gauss** point (٦)) for case(٢) greater than it's for case (١) , as shown in Figures (٥-١٠٣),(٥-١٠٤) and (٥-١٠٥) .

The shear stresses at supported (Gauss point (٣٥)) for case (١) greater than it's for case (٢) , as shown in Figures (٥-١٠٦),(٥-١٠٧) .

Table (٥-٨) Material Properties and Additional Parameters .

	Material Properties and Additional Parameter	Symbol , unit	
Concrete	Young's Modulus	E_C (kg/cm^2)	٢٨٤٠٠٠
	Compressive Strength	F_c (kg/cm^2)	٣٦٦
	Tensile Strength	F_t (kg/cm^2)	٤٦
	Poisson's Ratio	ψ	٠.١٥
	Ultimate Compressive Strain	ε_{cu}	٠.٠٠٤
	Fracture Energy	G_f (kg/cm)	٠.١٥٣
	Yield Surface Function	α_c	١٠
	Mass Density	ρ_c (kg.sec^2/cm^4)	٠.٢٤٥E-٠٥
	Fluidity Parameter	a_0	٠.٣٠٥٥
		a_1	٠.٧٦
	Failure Surface Function	β_0	١.٨٤
		β_1	١.٠٩
Steel	Young's Modulus	E_S (kg/cm^2)	٢١٠٠٠٠٠
	Yield Stresses	F_y (kg/cm^2)	٤١٤٠
	Mass Density	ρ_s (kg.sec^2/cm^4)	١٤
	Poisson's Ratio	ψ	٠.٢
Newmark's Parameters		δ	٠.٥
		β	٠.٢٥

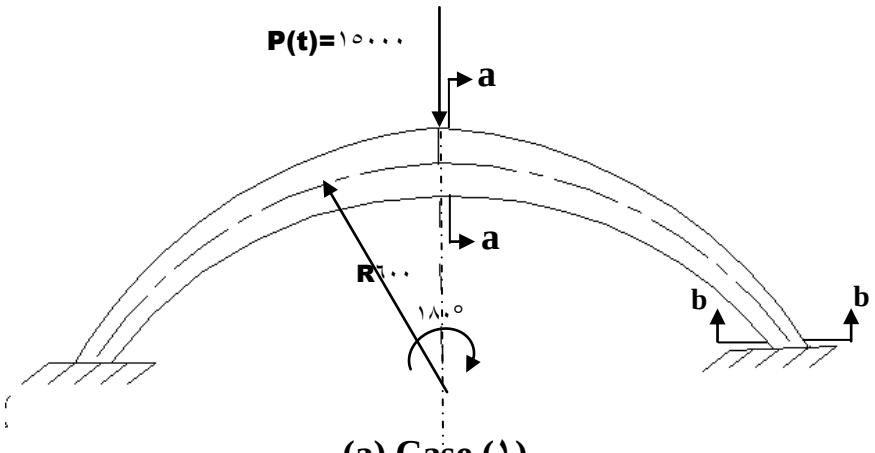

(a) Case (١)

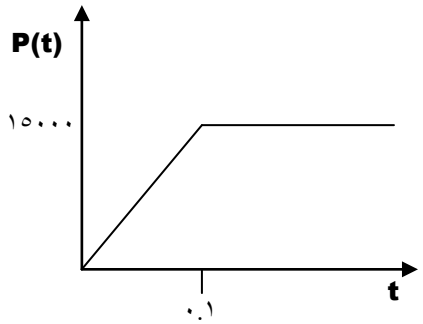

(c)

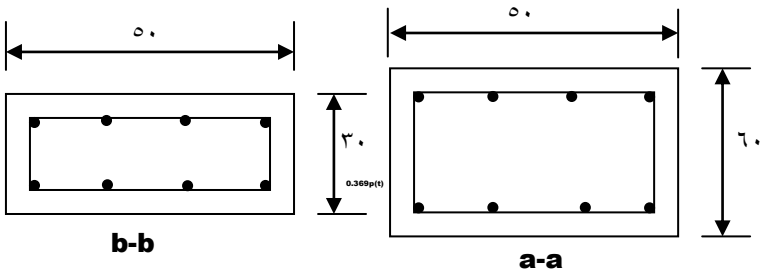

Reinforcement Details :
Main Reinforcement ٨-φ١.٢cm
Web Reinforcement φ١.٢cm @ ١٠cm

(b)

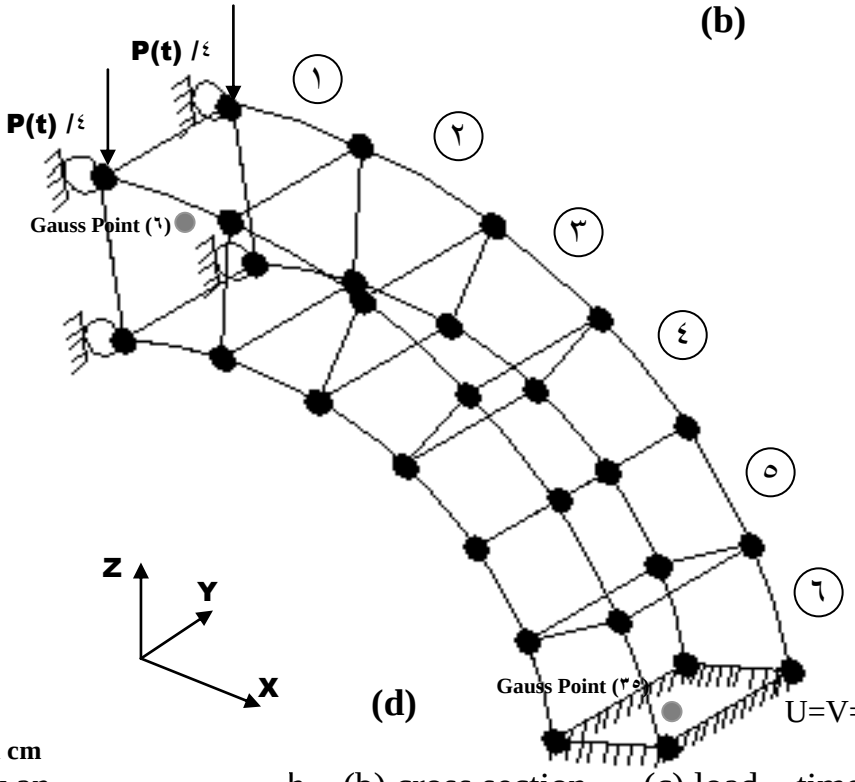

(d)

U=V=W=٠

Note:
All Load in kg
All Dimension in cm

(a) geometry and loading of arch (b) cross section (c) load – time relation
(d) finite element idealization and numbering of half of the arch

Figure (٥-٩٨a) Non-prismatic Clamped Circular Arch Structure of Continuously Varying Cross – Section

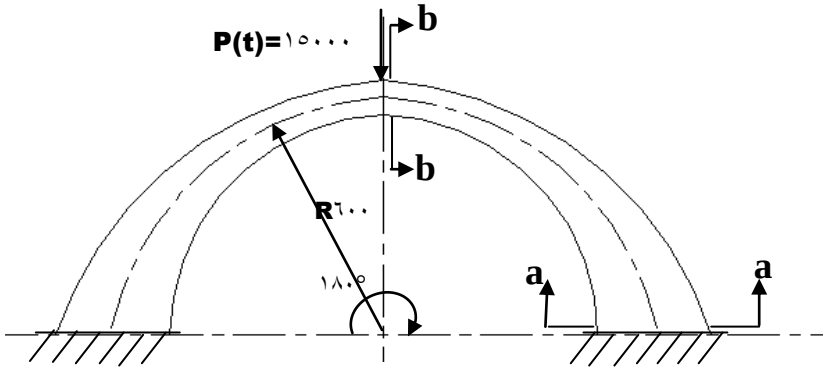

(a) Case (٢)

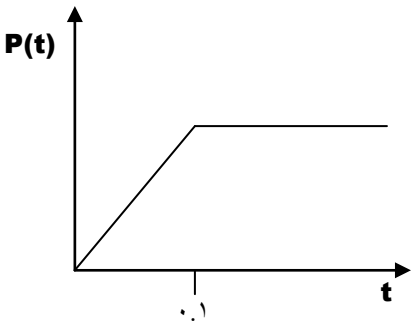

(c)

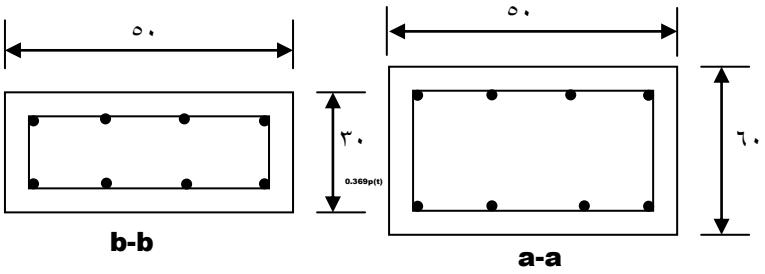

Reinforcement Details :
Main Reinforcement ٨-φ١.٢cm
Web Reinforcement φ١.٢cm @ ١٠cm

(b)

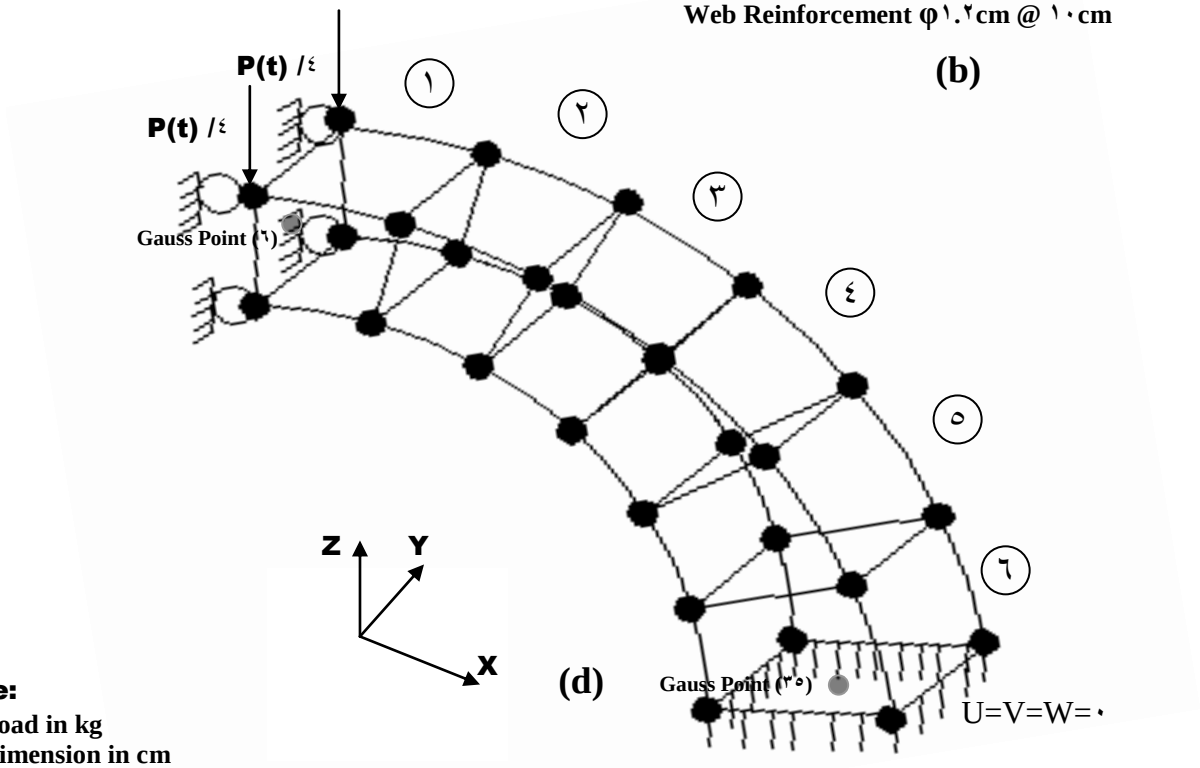

(d)

Note:
All Load in kg
All Dimension in cm

(a) geometry and loading of arch (b) cross section (c) load – time relation
(d) finite element idealization and numbering of half of the arch

Figure (٥-٩٨b) Non-prismatic Clamped Circular Arch Structure of Continuously Varying Cross – Section

Figure(٥-١٠٠) Time – Displacement in Y – Direction Response of the Circular Arch at (α=٤٥°)

Figure(٥-٩٩)Time – Displacement in Z – Direction Response of The Center Circular Arch

Figure(٥-١٠١)Time – Displacement in X – Direction Response of the Circular Arch at (α=٤٥°)

Figure(٥-١٠٢)Time – Displacement in Z – Direction Response of the Circular Arch at (α=٤٥°)

Figure(٥-١٠٣) Time – Stresses in X – Direction Response at Gauss Point (٦) of Center Circular Arch

Figure(٥-١٠٤)Time – Stresses in Y – Direction Response at Gauss Point (٦) of Center Circular Arch

Figure(٥-١٠٥)Time – Stresses in Z – Direction Response at Gauss Point (٦)of Center Circular Arch

Figure(٥-١٠٧) Time – Shear Stresses in XY - Plane Response at Gauss Point (٣٥) with Various Boundary Conditions.

Figure(٥-١٠٦) Time – Shear Stresses in YZ - Plane Response at Gauss Point (٣٥) with Various Boundary Conditions.

CHAPTER SIX

CONCLUSIONS AND RECOMMENDATIONS

٦.١ Conclusions

Based on the results obtained from the nonlinear finite element analysis of dynamic response of arch structures and comparison with other available results, the following conclusions can be drawn :

١- The comparison between the results of reinforced concrete arch structures under dynamic loading obtained from the present study by **(DARC٣)** and results obtained from another numerical methods gave a good agreement . From this was found that the program of **(DARC٣)** can solve the reinforced concrete arch structures .

٢- The deflection and shear stresses of arch without damping is greater than deflection and shear stresses for damping by difference about (٦٠.٢٩٪) and (٧٩.٦٪) respectively .

٣- For cantilever arch , for the subtended angle less than (٦٠º) the shear stresses in XZ and XY – plane at supported increased when the subtended angle decreases . Shear stresses in YZ – plane for subtended angles equals to (٣٠º and ٩٠º) is less than the shear stresses in this plane for subtended angle equals to (٦٠º) .

٤- The effect of the width of cross sections was noticed to have most pronounced effect on the time – deflection curve of arch structure . It was found that the increase of width from (٤٠)cm to (٥٠)cm , the maximum central deflection decreases of about (١٨%) .

٥- The maximum central deflection for arch structure plain concrete is greater than it is of reinforced arch with (٠.٢٣٦)cm thick for main layers and (٠.١٢٧)cm thick for web layers reinforcement by about (٧.٤٪) . But the maximum stresses in arch's center for plain concrete is less than it is for this reinforced arch with main and web reinforcement by about (٣٠٪) that in elastic stage .

٦- The maximum deflections in Z and Y – direction under point load at (α=٥٠°) for hinge ends arch is greater than it is for fixed ends arch , but the inverse happened for horizontal deflection . And the maximum deflection in Z and Y – direction under point load at (α=٥٠°) for hinge – fixed ends arch is greater than it is for fixed – hinge ends arch , but for maximum horizontal deflection the inverse is happened .

٧- If initial displacement happened in the supported of arch , the maximum central deflection increases , when this displacement in the direction and opposite the direction of X – axis with magnitude equals to (٠.٢,-٠.٢)cm the maximum difference of central deflection by about (٥٧.٥٪) .

٦.٢ Recommendations

١- Extending of the present work to include the geometric nonlinearity .
٢- Study the effect of earthquake on the reinforced concrete arch structures.
٣- Supporting the behavior of reinforced concrete arch structures experimentally .
٤- Investigating the behavior of arch structures with taking into account the bond slip between the concrete and steel bars .
٥- The construction of prestressed concrete structures such as long span bridges have been increasing used in the past few decades , so prestressing can be incorporated into the adopted three dimensional brick element .
٦- The failure surface used to characterize concrete material can be modified by incorporating a highly sophisticated triaxial concrete failure surface .

٧- Fiber reinforced concrete arch structures which are believed to improve the tensile properties of concrete can be incorporated in the developed program in this study .

٨- Extending the proposed method to the analysis of reinforced concrete arches under moving loads .

٩- Another approach by **Gilbert** [٣٧] is generally termed as the steel referred method can be adopted in the analysis to represent the tension stiffening effects . This model takes into account the direction and location of the reinforcement in the thickness direction relative to the crack .

١. **Abdul Kreem, I. M.,** " Nonlinear Analysis of Reinforced concrete Thick Plate Foundation on Cohesive Soil ", M.SC. Thesis, University of Babylon, Hill, Iraq, ٢٠٠٣ .

٢. **AL – Gharbawi, A.A.S.,** " Comparative Study of Recent Constitutive Relation of Continua ", M.SC. Thesis, Baghdad University, ١٩٨٤ .

٣. **AL – Naimi, H.A.,** " ٣-Dimensional Dynamic and Static Time – Dependent Finite Element Analysis of R.C. Members ", Ph.D. Thesis, Baghdad University, ١٩٩٦ .

٤. **Ali, A.A.,** " Nonlinear Analysis of Structures with Prismatic or Non - Prismatic Members Under Static and Dynamic Loading ", Ph.D. Thesis, University of Technology, ١٩٩٩ .

٥. **Arnesen, A., Sqresen, S.I.** and **Bergan, P.G.,** " Nonlinear Analysis of Reinforced Concrete ", Computers and Structures, Vol. ١٢, PP. ٥٧١-٥٧٩, ١٩٨٠ .

٦. **AL-Maroof, M.A.,** " Dynamic Analysis of Curved Members Using Curved Finite Element ", M.SC. Thesis, University of Baghdad, Iraq, ١٩٨٧ .

٧. **AL-Daami. H.H.M.,** " Transient Response of Systems with Non – Prismatic Members by Characteristics ", M.SC. Thesis, Saddam University, Iraq, ١٩٩٢ .

٨. **Ashwell, D.G., Sabir, A.B.** and **Roberts, T.M.,** " Further Studies in the Application of Curved Finite Element to the Circular Arches ", Internatinal Journal of Mechanical Sciences, Vol. ١٣, PP. ٥٠٧-٥١٧, ١٩٧١ .

٩. **Ashwell, D.G.** and **Gallagher, R.H.,** " Finite Element for Thin shells and Curves Members ", John Wily & Sons, London, ١٩٧٦ .

١٠. **Antoon, S.R.,** " General – Purpose Finite Element Program for Static Three – Dimensional Analysis of Elastic Structures ", M.SC. Thesis, University of Baghdad, Iraq, ١٩٨٥ .

١١. **Akhtar, M.N.,** " Element Stiffness of Circular Member ", Journal of Structural Engineering, Vol. ١١٣, No. ٤, April, PP. ٨٦٧-٨٧٢, April, ١٩٨٧.

١٢. **Abdul – Hameed, M.F.,** " Plastic Analysis of Non – Prismatic Arches " M.SC. Thesis, University of Baghdad, December, ١٩٩٢ .

١٣. **AL-Daami, H.H.,** " Linear and Nonlinear Static and Free Vabration Analysis of Thin – Walled Cellular and Ribbed Spherical Domes by Spherical Grillage Analogy ", Ph.D. Thesis, Department of Civil Engineering, University of Baghdad, Iraq, ٢٠٠٠ .

١٤. **AL – Naimi, H.A.,** " Dynamic Analysis of Axisymmetric Bodies Under Arbitrary Loadings " M.SC. Thesis for University of Babylon, ١٩٨٨ .

١٥. **AL – Temeemi, M.A.,** " Nonlinear Analysis of Reinforced Concrete Curved Beam on Elastic Foundation ", M.SC. Thesis, University of Babylon, Iraq, ٢٠٠٥ .

١٦. **Austin, W.J.** and **Veletsos, A.S.,** " Free Vibration of Arches Flexible in Shear ", JEMDiv. Vol. ٩٩, No. EM٤, pp. ٧٣٥ – ٧٥٣, ١٩٧٣ .

١٧. **Bicanic, N.** " Nonlinear Finite Element Transient Response of Concrete Structures ", Ph.D. Thesis, University of Wales, Swansea, ١٩٧٨ .

١٨. **Bicanic, N.** and **Zienkiewicz, O.C.,** " Constitutive Model for Concrete Under Dynamic Loading ", Earthquake Engineering and Structure Dynamic, ١١, ٦٨٩ – ٧١٠, ١٩٧٣ .

١٩. **Bazant, Z.P.** and **Gedolin, L.,** " Fracture Mechanics of Reinforced Concrete ", ASCE, EM٦, Vol. ١٠٦, PP. ١٢٨٧ – ١٣٠٦, ١٩٨٠ .

٢٠. **Bathe, K.J.** and **Ramaswamy, S.,** " On Three – Dimensional Nonlinear Analysis of Concrete Structures ", Nuclear Engineering and Design, Vol. ٥٢, PP. ٣٨٥ – ٤٠٩, ١٩٧٩ .

References

٢١. **Bath, K.J., Wakazak, J., Welch, A.** and **Mistry, N.,** " Nonlinear Analysis of Concrete Structures ", Computers and Structures, Vol. ٣٢, No. ٣١٤, PP. ٥٦٣ – ٥٩٠, ١٩٨٩ .

٢٢. **Bathe, K.J.,** " Finite Element Procedures in Engi~eering Analysis ", Prentic – Hall, ١٩٨٢ .

٢٣. **Chen, W.F.,** " Plasticity in Reinforced Concrete ", McGraw, Hill co., ١٩٨٢ .

٢٤. **Cook, R.D.,** " Concepts and Application of Finite Element Analysis ", ٢nd Edition, John Wiley & Sons, New York, ١٩٨١ .

٢٥. **Cervera, M., Hinton, E.** and **Hassan, O.,** " Nonlinear Analysis of Reinforced Concrete Plates and Shell Structures Using ٢٠ – Noded Isoparametric Element ", Computers and Structures, Vol. ٢٥, No. ٦, ١٩٨٧.

٢٦. **Cappelli, A.P., Aprawal, G.L.,** and **Romero, V.E.,** "A computer Program for Elastic Plastic Analysis of Dame Structures and Arbitrary Solids of Revolution Subjected to Unsymmetrical Loadings ", Service Bureau Corporation, Inglewood, Galifornia, AFWL – TR -٦٩ – ١٤٦ .Air force weapons laboratory, Kirtland AFB, New Mexico, ١٩٧٠ .

٢٧. **Clough, R. w.** and **Penzien, J.,** "Dynamics of Structures " Inteenational STtudent Edition, McGraw, Hill co., ١٩٨٢ .

٢٨. **Chaudhuri, S.K.** and **Shore, S.,** " Thin – Walled Curved Beam Finite Element ", JEMDiv, Vol. ١٠٣, No. EMS, PP. ٩٢١ – ٩٣٧, ١٩٧٧ .

٢٩. **Chen, F., Liang, J., Chen, Y., Liu, Y.** and **Ma, H.** " Bifurcation Analysis of An arch Structure with Parametric and Forced Excitation", Journal of Mechanics Research Communications, ٢٠٠٥ .

٣٠. **Desai, C.S.,** and **Abel, J.F.,** " Introduction to the Finite Element ", Van Nostrand Reinhold, ١٩٧٢ .

٣١. **Dawe, D.J.,** " Curved Finite Elements for the Analysis of Shallow and Deep Arches ", Computers and Structures, Vol. ٤, PP. ٧٢٩ – ٧٤٠, ١٩٧٤.

٣٢. **Dabrowski, R.,** " Curved Thin – Walled Girders ", Translated from the German by Amerongen, C.V., Springer Verlag Berlin, ١٩٦٨ .

٣٣. **Duham, R.S.,** and **Nickell, R.E.,** " Finite Element Analysis of Axisymmetric Solids with Arbitrary Loadings ", Structural Engineering Laboratory, Report (٦٧ – ٦), University of California, Berkeley, ١٩٦٧ .

٣٤. **Dai, H.H.** and **Bi, Q.,** " Analysis of Nomlinear Dynamic and Bifurcations of A shallow Arch Subjected to Periodic Excitation with Internal Resonance ", Journal of Sound and Vibration, ٢٠٠٠ .

٣٥. **Darzy, S.Y.,** " Static and Dynamic Analysis of Reinforced Concrete Bridges ", M.SC. Thesis for University of Mosul, ١٩٨٨ .

٣٦. **Evans, H.R.,** and **AL – Rifaie, W.N.,** " An experimental and Theoretical Investigation of the Behavior of Box Girders Curved in Plane ", Proc., Instn. Civil Engineering , London, England, ٢(٥a), PP. ٣٢٣ – ٣٥٢, ١٩٧٥ .

٣٧. **Gilbert, R.I.** and **Warner, R.F.,** " Tension Stiffening in Reinforced Concrete Slabs ", Journal of Structural Div., ASCE, Vol. ١٠٤, No. ST١٢, ١٩٧٨ .

٣٨. **Ghosh, S.,** and **Wilson, E.L.,** " Dynamic Stresses Analysis of Axisymmetric Structures Under Arbitrary Loading ", Earthquake Research Center, Report (EERC ٦٩ – ١٠), University of California, Berkely, ١٩٦٩ .

٣٩. **Gutierrez, R.H.** and **Laura, P.A.A.** " In Plane Vibrations of Non Circular Arcs of Non Uniform Cross – Section " Journal of Sound and Vibration, ١٢٩(٢), PP.١٨١ – ٢٠٠, ١٩٨٩ .

٤٠. **Hatano, T.** " Dynamic Behavior of Concrete Under Periodical Compressive Load ", Central Research Institute of Electric Power Industry, C. ٦١٠٤, Tokyo, ١٩٦٢ .

٤١. **Hatano, T.** " Dynamic Behavior of Concrete Under Impulsive Tensile Load ", Central Research Institute of Electric Power Industry, C.٦٠٠٢, Tokyo, ١٩٦٠ .

٤٢. **Hatano, T.** " Relations Between Strength of Failure, Strain Ability Elastic Modulus and Failure Time of Concrete ", CeNTRAL Research Institute of Electric Power Industry, C.٦٠٠١, Tokyo, ١٩٦٠ .

٤٣. **Husain, A.H.** " Static Analysis Shell Foundation by Finite Elements ", M.SC. Thesis University of Kufa, Najaf, Iraq, ٢٠٠٢ .

٤٤. **Hinton, E.** " Numerical Method and Software for Dynamic Analysis of Plate and Shell ", Pineridge Press limited, ١٩٨٨ .

٤٥. **Hinton, E.** and **Owen, D.R.J.,** " Finite Element Programming ", Academic Press, Swansea, U.K., ١٩٧٧ .

٤٦. **Hatano, T.** and **Tsutsumi, H.,** " Dynamic Compressive Deformation and Failure of Concrete Under Earthquake Load " Proc. ٢nd WCEE, Tokyo, PP. ١٩٦٣ – ١٩٧٨, ١٩٦٠ .

٤٧. **Hatano, T. a**nd **Watanabe, H.** " Fatigue Failure of Concrete Under Periodic Compressive Load ", Transactions JSCE, PP. ١٠٦ – ١٠٧, ١٩٧١ .

٤٨. **Henrych, J.,** " The Dynamic of Arches and Frames ", Elsevier Scientific Publishing Company, ١٩٨١ .

٤٩. **Hsiao, K.M.** and **Yang, R.T.** " A co-rotational Formulation for Nonlinear Dynamic Analysis of Curved Eular Beam ", Journal of Computers and Structures, Vol. ٥٤, No. ٦, PP. ١٠٩١ – ١٠٩٧, ١٩٩٥ .

٥٠. **Huang, C.S., Nieh, K.Y.** and **Yang, M.C.,** " In – Plane Free Vibration and Stability of Loading and Shear – Deformation Circular Arches ", International Journal of Solid and Structures ٤٠, PP. ٥٨٦٥ – ٥٨٨٦, ٢٠٠٣ .

٥١. **Hadi, W.K.,** " Elastic – Plastic Analysis of Reinforced Concrete Shallow Arches Frames Using Curved Beam Element ", M.SC. Thesis of University of Babylon, ٢٠٠٢ .

٥٢. **Just, D.J.,** " Circularly Curved Beam Under Plane Loads ", Journal of the Structural Division, Vol. ١١٠٨, No. ST٨, PP. ١٨٥٨ – ١٨٧٣, August, ١٩٨٢ .

٥٣. **Kupfer, H., Hilsodorf, K.H.** and **Rush, H.,** " Behavior of Concrete Under Biaxial Stresses ", Proc. ACI, ٦٦, PP. ٦٥٦ – ٦٦٦, ١٩٦٩ .

٥٤. **Kang, Y.J.,** " Nonlinear Geometric Material and Time Dependent Analysis of Reinforced and Prestressed Concrete Frames ", UCSESM Report No. ٧٧ – ١, Division of Structural Engineering and Structural Mechanics, University of California, Berkeley, Journal ١٩٧٧ .

٥٥. **Krauthammer, J.** and **Puglisi, R.D.,** " Simplified Analysis of Buried Reinforced Concrete Arches Under Simulated Unclear Loads ", Journal of Computers and Structures, Vol. ٤٣, Issue ٦, PP. ١٠٢٩ – ١٠٣٩, ١٩٩٢ .

٥٦. **Lin, C.S. and Scodelies, A.C.,** " Nonlinear Analysis of Reinforced Concrete Shells of General Form ", Journal of Structural Division ASCE, Vol. ١٠١, No. ST٣, March, ١٩٧٥ .

٥٧. **Litewka, P.** and **Rakowski, j.,** " The Exact Thick Arch Finite Element ", Computers and Structures, Vol. ٦٨, PP. ٣٦٩ – ٣٧٩, ١٩٩٨ .

٥٨. **Liu, G.R.** and **Wu, T.Y.,** " In – Plane Vibration Analyses of Circular Arches by the Generalized Differential Quadrature Rule ", Vol. ٤٣, Issue ١١, PP. ٢٥٩٧ – ٢٦١١, ٢٠٠١ .

٥٩. **Lee, Y.Y., Poon, W.Y.** and **Ng, C.F.,** " Anti – Symmetric Mode Vibration of A curved Beam Subjected to Autoparametric Exicitation ", Journal of Sound and Vibration, Vol. ٢٩٠, Issue ١-٢, PP. ٤٨ – ٦٤, ٢٠٠٦ .

٦٠. **Lee, S.L., Swaddiwudhipong, S.** and **Alwis, W.A.M.,** " Dynamic Response of Elasto – Plastic Planar Arches ", Journal of Structural Engineering and Mechanics, Vol. ٤, No. ١, PP. ٩ – ٢٣, ١٩٩٦ .

٦١. **Mehlhorn, G.** and **Klein, D.,** " Finite Element of Reinforced Concrete Slabs and Panels ", PP. ٤٥٣ – ٤٧٣, " Nonlinear Finite Element Analysis ", Journal of Structural Mechanics, Bathe, ١٩٧٧ .

٦٢. **Martin, H.C.,** " Introduction to Matrix Method of Structural Analysis ", McGraw – Hill, New York, ١٩٦٦ .

٦٣. **Morris, D.L.,** " Curved Beam Stiffness Coefficients ", Journal of Structural Division, Vol. ٩٤, No. ST٥, PP. ١١٦٥ – ١١٧٤, ١٩٦٨ .

٦٤. **Meck, H.R.,** " An accurate Polynomial Displacement Function for Finite Rings Elements ", Journal Computers and Structural, Vol. ١١, PP. ٢٦٥ – ٢٦٩, ١٩٨٠ .

٦٥. **Ngo, D.** and **Scordelis, A.C.,** " Finite Element Analysis of Reinforced Concrete Beams ", ACI Journal, Vol. ٦٤, No. ٣, March, ١٩٦٧ .

٦٦. **Nelissen, L.J.M.,** " Biaxial Testing of Normal Concrete ", Heron, ١٨, No. ١, Delft, ١٩٧٢ .

٦٧. **Newmark, N.M.,** " A method of Computation for Structural Dynamic ", Journal Engineering Mechanics Division, ASCE, ٨٥, PP. ٦٧ – ٩٤, ١٩٥٩ .

٦٨. **Noor, A.K.** and **Knight, N.F.,** " Nonlinear Dynamic Analysis of Curved Beam ", Comp. Meth. in Appl. Mech. and Engng., Vol. ١٦, PP. ٢٣٥ – ٢٤٧, ١٩٧٩ .

٦٩. **Owen, D.R.J.** and **Hinton, E.** " Finite Element in Plasticity : Theory and Practice ", Pineridge Press Limited, Swansea, V.K., ١٩٨٠ .

٧٠. **Oden, J.T.,** " Finite Elements of Nonlinear Continua ", McGraw – Hill, ١٩٧٢ .

٧١. **Perzyna, P.,** " Fundamental Problems in Viscoplasticity ", Adv. Appl. Mech., ٩, PP. ٢٤٣ – ٣٧٧, ١٩٦٦ .

٧٢. **Prathap, G.** and **Bhashyam, G.R.,** " Reduced Integration and the Shear – Flexible Beam Element ", IJNME, Vol. ١٨, PP. ١٩٥ – ٢١٠, ١٩٨٢ .

٧٣. **Prathap, G.,** " The Curved Beam /Deep Arch/ Finite Ring Element Revisited ", IJNME, Vol. ٢١, PP. ٣٨٩ – ٤٠٧, ١٩٨٥ .

٧٤. **Prathap, G.,** and **Babu, R.C.,** " An isoparametric Quadratic Thick Curved Beam Element ", IJNME, Vol. ٢٣, PP. ١٥٨٣ – ١٦٠٠, ١٩٨٦ .

٧٥. **Palaninathan, R.** and **Chandrasekharan, P.S.,** " Curved Beam Element Stiffness Matrix Formulation ", Journal of Computers and Structural, Vol. ٢١, No. ٤, PP. ٦٦٣ – ٦٦٩, ١٩٨٥ .

٧٦. **Park, J.H.** and **Kim, J.H.** " Dynamic Analysis of Rotating Curved Beam with A tip Mass ", Journal of Sound and Vibration, PP. ١٠١٧ – ١٠٣٤, ١٩٩٩ .

٧٧. **Rao, S.S.,** " Mechanical Vibrations ", Purdue University, ١٩٨٦ .

٧٨. **Rogers, B.G.** and **Munse, W.H.,** " Plastic Analysis and Design of Non Prismatic Members ", Journal of tha structural Division, ASCE, Vol. ٩١, NO. St٥, PP. ٢٩٩ – ٣٢٤, ١٩٦٥ .

٧٩. **Sabir, A.B., Djoudi, M.S.** and **Sfendji, A.** " The Effect of Shear Deformation on the Vibration of Circular Arches by the Finite Element Method ", Thin – Walled Structures, Vol. ١٨, Issue ١, PP. ٤٧ – ٦٦, ١٩٩٤ .

٨٠. **Scanlon, A.** and **Murray, D.W.,** " Time Dependent Reinforced Concrete Slab Deflections ", Journal of Structural Division, ASCE, Vol. ١٠٠, ST٩, Sep., ١٩٧٤ .

٨١. **Shanmugam,N.E., Thevendran, V., Liew, J.Y.R.** and **Tan, L.O.,** Journal of Structural Engineering, Vol. ١٢١, No. ٢, February, ١٩٩٥ .

٨٢. **Tene, Y., Epstein, M.** and **Sheinman, I.** " Dynamics of Curved Beams Involving Shear Deformation ", IJsost, Vol. ١١, PP. ٨٢٧ – ٨٤٠, ١٩٧٥ .

٨٣. **Tessler, A.** and **Spiridigliozzi, L.,** " Curved Beam Elements with Penalty Relaxation ", IJNME, Vol. ٢٣, PP. ٢٢٤٥ – ٢٢٦٢, ١٩٨٦ .

٨٤. **Veletsos, A.S., Austin, W.J., Pereira, C.A.L.** and **Wung, S.J.,** " Free In – Plane Vibration of Circular Arches ", JEMDIV., Vol. ٩٨, PP. ٣١١ – ٣٢٩, ١٩٧٢ .

٨٥. **Winter, G.** and **Nilson, A.H.,** " Design of Concrete Structures ", McGraw – Hill Kogakusha, Ltd. PP. ٤٣١ – ٤٩٠, ١٩٧٢ .

٨٦. **Wang, C.K.,** " Statically Indeterminate Structures ", McGraw – Hill Book Company, INC., PP. ٣٤٥ – ٣٨٤, ١٩٥٢ .

٨٧. **Waldron, P.,** " Elastic Analysis of Curved Thin – Walled Girders Including the Effect of Warping Restraint ", Est., Vol. ١, April, PP. ٩٣ – ١٠٤, ١٩٨٥ .

٨٨. **Wu, J.S.** and **Chiang, L.K.,** " Dynamic Analysis of An arch Due to A moving Load ", Journal of Sound and Vibration ٢٦٩, PP. ٥١١ – ٥٣٤, ٢٠٠٤.

٨٩. **Xu, J.X., Huang, H., Zhang, P.Z. and Zhow, J.Q.,** " Dynamic Stability of Shallow Arch with Elastic Supports – Application in the Dynamic Stability Analysisi of Inner Winding of Transformer During Short Circuit", International Journal of Nonlinear Mechanics ٣٧, PP. ٩٠٩ – ٩٢٠, ٢٠٠٢ .

٩٠. **Yoo, C.H.** and **Fehrenbach, J.P.,** " Natural Frequencies of Curved Girders ", JEMDIV, Vol. ١٠٧, No. EM٢, PP. ٣٣٩ – ٣٥٤, ١٩٨١ .

٩١. **Yamada, Y.** and **Ezawa, Y.,** " On Curved Finite Elements for the Analysis of Circular Arches ", IJNME, Vol. ١١, PP. ١٦٤٥ – ١٦٥١, ١٩٧٧ .

٩٢. **Zong, Z.H., Jaishi, B.,Ge, J.P.** and **Ren, W.Y.,** " Dynamic Analysis of A half – Through Concrete – Filled Steel Tubular Arch Bridge ", Journal of Engineering Structures ٢٧, PP. ٣ – ١٥, ٢٠٠٥ .

٩٣. **Zienkiewicz, O.C.,** " The Finite Element Method ", McGraw – Hill Co., ٣rd Edition, ١٩٧٧ .